Elastic modeling of biopolymer spherical shells

by

Lei Zhang

A thesis submitted in partial fulfillment of the requirements for the degree of

Doctor of Philosophy

Department of Mechanical Engineering

University of Alberta

Abstract

Elastic modeling is essential for mechanical behavior of biopolymer spherical shells [such as ultrasound contrast agents (UCAs), spherical viruses and enzymes] characterized by high structural heterogeneity and geometric imperfection. The effects of structural heterogeneity and geometric imperfection on pressured buckling and free vibration of biopolymer spherical shells are studied in detail in three chapters of this thesis.

1) An axisymmetric geometric imperfection sensitivity analysis is conducted based on a refined shell model recently developed for pressured buckling of biopolymer spherical shells of high structural heterogeneity and thickness nonuniformity. The influence of related parameters (including the ratio of radius to average shell thickness, the ratio of transverse shear modulus to in-plane shear modulus, and the ratio of effective bending thickness to average shell thickness) on imperfection sensitivity is examined for pressured buckling. The actual maximum sustainable external pressures for typical imperfect spherical biopolymer shells (viral capsids and ultrasound contrast agents) are predicted based on physically realistic parameters.

2) Initial post-buckling and geometric imperfection sensitivity of a pressured biopolymer spherical shell based on non-axisymmetric buckling modes and associated mode interaction are studied. The comparison with the results obtained based on the axisymmetric imperfection sensitivity analysis identified the cases in which a more accurate non-axisymmetric analysis with the mode interaction is required for imperfection sensitivity of pressured buckling of biopolymer spherical shells. The implications of the non-axisymmetric analysis to two specific types of biopolymer spherical shells (viral capsids and ultrasound contrast agents) are discussed.

3) A refined shell model is employed to study the effect of high structural heterogeneity on natural frequencies and vibration modes of biopolymer spherical shells. With this model, the structural heterogeneity of a biopolymer spherical shell is characterized by an effective bending thickness and

the transverse shear modulus. With physically realistic parameters for spherical viruses and enzymes, the natural frequencies and vibration modes predicted by the present refined shell model are in better agreement with some known simulation results, which suggest that the refined shell model could offer a relatively simple model to simulate free vibration of biopolymer spherical shells of high structural heterogeneity.

The theoretical models and numerical results achieved in this thesis help clarify to what degree the structural heterogeneity and geometric imperfection in biopolymer spherical shells affect their global mechanical response such as pressured buckling and free vibration. Using physically realistic parameters for some typical biopolymer spherical shells, the predictions of actual maximum sustainable pressure and natural frequencies and associated vibration modes provide plausible comparisons with known simulations and experiments of specific biopolymer spherical shells.

Preface

The main body of this thesis is composed by three published/accepted journal papers. See below for details.

Chapter 2 of this thesis is based on a journal paper published as Lei Zhang and C.Q. Ru, Imperfection sensitivity of pressured buckling of biopolymer spherical shells, Physical Review E, 2016 (93):062403. I was responsible for all math derivations, results analysis and writing manuscript. C.Q. Ru is the supervisory author who proposed the research topic, instructed results, and revised the manuscript.

Chapter 3 of this thesis is based on a journal paper published as Lei Zhang and C.Q. Ru, Post-buckling of a pressured biopolymer spherical shell with the mode interaction, Proceedings of The Royal Society A: Mathematical, Physical and Engineering Sciences, 2018 (474): 20170834. I was responsible for all math derivations, results analysis and writing manuscript. C.Q. Ru is the supervisory author who proposed the research topic, instructed results, and revised the manuscript.

Chapter 4 of this thesis is based on a journal paper published as Lei Zhang and C.Q. Ru, Free vibration of biopolymer spherical shells of high structural heterogeneity, AIP Advances, 2018(8): 075006. I was responsible for all math derivations, results analysis and writing manuscript. C.Q. Ru is the supervisory author who proposed the research topic, instructed results, and revised the manuscript.

Acknowledgements

I would like to express my sincere thanks to my supervisor Dr. Chongqing Ru for his incredible guidance and prompt help during my doctoral program. His constructive and valuable comments and suggestions helped me a lot in all the time of research and writing of this thesis.

I would also like to thank my supervisory committee members, Dr. Tian Tang and Dr. Donald Raboud, for their valuable suggestions on my research.

The financial support from China Scholarship Council (CSC) and Natural Sciences and Engineering Research Council of Canada (NSERC) is greatly appreciated. With the support provided, I could immerse myself in this research deeply, which guarantees the quality of my work.

Last but not the least, I would like to thank my parents and my wife who always support me no matter what kind of difficulty I am faced with. Without their supports, I would have never finished my PhD.

Table of Contents

List of figures

List of tables

Nomenclature

E	Young's modulus
$e_{\varphi}, e_{\theta}, e_{\varphi\theta}$	membrane strains
$e_{\theta z}$, $e_{\varphi z}$	transverse shear strains
G	in-plane shear modulus
G^{*}	transverse shear modulus
h	average shell thickness
k_s	shear coefficient
k_{φ}, k_{θ}, $k_{\varphi\theta}$	change in curvatures
$M_{\varphi}, M_{\theta}, M_{\varphi\theta}$	bending moments
$N_{\varphi}, N_{\theta}, N_{\varphi\theta}$	in-plane resultant membrane forces
$P_n(\cos\varphi)$	Legendre-polynomial of degree n,
$\bar{P}_n^m(\cos\varphi)$	associated normalized Legendre-polynomial of degree n, order m
Q_{φ}, Q_{θ}	transverse shear forces
q	external pressure
R	middle surface radius
t	time
u, v, w	the displacements of the middle surface in φ, θ, z directions
$u_0, v_0, w_0, \alpha_0, \beta_0$	pre-buckling deformations prior to buckling
u_1, w_1, α_1	linearized buckling modes

u_2, w_2, α_2	auxiliary displacements
$u_1^*, v_1^*, w_1^*, \alpha_1^*, \beta_1^*$	deviations from the pre-buckling state
$u_2^*, v_2^*, w_2^*, \alpha_2^*, \beta_2^*$	deviations expanded in the second-order buckling modes
Y	two-dimensional Young's modulus
α, β	the rotations of the normal of the middle surface in φ, θ directions
λ	knockdown factor
ρ	the mass density of the shell
Ω	dimensionless natural frequency
φ, θ, z	spherical coordinates of a biopolymer spherical shell
γ	Foppl-von Kanman number
κ	bending modulus
ξ_0	nondimensional amplitude factor of axisymmetric displacement
$\bar{\xi}_0$	nondimensional axisymmetric imperfection amplitude
$\xi_m, \kappa_m \left(m = 1, 2, 3, ...\right)$	nondimensional amplitude factors of non-axisymmetric displacement
$\bar{\xi}_m, \bar{\kappa}_m \left(m = 1, 2, 3, ...\right)$	nondimensional non-axisymmetric imperfection amplitudes
μ	Poisson's ratio
ω	angular frequency
σ	membrane stress

Chapter 1: Introduction

1.1 Research background

Spherical shell-like geometrical structures are common in various biological objectives. One example is the micro-scaled shell-like ultrasound contrasts agents (UCAs), which are manufactured by encapsulating an insert gas into a thin biocompatible shell and can be used as carriers for target drug and gene delivery (Liu et al., 2006; Sboros, 2008). The other example is nano-sized spherical virus coated by a protein shell (known as capsid) (Mateu, 2013). Enzymes, generally spherical ("globular") proteins, is another example of the biopolymer spherical shells.

The pressured buckling and free vibration of bio-related spherical shells are critical to fulfill their functions through the life cycle. For the buckling behavior of biopolymer spherical shells, the study on pressured buckling and rupture of the spherical virus shells (capsid) is of particular interest as they determine the resistance to osmotic shocks and the maximum ejection pressure of DNA in the host cell (Bealle et al., 2011), which is relevant in understanding their biological functions such as protecting genetic materials, maturation, and infection of cells (Hernando et al., 2014; Mateu, 2013; Roos et al., 2007). Emerging biomedical applications (e.g. perfusion imaging, drug delivery (Guo et al., 2016; Liu et al., 2006; Qin et al., 2009; Sboros, 2008) involving ultrasound contrasts agents (UCAs) rely on an understanding of pressured buckling and rupture of UCAs at or above a predetermined incident acoustic pressure (Chitnis et al., 2010, 2013).

For the vibration behavior of biopolymer spherical shells, a viral capsid protects viral genome from hostile environment of the host cell, and excitation of capsid vibration could find application in either diagnosis or treatment of viral diseases (Babincová, 2000; Dykeman and Sankey, 2008; Ford, 2003; Talati and Jha, 2006; Yang et al., 2015). And it has been experimentally observed that the large-scale

conformational changes in a viral capsid can be described by low-frequency modes and are relevant to the fulfillment of viruses' specific functions (Dykeman and Sankey, 2009, 2010a, 2010b; Kononova et al., 2016; Peeters and Taormina, 2008; Tama and Brooks, 2005). Also, a detailed picture of the enzymes' vibrational modes and frequencies are useful for understanding their cooperative motion and changes in conformation, which can potentially lead to correlated active site opening and/or closure, a phenomenon important for substrate binding and product release (Dykeman and Sankey, 2010a; Mahajan and Sanejouand, 2015; Marques and Sanejouand, 1995; Pentikainen et al., 2008; Wells et al., 2015). Therefore, research on the elastic modeling (such as pressured buckling and free vibration) of biorelated spherical shells is of great importance to understand their biological functions through the life cycle and for their biomedical applications.

1.2 Research motivation

Compared with classical homogeneous thin shells, a common key feature of biopolymer spherical shells is their high structural heterogeneity and geometric imperfection, such as structural inhomogeneity and geometrical imperfection of UCAs confirmed by scanning electron microscopy (Chlon, 2009) (see Fig. 1.1), as well as structural inhomogeneity and high geometric nonuniformity of spherical virus shells revealed by x-ray crystallography (Verdaguer et al., 2013) and cryotransmission electron microscope tomography (Baker et al., 1999; Caston, 2013) (see Fig. 1.2). For many biopolymer structures such as microtubules that have similar structural heterogeneity and geometric imperfection, it is known that some important physical phenomena related to buckling and vibration behaviors are greatly influenced by transverse shear resistance, bending modulus and imperfect boundaries (intensively studied in many research work, see e.g. (Arani et al., 2017; Baninajjaryan and Beni, 2015; Beni et al., 2017; Civalek and Demir, 2010; Daneshmand and Amabili, 2012; Fu and Zhang, 2010; Gu et al., 2009; Heireche et al., 2010; Kis et al., 2002; Kučera et al., 2016; Liew et al.,

2015; Mehrbod and Mofrad, 2011; Pampaloni et al., 2006; Shi et al., 2008; Shen, 2010; Tounsi et al., 2010; Xiang and Liew, 2012; Zhang and Wang, 2015)). These phenomena cannot be explained by the simple homogeneous elastic shell model without transverse shear. As stated by Gibbons and Klug (Gibbons and Klug, 2008), "although homogenized continuum models provide an explanation of biopolymer spherical shell indentation mechanics consistent with experiments, the degree for which heterogeneity in these protein assemblies affects their global mechanical response is still unclear." Therefore, the present thesis aims to develop more accurate shell models for biopolymer spherical shells which can account for some high-order effects associated with their structural heterogeneity such as transverse shear, effective bending thickness and geometric imperfection.

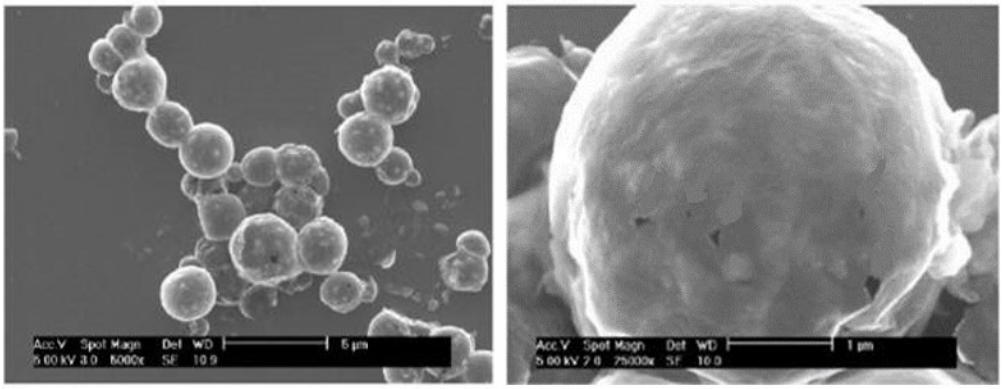

Fig. 1.1 Electronmicrographs of UCAs (Kooiman et al., 2009). Copyright 2009. Reproduced with permission from Elsevier.

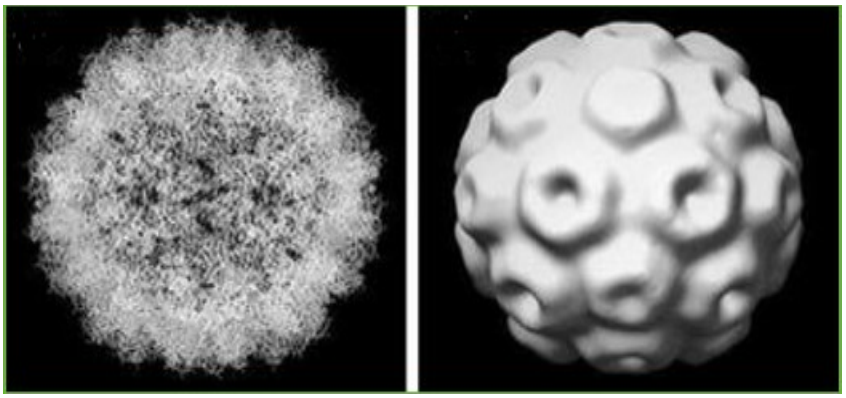

Fig. 1.2 Representations of the CCMV viral capsids (Gibbons and Klug, 2007a). Copyright 2007. Reproduced with permission from Springer Nature.

1.3 Literature review

1.3.1 Elastic modeling of classical homogeneous spherical shells

1.3.1.1 The pressured buckling modeling of classical homogeneous spherical shells

The calculations of the linearized buckling pressure of spherical shells were first made by Zoelly (Zoelly, 1915) and Schwerin (Schwerin, 1922), who considered that the buckling displacement is axisymmetric. Their solutions were based on the assumption of infinitesimal displacements from the linear pre-buckling solution, $\sigma = qR/(2h)$, $w/R = q/\left[(1-\mu^2)E\right](R/h)$ and were obtained in terms of Legendre functions. The critical pressure for linearized buckling is given by

$$q_{cr} = \frac{2E}{\sqrt{3(1-\mu^2)}}\left(\frac{h}{R}\right)^2, \tag{1.1}$$

where R is the radius of the spherical, h its thickness, q the external pressure, σ the membrane stress, w the radial displacement, and E and μ are Young's modulus and Poisson's ratio of the shell materials, respectively.

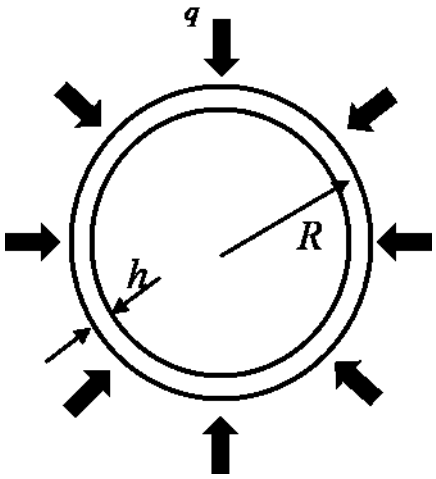

Fig. 1.3 A classical homogeneous spherical shell subject to external pressure

The first complete general analysis of the problem based on the linear theory of elastic stability is due to Van der Neut (Van der Neut, 1932). He found that the linear buckling pressure (1.1) corresponds to (2n+1) linearly independent buckling modes, only one of which is axisymmetric while all others are non-axisymmetric. The integer n can be determined as the nearest natural number by

$$2\sqrt{3(1-\mu^2)}R/h \approx n(n+1). \tag{1.2}$$

This classical shell model was developed based on the assumptions that the spherical shell is thin and therefore the transverse shear strains are neglected, the shell thickness is uniform, and the spherical shell is perfect. We call a spherical shell "perfect", if it is homogenous with uniform thickness and all points on the outer/inner surface have same distance from the centre (see Fig. 1.3). Otherwise, the spherical shell is imperfect. As we can see from Figs. 1.1 and 1.2, there exists imperfect boundaries, uneven surfaces and pores in the shells.

For decades, this theoretical prediction was found to be in disagreement with the experimental results (Carlson et al., 1967; Homewood et al., 1961; Kaplan and Fung, 1954; Krenzke et al., 1967; Seaman, 1962; Tsien, 1942). Early efforts to come to terms with this discrepancy between experiments and shell theory focused on the post-buckling behavior of imperfect shells (Karman and Tsien, 1939; Tsien, 1942) and their extreme sensitivity to initial imperfections (Hutchinson, 1967; Koiter, 1945, 1963, 1969; Thompson, 1962, 1964). Thompson (Thompson, 1962) made a simplified analysis of a spherical shell with initial imperfections but used only two terms to represent the deformation with a constant dimple angle. Thompson (Thompson, 1964) then performed a theoretical buckling stability analysis using Koiter's (Koiter, 1945, 1963) initial post-buckling theory for axisymmetric imperfection. Koiter's (Koiter, 1945, 1963) major contribution is to develop a general theory of elastic stability which connected imperfection sensitivity to the initial post-buckling behavior of the perfect structure. Hutchinson (Hutchinson, 1967) extended Thompson's (Thompson, 1962, 1964) use of Koiter's (Koiter,

1945, 1963) initial post-buckling theory to include non-axisymmetric modes. His simplified analysis by using shallow shell theory is limited to thin shells, for which classic buckling wavelengths are small compared to the cap dimensions. Koiter (Koiter, 1969) performed an extensive investigation of the post-buckling behavior of the complete spherical shell. This included some modifications of Hutchinson's non-axisymmetric analysis (Hutchinson, 1967) and a considerable amplification of Thompson's axisymmetric analysis (Thompson, 1962, 1964). He added the fourth-order terms in the axisymmetric analysis and the obtained results which are close to Hutchinson's (Hutchinson, 1967). Based on the seminal works done by (Hutchinson, 1967; Koiter, 1969; Thompson, 1962, 1964) and other extensive research work (Murray and Wright, 1961; Kalnins and Biricikoglu, 1970; Koga and Hoff, 1969; Sabir, 1964; Walker, 1968), it became well established that the primary cause for this discrepancy is the presence of geometric imperfections.

The intense study of the nonlinear buckling behavior of complete spherical shells largely ended almost five decades ago with the publication of Koiter's (Koiter, 1969) monumental paper on the post-buckling behavior and imperfection sensitivity of complete spherical shells subject to external pressure (Hutchinson, 2016). Until very recently, the post-buckling behavior and imperfection sensitivity of shells have been extensively studied numerically and experimentally (Evkina and Lykhachova, 2017; Hutchinson, 2016; Hutchinson and Thompson, 2016; Jimenez et al., 2017; Lee et al., 2016; Yu et al., 2017). Lee et al. (Lee et al., 2016) study the effect of a precisely fabricated dimplelike geometric imperfection on the critical buckling load of spherical elastic shells under pressure loading. For the first time, experimental results of imperfect spherical shells have been accurately predicted, through both finite element modeling and shell theory solutions. In particular, they found that the buckling pressure becomes independent of the amplitude of the dimplelike defect beyond a critical value. This phenomenon is also observed by Hutchinson (Hutchinson, 2016) (who considers several types of geometric imperfections including dimple-shaped undulations and sinusoidal-shaped equatorial

undulations and use the shell theory), and Jimenez et al. (Jimenez et al., 2017) (who consider precisely defined geometric imperfections and use finite-element analysis). This observation proves that the direct application of Koiter-type theory to complete spherical shells under external pressure, first presented by (Thompson, 1962, 1964) and somewhat later by (Hutchinson, 1967) and (Koiter, 1969), turns out to be valid for only small imperfections.

1.3.1.2 The free vibration modeling of classical homogeneous spherical shells

Vibration of elastic closed spherical shell was first examined by Lamb (Lamb, 1882), by means of the membrane theory, and then by Federhofer (Federhofer, 1937) who employed the classical bending theory of shells. More detailed treatments of axisymmetric vibration of a closed spherical shell were given by (Baker, 1961) and (Kalnins, 1964) who used membrane and classical bending theories, respectively. Wilkinson (Wilkinson, 1965) subsequently investigated the axisymmetric modes of a complete spherical shell including the effects of transverse shear and rotary inertia. Two frequency equations for the axisymmetric vibration of a closed spherical shell are derived in (Wilkinson, 1965). The first frequency equation for spheroidal vibration modes is written as a cubic equation in Ω^2 as follows (Wilkinson, 1965)

$$\begin{aligned}
&\Omega^6\left[2k_1\left(k_1k_r-k_2c_r\right)/\left(k_s\left(1-\mu\right)\right)\right]-\Omega^4\left\{\left(k_1k_r-k_2c_r\right)\left[r+4\left(1+\mu\right)/\left(k_s\left(1-\mu\right)\right)\right]\right.\\
&+k_1\left[12\left(R/h\right)^2\left(k_1+k_2\right)+\left(c_r+k_r\right)+2\left(k_1+k_r\right)\left(r/\left(1-\mu\right)-1\right)/k_s\right]\Big\}\\
&+\Omega^2\left\{\left(1+\mu\right)\left(2-r\right)\left(12\left(R/h\right)^2k_2+c_r\right)+k_r\left[r\left(r-3-\mu\right)+2\left(1+\mu\right)\left(\left(r-2\right)/k_s+1\right)\right]\right.\\
&\left.+k_1\left[2r\left(r+4\mu\right)/\left(k_s\left(1-\mu\right)\right)+r\left(r+12\left(R/h\right)^2+\mu\right)+\left(1+3\mu\right)\left(12\left(R/h\right)^2-2/k_s\right)-\left(1-\mu\right)\right]\right\}\\
&-\left(r-2\right)\left[r\left(r-2\right)+2\left(1+\mu\right)\left(r-1+\mu\right)/k_s+\left(1-\mu^2\right)\left(12\left(R/h\right)^2+1\right)\right]=0,
\end{aligned} \tag{1.3}$$

and the second frequency equation for torsional vibration modes is written as a quadratic equation in Ω^2 as follows (Wilkinson, 1965)

$$\Omega^4\left[4\left(k_1k_r-k_2c_r\right)/\left(k_s\left(1-\mu\right)\right)\right]-2\Omega^2\left[12\left(R/h\right)^2\left(k_1+k_2\right)+\left(c_r+k_r\right)+\left(k_1+k_r\right)\left(r-2\right)/k_s\right]$$
$$+\left(1-\mu\right)\left(r-2\right)\left[\left(r-2\right)/k_s+\left(12\left(R/h\right)^2+1\right)\right]=0, \tag{1.4}$$

where R is the radius of the spherical shell, h is its average thickness, μ is Poisson's ratio of shell material, k_s is the shear coefficient, the tracers are given by $k_1=1+\frac{1}{12}\left(\frac{h}{R}\right)^2$, $k_2=\frac{1}{6}\left(\frac{h}{R}\right)^2$, $k_r=1+\frac{3}{20}\left(\frac{h}{R}\right)^2$, $c_r=2$ (Kraus, 1967; Wilkinson and Kalnins, 1965), and $r=n\left(n+1\right)$, where n denotes the mode number. Ω denotes the dimensionless natural frequency defined by $\Omega^2=\frac{\rho R^2\omega^2(1-\mu^2)}{E}$, where E is Young's modulus, t is time, and ρ denotes the mass density of the shell, ω is the angular frequency.

It is known that this classical shell model for studying free vibration of spherical shells is developed based on the assumptions that the transverse shear modulus equals to in-plane shear modulus, the thickness of spherical shell is uniform, and the spherical shell is perfect.

Theoretical investigations regarding the non-axisymmetric modes have been reported as well (Niordson, 1984, 1988; Silbiger, 1962; Wilkinson and Kalnins, 1965). Silbiger (Silbiger, 1962) presents the first discussion of the presence of non-axisymmetric modes of spherical shells and claims that non-axisymmetric modes for a complete spherical shell do exist and that they are degenerate, meaning that the non-axisymmetric frequencies are identical to corresponding axisymmetric modes. Silbiger (Silbiger, 1962) attributes this to the spherical symmetry of the shell and goes on to state that, corresponding to each natural frequency, there exists $2n+1$ linearly independent modes at each mode number n. All other modes (at a given frequency) are linear combinations of these modes.

Attempts at correlating the theoretical results with either experimental or simulated results (both for axisymmetric and non-axisymmetric modes of vibration) are almost completely lacking (Duffey et al., 2007). Recently, Duffey et al. (Duffey et al., 2007) presented a comparison of natural frequencies and vibration modes obtained from axisymmetric and non-axisymmetric theories of vibration of complete spherical shells (Wilkinson, 1965) with finite element simulations and experimental results. Comparisons of the axisymmetric frequencies are good (see Table 1 and 2 in (Duffey et al., 2007)). Also, finite element calculations and experimental results support the existence of $2n+1$ independent vibration mode (see figures 4 and 5 in (Duffey et al., 2007)), in agreement with (Silbiger, 1962).

1.3.2 Pressured buckling of biopolymer spherical shells

Recently, the shell material properties of polymer-shelled UCAs have been explored based on mechanical deformation through an atomic-force microscope (AFM) (Sboros, 2007), and buckling and rupture (Chitnis et al., 2010, 2011a, 2011b, 2013; Marmottant et al., 2011) of polymer-shelled UCAs are studied in detail. In terms of spherical viruses, the complex mechanical properties have been studied extensively, using the method of AFM nanoindentation (Mateu, 2012; Michel, 2006), continuum elasticity by Nelson and Widom (Lidmar et al., 2003; Widom et al., 2007) and Bruisnma and Gelbart (Nguyen et al., 2005, 2006), and molecular dynamics simulation by May and Brooks (May, 2011; May and Brooks, 2011, 2012). In particular, the mechanical stability and rupture of viral capsid under different external and internal mechanical loadings (Nguyen et al., 2005; Siber, 2006; Siber and Podgornik, 2009; Zandi and Reguera, 2005) have been investigated by many researchers.

Based on the feature of biopolymer spherical shells, the effect of structural heterogeneity and geometric imperfection on the pressured buckling of biopolymer spherical shells has received considerable attention. For examples, a refined elastic spherical shell model has been developed in (Ru, 2009) to

explore the effect of structural heterogeneity and thickness nonuniformity on pressured buckling of biopolymer spherical shells; this model was recently employed by Chitnis et al. to study the rupture of ultrasound contrast agents (UCAs) (Chitnis et al., 2010, 2011a, 2011b, 2013). Wan et al. (Wan et al., 2015) showed that structural defects in spherical crystalline shells affect the shells' ability to sustain external hydrostatic pressure. Gibbons and Klug (Gibbons and Klug, 2006, 2007, 2008, 2015) demonstrated by finite element simulations that nonuniform geometry and geometric defects have meaningful effects on the mechanical failure of viral capsid. May et al. (May et al., 2011) and May and Brooks (May and Brooks, 2011, 2012) revealed nonuniform elastic properties of spherical viruses due to the heterogeneity of the structure and the anisotropy of the biomolecular interactions through molecular dynamics simulation based on a buckling transition predicted by Lidmar et al. (Lidmar et al., 2003) and Widom et al. (Widom et al., 2007). Chitnis et al. (Chitnis et al., 2010, 2011a, 2011b, 2013) emphasized that the shell imperfection influences the rupture load of polymer-shelled UCAs. Also, Nguyen-Thanh et al. (Nguyen-Thanh et al., 2015) developed an extended isogeometric element formulation (XIGA) based on Kirchhoff-Love shell theory for through-the-thickness cracks in thin shell structures, which is also significant for the future study on imperfect biopolymer shells.

It should also be noted that in more realistic biopolymer spherical shells, both the geometric imperfection and the buckling pattern can be non-axisymmetric. For examples, the structural model of spherical viruses' shell (capsid) obtained by X-ray crystallography shows the non-axisymmetric geometric imperfection (e.g. fig. 1 in (Michel et al., 2006)). Bealle et al. (Bealle et al., 2011) demonstrated that deformation patterns of osmotically induced buckling of capsid-like icosahedral vesicles are non-axisymmetric (see their fig. 3). Also, Chitnis et al. (Chitnis et al., 2010) showed different buckling modes and the asymmetric rupture of UCAs in their static pressure experiments (see their fig. 3), and Yin et al. (Yin et al., 2005) found various post-bifurcation modes with shape transitions in biomembrane cells.

Therefore, it is of great significance to study the effect of geometrical imperfection (both axisymmetric and non-axisymmetric) on pressured buckling of biorelated spherical shells (such as UCAs and spherical viruses) and the influence on their biological functioning. In particular, when a non-axisymmetric imperfection is involved, the effect of the non-axisymmetric modes and the mode interaction on the imperfection sensitivity of pressured biopolymer spherical shells is worthwhile to be investigated.

1.3.3 Vibrational properties of biopolymer spherical shells

The study on vibrational properties of biopolymer spherical shells is an area of growing interest recently due to its close relation with their biological functions. A number of approaches have been developed to investigate vibration behaviors of biopolymer spherical shells, such as experiments (Tama and Brooks, 2005; Tsen et al., 2006, 2007), continuum elastic models (Balandin and Fonoberov, 2005; Ford, 2003; Ghavanloo and Fazelzadeh, 2015; Kahn et al., 2001; Tsen et al., 2006, 2007; Widom et al., 2007; Yang et al., 2009), elastic network modeling (Bergman and Lezon, 2017; May et al., 2011; May and Brooks, 2011, 2012; May, 2014; Peeters and Taormina, 2008, 2009), and atomistic simulations (Dykeman and Sankey, 2008; 2009, 2010; Wells et al., 2015). To mention a few, Babincová et al. (Babincová et al., 2000) suggested that viruses can be inactivated by ultrasound resonance in the GHz region. Motivated by this hypothesis, several groups investigated vibrational modes of viruses (Balandin and Fonoberov, 2005; Dykeman and Sankey, 2008, 2010a, 2010b; Tsen et al., 2006). Ford (Ford, 2003) has reported theoretical estimates of vibrational frequencies of spherical virus particles using the liquid drop model and an elastic sphere model. Talati and Jha (Talati and Jha, 2006) used an elastic continuum model to calculate low-frequency vibrational modes of spherical viruses immersed in a medium. Widom et al. (Widom et al., 2007) identified and classified vibration

modes of a virus capsid based on a simple mass-and-spring model. Dykeman and Sankey (Dykeman and Sankey, 2008; 2009, 2010a, 2010b) calculated low-frequency vibration modes and frequencies of large protein assemblies (such as enzymes and viral capsids), where the vibration modes are modeled with full atomic detail. Yang et al. (Yang et al., 2009) predicted vibrational modes of several icosahedral viruses and an icosahedral enzyme using continuum models, and they estimated the macroscopic material properties such as the Young's modulus or Poisson's ratio by fitting the predictions to an anisotropic network model. May and Brooks (May et al., 2011; May and Brooks, 2011, 2012; May, 2014) applied two-dimensional elasticity theory to viral capsids and developed a framework for calculating elastic properties of viruses.

However, bio-related spherical shells are characterized by high structural heterogeneity and thickness non-uniformity. Such a key feature of bio-related spherical shells has not been well addressed in the previous related studies on free vibration behavior. In particular, almost all previous continuum models are based on the classical homogeneous shell model and are often limited to axisymmetric vibration. Therefore, it is of great interest to investigate the role of high structural heterogeneity and thickness nonuniformity on axisymmetric and non-axisymmetric free vibration of biopolymer spherical shells.

1.4 Research objectives

In view of the fact that biopolymer spherical shells are characterized by high structural heterogeneity and thickness non-uniformity, a refined elastic spherical shell model was developed in (Ru, 2009) based on axisymmetric assumption, which was recently used to study the rupture of ultrasound contrasts agents (UCAs) by Chitnis et al. (Chitnis et al., 2011a, 2011b, 2013). The effect of structural heterogeneity and thickness non-uniformity on the linear critical pressure q_{cr} for small-deflection linearized axisymmetric buckling of a perfect biopolymer spherical shell given by the refined model is

$$q_{cr}=\left(\frac{2E}{\sqrt{3\left(1-\mu^2\right)}}\right)\left(\frac{h_0}{h}\right)^{\frac{3}{2}}\left(\frac{h}{R}\right)^2-\left(\frac{E}{3(1-\mu)k_s}\right)\left(\frac{h_0}{h}\right)^3\left(\frac{h}{R}\right)^2\left(\frac{G}{G^*}\right), \tag{1.5}$$

where E is Young's modulus, μ is Poisson's ratio of the biopolymer spherical shell, k_s is the shear coefficient, R is the average radius, h is the average thickness, G is the in-plane shear modulus, G^* is the transverse shear modulus, and h_0 is the effective bending thickness. Clearly, the critical value (1.5) given by the refined model reduces to the classical formula (1.1) when transverse shear strains are neglected ($G^*/G=\infty$) and $h_0=h$, as shown in (Ru, 2009). Here, the deviation of trasverse shear modulus G^* and effective bending thickness h_0 from the in-plane shear modulus G and the average thickness h indicate the structural heterogeneity and the thickness nonuniformity, respectively. The deviation of G^* from G indicates the anisotropy, which is due to the underlying heterogenous microstructures. It should be noted that the terminology "heterogeniety" in this thesis is referring to the inhomogeneous microscopic structures of which the characteristic length is far smaller than the radius of spherical shells. The separation of scales permits the homogenization of microstructures. Therefore, in the model of this thesis, the material is assumed to be homogenous and possesses effective material properties.

Owing to the axisymmetric assumption made in (Ru, 2009), only one axisymmetric buckling mode exists. The linearized axisymmetric buckling mode is given by the n-degree Legendre functions $P_n(\cos\varphi)$ (Koiter, 1969; Zhang and Ru, 2016), where the integer n can be determined as the nearest natural number by the following formula (Ru, 2009; Zhang and Ru, 2016)

$$\frac{6(1-\mu)k_s\dfrac{G^*}{G}(\dfrac{R}{h})^2(\dfrac{h}{h_0})^3}{\dfrac{k_s\sqrt{3(1-\mu^2)}}{1+\mu}\dfrac{G^*}{G}\dfrac{R}{h}(\dfrac{h}{h_0})^{\frac{3}{2}}-1}\approx n(n+1). \tag{1.6}$$

Also, it is seen that the formula (1.6) reduces to (1.2) when transverse shear strains are neglected ($G^*/G=\infty$) and $h_0=h$.

It is known that for some typical biopolymer shells (such as microtubules), transverse shear modulus can be much lower than in-plane shear modulus (Kis et al., 2002; Pampaloni et al., 2006; Shi et al., 2008), and therefore transverse shear could become significant for shorter-wavelength deformation. For biopolymer spherical shells, because wavelengths are always shorter as compared to the diameter, it is expected that transverse shear could be relevant for biopolymer spherical shells. In particular, in view of similar thickness non-uniformity and structural heterogeneity of microtubules and biopolymer spherical shells, it is assumed here that the transverse shear modulus G^* could be much lower than the in-plane shear modulus G and the effective bending thickness h_0 can be different from the average shell thickness h (Ru, 2009).

Based on this refined model, we carry out the study on the following topics:

(1) Investigate the effect of axisymmetric geometric imperfection on pressured buckling of a biopolymer spherical shell.

(2) Non-axisymmetric geometrical imperfections and mode-interaction on the imperfection sensitivity of pressured biopolymer spherical shells.

(3) Investigate the effect of structural heterogeneity and thickness non-uniformity on natural frequencies and vibration modes of biopolymer spherical shells.

1.5 Thesis layout

The present thesis is organized as follows:

Chapter 1 provides a general research background and motivation of the involved research topics, the literature review and the objectives of my research.

Chapter 2 investigates the post-buckling behavior and imperfection sensitivity of pressured buckling of a biopolymer spherical shell based on axisymmetric assumption and the above-mentioned refined shell model. Detailed research on the influence of related parameters (including the ratio of radius to average shell thickness, the ratio of transverse shear modulus to in-plane shear modulus, and the ratio of effective bending thickness to average shell thickness) on imperfection sensitivity is conducted. In addition, with physically relevant data in the literature for viral capsids and ultrasound contrast agents, the actual maximum external pressure an imperfect biopolymer spherical shell can sustain is predicted.

Chapter 3 extends the axisymmetric imperfection sensitivity analysis proposed in chapter 2 to a non-axisymmetric analysis with the mode interaction. The cases that need the more accurate non-axisymmetric analysis with the mode interaction are discussed in detail. The actual maximum external pressures predicted in chapter 2 for two types of biopolymer spherical shells are modified based on the non-axisymmetric analysis.

Chapter 4 proposes a refined shell model to study the effect of high structural heterogeneity on natural frequencies and vibration modes of biopolymer spherical shells. With physically realistic parameters of spherical viruses and enzymes, the results predicted by the refined shell model are compared with known simulation results and the results obtained by the classical homogeneous shell model.

Chapter 5 summarizes the major conclusions of this research and suggests a few research topics for future studies.

Chapter 2: Axisymmetric imperfection sensitivity on pressured buckling of a biopolymer spherical shell

2.1 Introduction

This chapter aims to examine axisymmetric imperfection sensitivity of biopolymer spherical shells of high structural heterogeneity using the refined shell model (Eqs. (1.5) and (1.6)) developed in (Ru, 2009). The methods for axisymmetric post-buckling of classical homogeneous spherical shells developed in previous seminal works, e.g. by Thompson (Thompson, 1962, 1964), Hutchinson (Hutchinson, 1967), Koiter (Koiter, 1945,1963,1969) and Budiansky and Hutchinson (Budiansky and Hutchinson, 1964), will be employed to study the imperfection sensitivity of structurally heterogeneous biopolymer spherical shells based on the refined shell model (Ru, 2009). In section 2.2, the axisymmetric post-buckling modes of a pressured perfect biopolymer spherical shell are derived. Furthermore, the axisymmetric imperfection sensitivity is studied in section 2.3 with an emphasis on the influence of key parameters on the axisymmetric imperfection sensitivity for two specific types of biopolymer spherical shells (ultrasound contrasts agents UCAs and spherical viruses). Finally, main conclusions are summarized in section 2.4.

2.2 Axisymmetric post-buckling modes of a pressured perfect biopolymer spherical shell

In this section, post-buckling modes of a prefect biopolymer spherical shell defined by the refined model (Ru, 2009) are studied. The present chapter focuses on buckling under static pressure, and viscous effect can be ignored reasonably although such viscoelastic effect may play a significant

role in high frequency vibration of some biopolymer shells. The procedures and formulations given in this section were developed in Budiansky and Hutchinson's work (Budiansky and Hutchinson, 1964) on post-buckling of elastic structures, based on Koiter's general nonlinear theory of elastic stability (Koiter, 1945,1963). Since geometric imperfection of the biopolymer shells can be assumed to be axisymmetric, we shall confine ourselves to axisymmetric postbuckling.

Spherical coordinates φ ($0 \le \varphi \le \pi$), θ ($0 \le \theta \le 2\pi$) and z ($-h/2 \le z \le h/2$) are used to describe a biopolymer spherical shell of middle surface radius R and average shell thickness h, where the radial coordinate z, whose sign is taken positive outward, indicates the distance of a point in the shell to the middle surface. The linear mid-face strains (including 2 transverse shear strains $e_{\varphi z}$, $e_{\theta z}$ and the change in curvatures k_φ, k_θ and $k_{\varphi\theta}$) of a spherical shell are given in terms of the displacements of the middle surface u, v, w and the rotations α, β of the normal of the middle surface in φ, θ directions by (Ru, 2009) (the detailed derivation is given in Appendix A)

$$
\begin{aligned}
e_\varphi &= \frac{1}{R}\frac{\partial u}{\partial \varphi} + \frac{w}{R}, \qquad e_\theta = \frac{u}{R}\cot\varphi + \frac{1}{R\sin\varphi}\frac{\partial v}{\partial \theta} + \frac{w}{R}, \qquad e_{\varphi\theta} = \frac{1}{R\sin\varphi}\frac{\partial u}{\partial \theta} + \frac{1}{R}\frac{\partial v}{\partial \varphi} - \frac{v}{R}\cot\varphi, \\
e_{\theta z} &= \frac{1}{R\sin\varphi}\frac{\partial w}{\partial \theta} - \frac{v}{R} + \beta, \qquad e_{\varphi z} = \frac{1}{R}\frac{\partial w}{\partial \varphi} - \frac{u}{R} + \alpha, \\
k_\varphi &= \frac{1}{R}\frac{\partial \alpha}{\partial \varphi}, \qquad k_\theta = \frac{\alpha}{R}\cot\varphi + \frac{1}{R\sin\varphi}\frac{\partial \beta}{\partial \theta}, \qquad k_{\varphi\theta} = \frac{1}{R\sin\varphi}\frac{\partial \alpha}{\partial \theta} + \frac{1}{R}\frac{\partial \beta}{\partial \varphi} - \frac{\beta}{R}\cot\varphi
\end{aligned}
\tag{2.1}
$$

For axisymmetric post-buckling of an elastic spherical shell (with $v = \beta = 0$ and $\partial(\ )/\partial\theta = 0$, see e.g. (Ru, 2009)), based on the simplifications (Kraus, 1967; Ru, 2009) that the contribution of two in-plane displacements u and v to the transverse shear strains $e_{\theta z}$, $e_{\varphi z}$ is negligible, and using the simple nonlinear term of Sander's nonlinear kinematic relations (Sanders, 1961) and the shear deformation theory of Reddy and Liu (Reddy and Liu,1985), Eq. (2.1) is replaced by

$$e_\varphi = \frac{1}{R}\frac{\partial u}{\partial \varphi} + \frac{w}{R} + \frac{1}{2}\left(\frac{\partial w}{R\partial \varphi}\right)^2, \quad e_\theta = \frac{u}{R}\cot\varphi + \frac{w}{R},$$
$$e_{\varphi\theta} = 0, \quad e_{\theta z} = 0, \quad e_{\varphi z} = \frac{1}{R}\frac{\partial w}{\partial \varphi} + \alpha, \tag{2.2}$$
$$k_\varphi = \frac{1}{R}\frac{\partial \alpha}{\partial \varphi}, \quad k_\theta = \frac{\alpha}{R}\cot\varphi, \quad k_{\varphi\theta} = 0$$

Here, transverse shear deformation is included as a potentially significant factor for thick biopolymer spherical shells (Gibbons and Klug, 2007).

Based on Hooke's law, the relationship between the stresses and strains ($\varepsilon_\varphi, \varepsilon_\theta, \gamma_{\varphi\theta}, \gamma_{\varphi z}, \gamma_{\theta z}$, see definitions in Appendix A) on the biopolymer spherical surface are given by

$$\sigma_\varphi = \frac{E}{1-\mu^2}\left(\varepsilon_\varphi + \mu\varepsilon_\theta\right), \quad \sigma_\theta = \frac{E}{1-\mu^2}\left(\varepsilon_\theta + \mu\varepsilon_\varphi\right)$$
$$\sigma_{\varphi\theta} = G\gamma_{\varphi\theta}, \quad \sigma_{\varphi z} = G^*\gamma_{\varphi z}, \quad \sigma_{\theta z} = G^*\gamma_{\theta z}. \tag{2.3}$$

where E is Young's modulus, μ is Poisson's ratio of the biopolymer shell, G^* is the transverse shear modulus, and G is the common in-plane shear modulus determined by (E , μ).

Furthermore, based on the isotropic linear plane-stress stress-strain relation, the in-plane resultant membrane forces, bending moments and transverse shear forces are given by (Ru, 2009)

$$\begin{bmatrix} N_\varphi \\ N_\theta \end{bmatrix} = \frac{Eh}{1-\mu^2}\begin{bmatrix} 1 & \mu \\ \mu & 1 \end{bmatrix}\begin{bmatrix} e_\varphi \\ e_\theta \end{bmatrix}, \quad N_{\varphi\theta} = Ghe_{\varphi\theta},$$
$$\begin{bmatrix} M_\varphi \\ M_\theta \end{bmatrix} = D\begin{bmatrix} 1 & \mu \\ \mu & 1 \end{bmatrix}\begin{bmatrix} \kappa_\varphi \\ \kappa_\theta \end{bmatrix}, \quad M_{\varphi\theta} = D_{12}\kappa_{\varphi\theta}, \tag{2.4}$$
$$Q_\varphi = k_s G^* he_{\varphi z}, \quad Q_\theta = k_s G^* he_{\theta z},$$

where k_s is the shear coefficient, which is a dimensionless quantity and depends on the shape of the cross section (defined by $k_s = 6(1+\mu)^2/(7+12\mu+4\mu^2)$ for the circular section and $k_s = 5(1+\mu)/(6+5\mu)$ for the rectangle section) (Stephen, 1980). It is introduced to account for the

fact that the shear stress and shear strain are not uniformly distributed over the cross section (Stephen, 1980). The bending stiffnesses of a biopolymer spherical shell are assumed to be determined by an effective bending thickness h_0 as

$$D = \frac{Eh_0^3}{12\left(1-\mu^2\right)}, \qquad D_{12} = \frac{Gh_0^3}{12} \tag{2.5}$$

For biopolymer spherical shells, as stated above, it is assumed here that the transverse shear modulus G^* could be much lower than the in-plane shear modulus G and the effective bending thickness h_0 can be different from the average shell thickness h (Ru, 2009). It is the two new parameters (G^*, h_0) of the refined model (Ru, 2009) which distinguish biopolymer spherical shells of high structural heterogeneity and thickness non-uniformity from classical elastic shells defined by (E, μ, h).

For a spherical shell, when the uniform external pressure q reaches to the critical value of buckling pressure (bifurcation point), the spherical shell suffers deviation from its spherical geometrical shape. The displacement of the spherical shell in initial post-buckled state can be written in the asymptotic expansions (Budiansky and Hutchinson, 1964; Danielson, 1974)

$$\begin{aligned} u &= u_0 + \xi_0 u_1 + \xi_0^{\,2} u_2 + \mathrm{O}(\xi_0^{\,3}), \\ w &= w_0 + \xi_0 w_1 + \xi_0^{\,2} w_2 + \mathrm{O}(\xi_0^{\,3}), \\ \alpha &= \alpha_0 + \xi_0 \alpha_1 + \xi_0^{\,2} \alpha_2 + \mathrm{O}(\xi_0^{\,3}) \end{aligned} \tag{2.6}$$

where the displacement (u_0, w_0, α_0) are pre-buckling deformations prior to buckling, (u_1, w_1, α_1) are linearized buckling modes, the auxiliary displacements (u_2, w_2, α_2), which will be used to analyze the instability of post-buckling behavior in Appendix B, are all taken to be orthogonal to the buckling

mode (u_1, w_1, α_1) (defined by $\int_0^{2\pi}\int_0^{\pi}\left(\frac{\partial w_1}{\partial \varphi}\right)\left(\frac{\partial w_2}{\partial \varphi}\right)R^2\sin\varphi d\varphi d\theta = 0$), and ξ_0 is a nondimensional amplitude factor.

Substituting the displacements (2.6) into the midface strains (2.2) and then into Eq. (2.4), and considering that the spherical shell under uniform external pressure q prior to buckling is in a uniform membrane state of stress ($N_{\varphi 0} = N_{\theta 0} = -qR/2$) with a pre-buckling inward radial displacement w_0 ($u_0 = 0, \alpha_0 = 0, w_0 = -(1-\mu)qR^2/(2Eh)$) (Hutchinson, 1967), the in-plane resultant membrane forces, bending moments and transverse shear forces have the asymptotic expansions (Budiansky and Hutchinson, 1964; Danielson, 1974)

$$\begin{bmatrix} N_\varphi \\ N_\theta \\ M_\varphi \\ M_\theta \\ Q_\varphi \end{bmatrix} = \begin{bmatrix} N_{\varphi 0} \\ N_{\theta 0} \\ 0 \\ 0 \\ 0 \end{bmatrix} + \xi_0 \begin{bmatrix} N_{\varphi 1} \\ N_{\theta 1} \\ M_{\varphi 1} \\ M_{\theta 1} \\ Q_{\varphi 1} \end{bmatrix} + \xi_0^{\,2} \begin{bmatrix} N_{\varphi 2} + \frac{1}{2}\frac{Eh}{1-\mu^2}\left(\frac{\partial w_1}{R\partial \varphi}\right)^2 \\ N_{\theta 2} + \frac{1}{2}\frac{Eh}{1-\mu^2}\mu\left(\frac{\partial w_1}{R\partial \varphi}\right)^2 \\ M_{\varphi 2} \\ M_{\theta 2} \\ Q_{\varphi 2} \end{bmatrix} + \mathrm{O}(\xi_0^{\,3}),$$
$$N_{\varphi\theta} = 0, \quad M_{\varphi\theta} = 0, \quad Q_\theta = 0 \tag{2.7}$$

where $N_{\varphi i}$ and $N_{\theta i}$ $(i = 0,1,2)$ represent membrane forces with linear strains.

The equilibrium equations of a spherical shell can be derived from the variational principle (Budiansky and Hutchinson, 1964; Danielson, 1974)

$$\frac{1}{2}\int_0^{\pi}\int_0^{2\pi}(N_\varphi \delta e_\varphi + N_\theta \delta e_\theta + N_{\varphi\theta}\delta e_{\varphi\theta} + M_\varphi \delta k_\varphi + M_\theta \delta k_\theta + M_{\varphi\theta}\delta k_{\varphi\theta} + Q_\varphi \delta e_{\varphi z} + Q_\theta \delta e_{\theta z})$$
$$R^2\sin\varphi d\varphi d\theta = \frac{1}{2}\int_0^{\pi}\int_0^{2\pi}\left[N_{\varphi 0}\delta\left(\frac{1}{R}\frac{\partial u}{\partial \varphi} + \frac{w}{R}\right) + N_{\theta 0}\delta e_\theta\right]R^2\sin\varphi d\varphi d\theta \tag{2.8}$$

The integral on the left-hand side of Eq. (2.8) is the internal virtual work, while the right-hand side of Eq. (2.8) is the external virtual work represented by the work of pre-buckling state membrane forces, and $\left(\frac{1}{R}\frac{\partial u}{\partial \varphi}+\frac{w}{R}\right)$ is the linear part of e_φ since the pre-buckling state is described by linear membrane theory.

The midface strains (2.2), the displacement w given in (2.6) and the expansions (2.7) are then substituted into Eq. (2.8), which gives, on using the integration by parts and collecting the coefficients of δu, δw and $\delta\alpha$ separately (Budiansky and Hutchinson, 1964; Reddy, 2002)

$$
\begin{aligned}
0=\xi_0\Bigg\{&\int_0^{\pi}\int_0^{2\pi}\Bigg[\left(-\frac{\partial}{\partial\varphi}(N_{\varphi 1}R\sin\varphi)+N_{\theta 1}R\cos\varphi\right)\delta u\\
&+\left(-\frac{\partial}{\partial\varphi}(N_0\sin\varphi\frac{\partial w_1}{\partial\varphi})+N_{\varphi 1}R\sin\varphi+N_{\theta 1}R\sin\varphi-\frac{\partial}{\partial\varphi}(Q_{\varphi 1}R\sin\varphi)\right)\delta w\\
&+\left(-\frac{\partial}{\partial\varphi}(M_{\varphi 1}R\sin\varphi)+M_{\theta 1}R\cos\varphi+Q_{\varphi 1}R^2\sin\varphi\right)\delta\alpha\Bigg]d\varphi d\theta\\
&+\iint_{\partial S}\Big[(N_{\varphi 1}R\sin\varphi)n_\varphi\delta u+(N_0\sin\varphi\frac{\partial w_1}{\partial\varphi}+Q_{\varphi 1}R\sin\varphi)n_\varphi\delta w+(M_{\varphi 1}R\sin\varphi)n_\varphi\delta\alpha\Big]dS\Bigg\}\\
+\xi_0^{\,2}\Bigg\{&\int_0^{\pi}\int_0^{2\pi}\Bigg[\left(-\frac{\partial}{\partial\varphi}(\frac{1}{2}\frac{Eh}{1-\mu^2}(\frac{\partial w_1}{R\partial\varphi})^2R\sin\varphi)-\frac{\partial}{\partial\varphi}(N_{\varphi 2}R\sin\varphi)\right.\\
&\left.+\frac{1}{2}\frac{Eh}{1-\mu^2}\mu(\frac{\partial w_1}{R\partial\varphi})^2R\cos\varphi+N_{\theta 2}R\cos\varphi\right)\delta u\\
&+\left(-\frac{\partial}{\partial\varphi}(N_0\sin\varphi\frac{\partial w_2}{\partial\varphi})-\frac{\partial}{\partial\varphi}(N_{\varphi 1}\sin\varphi\frac{\partial w_1}{\partial\varphi})+\frac{1}{2}\frac{Eh}{1-\mu}(\frac{\partial w_1}{R\partial\varphi})^2R\sin\varphi\right.\\
&\left.+N_{\varphi 2}R\sin\varphi+N_{\theta 2}R\sin\varphi-\frac{\partial}{\partial\varphi}(Q_{\varphi 2}R\sin\varphi)\right)\delta w\\
&+\left(-\frac{\partial}{\partial\varphi}(M_{\varphi 2}R\sin\varphi)+M_{\theta 2}R\cos\varphi+Q_{\varphi 2}R^2\sin\varphi\right)\delta\alpha\Bigg]d\varphi d\theta\\
&+\iint_{\partial S}\Big[(N_{\varphi 2}R\sin\varphi+\frac{1}{2}\frac{Eh}{1-\mu^2}(\frac{\partial w_1}{R\partial\varphi})^2R\sin\varphi)n_\varphi\delta u\\
&+(N_0\sin\varphi\frac{\partial w_2}{\partial\varphi}+N_{\varphi 1}\sin\varphi\frac{\partial w_1}{\partial\varphi}+Q_{\varphi 2}R\sin\varphi)n_\varphi\delta w+(M_{\varphi 1}R\sin\varphi)n_\varphi\delta\alpha\Big]dS\Bigg\}\\
&+\mathrm{O}(\xi_0^{\,3})
\end{aligned}
\tag{2.9}
$$

where $N_0 = N_{\varphi 0}$, n_φ is the unit normal vector at the edge of the spherical shell. In the case of a spherical shell section clamped along its boundary, the boundary condition is $u = w = \alpha = 0$ and the boundary expressions vanish, whereas in the case of a closed spherical shell, the boundary expressions also vanish owing to the continuity of all displacements.

Since δu, δw and $\delta\alpha$ are arbitrary and independent, the linear ξ_0-term leads to the (first-order) Euler equations for (u_1, w_1, α_1) (Budiansky and Hutchinson, 1964; Reddy, 2002)

$$\begin{gathered} \frac{\partial N_{\varphi 1}}{\partial \varphi} + (N_{\varphi 1} - N_{\theta 1})\frac{\cos\varphi}{\sin\varphi} = 0 \\ \frac{\partial Q_{\varphi 1}}{\partial \varphi} + Q_{\varphi 1}\frac{\cos\varphi}{\sin\varphi} - (N_{\varphi 1} + N_{\theta 1}) + N_0 R\nabla^2 w_1 = 0 \\ RQ_{\varphi 1} = \frac{\partial M_{\varphi 1}}{\partial \varphi} + (M_{\varphi 1} - M_{\theta 1})\frac{\cos\varphi}{\sin\varphi} \end{gathered} \tag{2.10}$$

Following the procedure given in (Ru, 2009) which define u_1 and $Q_{\varphi 1}$ in terms of two new functions $f_1(\varphi)$ and $g_1(\varphi)$ as

$$u_1 = \frac{\partial f_1}{\partial \varphi}, \qquad Q_{\varphi 1} = \frac{\partial g_1}{\partial \varphi} \tag{2.11}$$

and substituting Eq. (2.11) into Eq. (2.10) gives 3 equations for (f_1, w_1, g_1)

$$\begin{gathered} \left[R^2\nabla^2 + (1-\mu)\right] f_1 + (1+\mu) w_1 = 0 \\ R\nabla^2 g_1 - \frac{Eh}{1-\mu}\left(\nabla^2 f_1 + \frac{2w_1}{R^2}\right) + N_0\nabla^2 w_1 = 0 \\ \left(R\nabla^2 + \frac{1-\mu}{R} - \frac{R}{D}k_s G^* h\right) g_1 - \left(k_s G^* h\nabla^2 + k_s G^* h\frac{1-\mu}{R^2}\right) w_1 = 0 \end{gathered} \tag{2.12}$$

Finally, eliminating $f_1(\varphi)$ and $g_1(\varphi)$ in (2.12) leads to a decoupled equation for w_1, the linearized critical value of the external pressure, as given by (1.5) in the form of $\left(\frac{N_0}{Eh}\right)_{cr}$ (considering $N_0 = -qR/2$), is determined by the minimum value of N_0 for a non-zero w_1 as

$$\left(\frac{N_0}{Eh}\right)_{cr} = -\left(\frac{1}{\sqrt{3(1-\mu^2)}}\right)\left(\frac{h_0}{h}\right)^{\frac{3}{2}}\left(\frac{h}{R}\right)+\left(\frac{1}{6(1-\mu)k_s}\right)\left(\frac{h_0}{h}\right)^3\left(\frac{h}{R}\right)^2\left(\frac{G}{G^*}\right). \tag{2.13}$$

Clearly, the critical value (2.13) given by the refined model reduces to the classical formula (1.1) when transverse shear strains are neglected ($G^*/G = \infty$) and $h_0 = h$, as shown in (Ru, 2009).

The linearized axisymmetric normalized buckling mode is given by (Koiter, 1969)

$$w_1 = -hP_n(\cos\varphi) \tag{2.14}$$

where P_n is the n-degree Legrende function and the integer n can be determined as the nearest natural number by the following formula (Ru, 2009)

$$\frac{\frac{R^2}{D}k_sG^*h}{\sqrt{\frac{R^2}{EhD}k_sG^*h-1}} = \frac{6(1-\mu)k_s\frac{G^*}{G}\left(\frac{R}{h}\right)^2\left(\frac{h}{h_0}\right)^3}{\frac{k_s\sqrt{3(1-\mu^2)}}{1+\mu}\frac{G^*}{G}\frac{R}{h}\left(\frac{h}{h_0}\right)^{\frac{3}{2}}-1} \approx n(n+1) >> 1 \tag{2.15}$$

Actually the buckling mode w_1 is the nth eigenfunction of the following eigenvalue problem (Ru, 2009)

$$\nabla^2 w = \frac{-n(n+1)}{R^2}w \tag{2.16}$$

and therefore is determined by

$$\nabla^2 w_1 = \frac{-n(n+1)}{R^2} w_1 \tag{2.17}$$

where the integer n is determined by (2.15). Also, it is proved in (Ru, 2009) that the inequality condition ($n(n+1) >> 1$) listed in (2.15) is met as long as the following condition is satisfied

$$\frac{G^*}{G} > \frac{(1+\mu)}{k_s\sqrt{3(1-\mu^2)}}\left(\frac{h_0}{h}\right)^{3/2}\frac{h}{R} \tag{2.18}$$

In particular, all physically realistic parameters of biopolymer shells used in this chapter well satisfy the condition (2.18).

To derive formulas of u_1 and α_1 , it follows from the first and third equations of (2.12) that the expressions of f_1 and g_1 have similar form as Eq. (2.14). Therefore, combined with Eq. (2.17), the first Laplacian of f_1 and g_1 gives

$$\nabla^2 f_1 = \frac{-n(n+1)}{R^2} f_1, \qquad \nabla^2 g_1 = \frac{-n(n+1)}{R^2} g_1 \tag{2.19}$$

Subsequently, we can get specific expressions of f_1 and g_1 by introducing Eqs. (2.14), (2.17) and (2.19) into the first and third equations of (2.12). Then substituting f_1 and g_1 into Eq. (2.11), the buckling mode u_1, α_1 are determined as

$$\begin{aligned} u_1 &= h\frac{-(1+\mu)}{n(n+1)-(1-\mu)}\frac{\partial}{\partial\varphi}P_n(\cos\varphi) \\ \alpha_1 &= \frac{h}{R}\frac{6(1-\mu)k_s\dfrac{G^*}{G}\left(\dfrac{R}{h}\right)^2\left(\dfrac{h}{h_0}\right)^3}{n(n+1)-(1-\mu)+6(1-\mu)k_s\dfrac{G^*}{G}\left(\dfrac{R}{h}\right)^2\left(\dfrac{h}{h_0}\right)^3}\frac{\partial}{\partial\varphi}P_n(\cos\varphi) \end{aligned} \tag{2.20}$$

Therefore, (2.14) and (2.20) are the linearized buckling modes given by the refined model developed for biopolymer spherical shells with the integer n determined by (2.15).

Next, to determine the auxiliary displacements (u_2, w_2, α_2), setting δu, δw and $\delta\alpha$ orthogonal to (u_1, w_1, α_1) in Eq. (2.9), dividing by $\xi_0^{\,2}$ and then letting ξ_0 vanish, the rearranged equations give the second-order Euler equations for (u_2, w_2, α_2) (Budiansky and Hutchinson, 1964; Reddy, 2002)

$$\begin{gathered}
\frac{\partial N_{\varphi 2}}{\partial\varphi}+(N_{\varphi 2}-N_{\theta 2})\frac{\cos\varphi}{\sin\varphi}+\frac{Eh}{2(1+\mu)}\frac{\cos\varphi}{\sin\varphi}\left(\frac{\partial w_1}{R\partial\varphi}\right)^2+\frac{Eh}{1-\mu^2}\frac{\partial w_1}{R\partial\varphi}\frac{\partial^2 w_1}{R\partial\varphi^2}=0 \\
\frac{\partial Q_{\varphi 2}}{\partial\varphi}+Q_{\varphi 2}\frac{\cos\varphi}{\sin\varphi}-(N_{\varphi 2}+N_{\theta 2})+N_0R\nabla^2 w_2+\frac{\partial N_{\varphi 1}}{\partial\varphi}\frac{\partial w_1}{R\partial\varphi}+N_{\varphi 1}R\nabla^2 w_1-\frac{Eh}{2(1-\mu)}\left(\frac{\partial w_1}{R\partial\varphi}\right)^2=0 \qquad (2.21) \\
\frac{\partial M_{\varphi 2}}{\partial\varphi}+(M_{\varphi 2}-M_{\theta 2})\frac{\cos\varphi}{\sin\varphi}-RQ_{\varphi 2}=0
\end{gathered}$$

Likewise, define u_2 and $Q_{\varphi 2}$ in terms of two new functions $f_2(\varphi)$ and $g_2(\varphi)$

$$u_2=\frac{\partial f_2}{\partial\varphi}, \qquad Q_{\varphi 2}=\frac{\partial g_2}{\partial\varphi} \qquad (2.22)$$

Inserting Eq. (2.22) into Eq. (2.21) leads to 3 equations for (f_2, w_2, g_2)

$$\begin{gathered}
\left[R^2\nabla^2+(1-\mu)\right]f_2+(1+\mu)w_2+\int\left[\frac{\partial w_1}{R\partial\varphi}\frac{\partial^2 w_1}{\partial\varphi^2}+\frac{1-\mu}{2R}\cot\varphi\left(\frac{\partial w_1}{\partial\varphi}\right)^2\right]d\varphi=0 \\
R\nabla^2 g_2-\frac{Eh}{1-\mu}\left(\nabla^2 f_2+\frac{2w_2}{R^2}\right)+N_0R\nabla^2 w_2+\frac{\partial N_{\varphi 1}}{\partial\varphi}\frac{\partial w_1}{R\partial\varphi}+N_{\varphi 1}R\nabla^2 w_1-\frac{Eh}{2(1-\mu)}\left(\frac{\partial w_1}{R\partial\varphi}\right)^2=0 \qquad (2.23) \\
\left(R\nabla^2+\frac{1-\mu}{R}-\frac{R}{D}k_sG^*h\right)g_2-\left(k_sG^*h\nabla^2+k_sG^*h\frac{1-\mu}{R^2}\right)w_2=0
\end{gathered}$$

By introducing the buckling mode w_1 (Eq. (2.14)) into the third term on left hand side of the first equation of (2.23), it can be proved through *Mathematica* that the formula gives

$$\int\left[\frac{\partial w_1}{R\partial\varphi}\frac{\partial^2 w_1}{\partial\varphi^2}+\frac{1-\mu}{2R}\cot\varphi\left(\frac{\partial w_1}{\partial\varphi}\right)^2\right]d\varphi=h\sum_{k=0}^{n}H_{2k}P_{2k}(\cos\varphi) \tag{2.24}$$

where P_{2k} are Legrende functions of degree $2k$, and H_{2k} can be obtained easily through *Mathematica*.

Then, it follows from Eq. (2.23) that the formulas of w_2, f_2 and g_2 are

$$w_2=-h\sum_{k=0}^{n}C_{2k}P_{2k}(\cos\varphi),\qquad f_2=h\sum_{k=0}^{n}D_{2k}P_{2k}(\cos\varphi),\qquad g_2=h\sum_{k=0}^{n}G_{2k}P_{2k}(\cos\varphi) \tag{2.25}$$

Where C_{2k}, D_{2k} and G_{2k} are some undetermined coefficients. Accordingly, with the use of Eqs. (2.17) and (2.19), the first Laplacian of w_2, f_2 and g_2 gives

$$\begin{aligned}\nabla^2 w_2&=-h\sum_{k=0}^{n}\frac{-2k(2k+1)}{R^2}C_{2k}P_{2k}(\cos\varphi),\\ \nabla^2 f_2&=h\sum_{k=0}^{n}\frac{-2k(2k+1)}{R^2}D_{2k}P_{2k}(\cos\varphi),\\ \nabla^2 g_2&=h\sum_{k=0}^{n}\frac{-2k(2k+1)}{R^2}G_{2k}P_{2k}(\cos\varphi)\end{aligned} \tag{2.26}$$

Introduction of Eq. (2.24), (2.25) and (2.26) into the first and third equations of (2.23) gives the expressions of D_{2k} and G_{2k} in terms of the unknown C_{2k}. Then substituting the resulting expressions D_{2k} and G_{2k} into (2.25) and combining with (2.22), the auxiliary displacements (u_2,α_2) in terms of the unknown C_{2k} are given by

$$\begin{aligned}u_2&=h\frac{\partial}{\partial\varphi}\left[\sum_{k=0}^{n}\frac{-(1+\mu)C_{2k}+H_{2k}}{2k(2k+1)-(1-\mu)}P_{2k}(\cos\varphi)\right],\\ \alpha_2&=\frac{h}{R}\frac{\partial}{\partial\varphi}\left[\sum_{k=0}^{n}\left(\frac{2k(2k+1)-(1-\mu)}{-2k(2k+1)+(1-\mu)-\dfrac{G^*}{G}\left(\dfrac{R}{h}\right)^2\left(\dfrac{h}{h_0}\right)^3 6(1-\mu)k_s}+1\right)C_{2k}P_{2k}(\cos\varphi)\right]\end{aligned} \tag{2.27}$$

Now we consider the orthogonality condition, expressed by the equation (Koiter, 1969; Reddy, 2002)

$$\int_0^{\pi}\int_0^{2\pi}\left(\frac{\partial w_1}{\partial \varphi}\right)\left(\frac{\partial w_2}{\partial \varphi}\right)R^2\sin\varphi d\varphi d\theta = 0 \tag{2.28}$$

The orthogonality condition requests that the expansion of w_2 in a series of Legrende functions does not contain any term of degree n. In the case of an odd integer n of the buckling mode, it follows immediately from the expression of w_2 in (2.25) that the orthogonality condition (2.28) is satisfied. On the other hand, for an even integer n, this orthogonality condition requires $C_{2k} = 0$ for $k = n/2$ or $C_n = 0$. Therefore, a unified form of these two cases is given by, instead of (2.25) and (2.27)

$$\begin{aligned} w_2 &= -h\sum_{k=0}^{n}{}^{*} C_{2k}P_{2k}(\cos\varphi), \\ u_2 &= h\frac{\partial}{\partial\varphi}\left[\sum_{k=0}^{n}{}^{*}\frac{-(1+\mu)C_{2k}+H_{2k}}{2k(2k+1)-(1-\mu)}P_{2k}(\cos\varphi)\right], \\ \alpha_2 &= \frac{h}{R}\frac{\partial}{\partial\varphi}\left[\sum_{k=0}^{n}{}^{*}\left(\frac{2k(2k+1)-(1-\mu)}{-2k(2k+1)+(1-\mu)-\dfrac{G^*}{G}\left(\dfrac{R}{h}\right)^2\left(\dfrac{h}{h_0}\right)^3 6(1-\mu)k_s}+1\right)C_{2k}P_{2k}(\cos\varphi)\right] \end{aligned} \tag{2.29}$$

where the star on the summation sign denotes that the terms $k = n/2$ is omitted if n happens to be even. The expression of w_2 derived here is the same as the expression developed by Koiter (Koiter, 1969). In conclusion, Eq. (2.29) represents the auxiliary displacements (u_2, w_2, α_2) with unknown C_{2k} to be determined by minimizing the energy increment for any fixed value of ξ_0. The determinant of C_{2k} is illustrated in Appendix B.

2.3 Axisymmetric imperfection sensitivity of an imperfect biopolymer spherical shell

Before analyzing the imperfection sensitivity of a pressured imperfect biopolymer spherical shell, it is relevant to examine post-buckling behavior of a pressured perfect biopolymer spherical shell defined by the refined model (Ru, 2009). Based on Koiter's general nonlinear theory of elastic stability (Koiter, 1945,1963) and the procedure developed in his work on post-buckling behavior of a complete spherical shell (Koiter, 1969), with the use of Eq. (2.7) and (2.8), the potential energy for a spherical shell is given by

$$\begin{aligned} P = & \frac{1}{2}\int_0^{\pi}\int_0^{2\pi}(N_{\varphi}e_{\varphi}+N_{\theta}e_{\theta}+M_{\varphi}k_{\varphi}+M_{\theta}k_{\theta}+Q_{\varphi}e_{\varphi z})R^2\sin\varphi d\varphi d\theta \\ & -\frac{1}{2}\int_0^{\pi}\int_0^{2\pi}\left[N_{\varphi 0}\left(\frac{1}{R}\frac{\partial u}{\partial\varphi}+\frac{w}{R}\right)+N_{\theta 0}e_{\theta}\right]R^2\sin\varphi d\varphi d\theta \end{aligned} \tag{2.30}$$

We denote the potential energy of a spherical shell in the pre-buckling equilibrium state I whose stability is to be investigated by P_I. The energy criterion requires a comparison of P_I with the potential energy P_{II} of an arbitrary state II in the neighborhood of the pre-buckling equilibrium state I. The increment in the potential energy of the spherical shell due to the transmission from state I to state II, $P[\hat{u}]=P_{II}-P_I$, is a potential energy functional of the displacement field $\hat{u}$ from the state I to state II. According to the displacements (2.6), the displacement field $\hat{u}$ is $(u-u_0, w-w_0, \alpha-\alpha_0)$. Therefore, the increment in potential energy is obtained as (Danielson, 1974)

$$\begin{aligned} P[\hat{u}] = & \frac{1}{2}\int_0^{\pi}\int_0^{2\pi}\left[N_{\varphi}(e_{\varphi}-e_{\varphi 0})+N_{\theta}(e_{\theta}-e_{\theta 0})+M_{\varphi}k_{\varphi}+M_{\theta}k_{\theta}+Q_{\varphi}e_{\varphi z}\right]R^2\sin\varphi d\varphi d\theta \\ & -\frac{1}{2}\int_0^{\pi}\int_0^{2\pi}\left[N_{\varphi 0}\left(\frac{1}{R}\frac{\partial(u-u_0)}{\partial\varphi}+\frac{(w-w_0)}{R}\right)+N_{\theta 0}(e_{\theta}-e_{\theta 0})\right]R^2\sin\varphi d\varphi d\theta \end{aligned} \tag{2.31}$$

Equations (2.2), (2.6) and (2.7) are then substituted into Eq. (2.31) to give

$$P[\hat{u}] = 2\pi Eh^3 \left\{ \xi_0^{\,2} P_2 \left[(u_1, w_1, \alpha_1); \frac{N_0}{Eh} \right] + \xi_0^{\,3} \left\{ P_3[u_1, w_1, \alpha_1] + P_{11} \left[(u_1, w_1, \alpha_1), (u_2, w_2, \alpha_2); \frac{N_0}{Eh} \right] \right\} \right.$$
$$\left. + \xi_0^{\,4} \left\{ P_4[u_1, w_1, \alpha_1] + P_{21}[(u_1, w_1, \alpha_1), (u_2, w_2, \alpha_2)] + P_2 \left[(u_2, w_2, \alpha_2); \frac{N_0}{Eh} \right] \right\} + \mathrm{O}(\xi_0^{\,5}) \right\} \tag{2.32}$$

where the first order terms are absent because the pre-buckling state I is an equilibrium configuration; see Appendix C.

Therefore, post-buckling behavior of a pressured perfect biopolymer spherical shell defined by the refined model (Ru, 2009) can be described by the potential energy functional (2.32). The analysis of stability of post-buckling behavior and calculation of the potential energy functional (2.32) can be carried out by following the procedure developed in Koiter's work (Koiter, 1969) on post-buckling behavior of a complete spherical shell. In doing so (the detailed derivation and analysis are provided in Appendix B), two conclusions, similar to that given in Koiter's work (Koiter, 1969), can be summarized as: (i) the post-buckling behavior of a pressured prefect spherical shell described by (2.32) is actually unstable, therefore the linearized critical value $\left(\frac{N_0}{Eh} \right)_{cr}$ given by Eq. (2.13) is actually the maximum loading a prefect spherical shell can sustain; and (ii) the third order term of (2.32) is negligible over the initial post-buckling range, which indicates that the potential energy functional (2.32), which describes the post-buckling behavior of a pressured perfect biopolymer spherical shell defined by the refined model (Ru, 2009), can be finally simplified as

$$P[\hat{u}] = 2\pi Eh^3 \left[\xi_0^{\,2} A_2 \left(\frac{N_0}{Eh} \right) + \xi_0^{\,4} A_4 \left(\frac{N_0}{Eh} \right) \right] \tag{2.33}$$

where the expressions of $A_2\left(\frac{N_0}{Eh} \right)$ and $A_4\left(\frac{N_0}{Eh} \right)$ are showed in Appendix B.

2.3.1 Imperfection sensitivity and a verification of the refined model

Based on the above two conclusions for post-buckling behavior of a pressured perfect biopolymer spherical shell defined by the refined model (Ru, 2009), now let us study the imperfection sensitivity of an imperfect biopolymer spherical shell. We shall restrict our investigation to the effect of initial geometric imperfection in the shape of the linear buckling mode. Any types of imperfections can be projected to a function space spanned by the buckling modes, which form an orthogonal basis. The compressed component is negligible in practice (Koiter, 1969). Due to the orthogonality, each component of the imperfection only affects the critical load of the corresponding mode. So the component of the buckling mode, which gives the lowest critical load of perfect spherical shell, lead to the lowest critical load of imperfect spherical load (Hutchinson, 1967). Therefore, we consider a small stress-free initial imperfection described by $\bar{w} = \bar{\xi}_0 w_1$ (see Fig. 2.1), where w_1 is the linear buckling mode defined by $w_1 = -hP_n(\cos\varphi)$ (see Eq. (2.14)) and $\bar{\xi}_0$ is the nondimensional imperfection parameter normalized by the average thickness h (Koiter, 1969). Here, the spherical shell with imperfections is assumed to be initially stress free when no deformation occurs on the original shape. Then the term $\bar{\xi}_0 \frac{\partial w}{R\partial\varphi}\frac{\partial w_1}{R\partial\varphi}$ is added to e_φ and other strain-displacement relations in (2.2) keep unchanged (Budiansky and Hutchinson, 1964)

$$\begin{aligned} e_\varphi &= \frac{1}{R}\frac{\partial u}{\partial\varphi} + \frac{w+\bar{w}}{R} + \frac{1}{2}\left(\frac{\partial\left(w+\bar{w}\right)}{R\partial\varphi}\right)^2 - \left(\frac{\bar{w}}{R} + \frac{1}{2}\left(\frac{\partial\bar{w}}{R\partial\varphi}\right)^2\right) \\ &= \frac{1}{R}\frac{\partial u}{\partial\varphi} + \frac{w}{R} + \frac{1}{2}\left(\frac{\partial w}{R\partial\varphi}\right)^2 + \bar{\xi}_0\frac{\partial w}{R\partial\varphi}\frac{\partial w_1}{R\partial\varphi} \end{aligned} \tag{2.34}$$

The expression (2.7) for membrane forces (N_φ, N_θ) are augmented by terms involving the order $\xi_0\bar{\xi}_0$ and higher; similarly, the term $2\pi Eh^3\xi_0\bar{\xi}_0\int_0^\pi \frac{N_0}{Eh}\left(\frac{\partial w_1}{h\partial\varphi}\right)^2 \sin\varphi d\varphi$ together with others of higher orders than $\xi_0\bar{\xi}_0$ are added to Eq. (2.33). Following Koiter (Koiter, 1945, 1963, 1969), we now limit ourselves to the lowest-order approximation by neglecting all terms of higher orders than $\xi_0\bar{\xi}_0$

$$P[\hat{u}] = 2\pi Eh^3\left[\xi_0^{\,2}A_2\left(\frac{N_0}{Eh}\right)+\xi_0^{\,4}A_4\left(\frac{N_0}{Eh}\right)+\xi_0\bar{\xi}_0A_1\left(\frac{N_0}{Eh}\right)\right] \tag{2.35}$$

where

$$A_1\left(\frac{N_0}{Eh}\right)=\int_0^\pi \frac{N_0}{Eh}\left(\frac{\partial w_1}{h\partial\varphi}\right)^2 \sin\varphi d\varphi = A_{10}\frac{N_0}{Eh} \tag{2.36}$$

where A_{10} can be obtained by introducing the buckling mode (2.14) and using *Mathematica*.

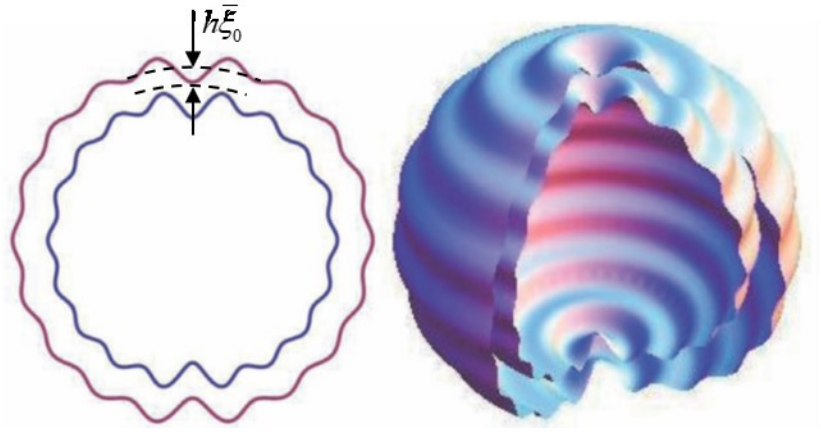

Fig. 2.1 The initial geometric imperfection in the shape of the linear buckling mode (Sato, 2015). Copyright 2015. Reproduced with permission from Cambridge University Press.

Therefore, the equilibrium state of the imperfect biopolymer spherical shell in the neighborhood of the critical bifurcation point is characterized by the stationary value of Eq. (2.35) with respect to the amplitude factor ξ_0, which gives

$$\frac{\partial P[\hat{u}]}{\partial \xi_0} = 2\xi_0 A_2\left(\frac{N_0}{Eh}\right) + 4{\xi_0}^3 A_4\left(\frac{N_0}{Eh}\right) + \bar{\xi}_0 A_1\left(\frac{N_0}{Eh}\right) = 0 \tag{2.37}$$

Since stable equilibrium state of the imperfect shell is defined by a positive second variation of the energy expression (2.35), to determine the maximum value of $\frac{N_0}{Eh}$ an imperfect spherical shell can sustain, we consider the zero of the second variation of the energy expression (2.35)

$$\frac{\partial^2 P[\hat{u}]}{\partial {\xi_0}^2} = 2A_2\left(\frac{N_0}{Eh}\right) + 12{\xi_0}^2 A_4\left(\frac{N_0}{Eh}\right) = 0 \tag{2.38}$$

Eliminating the amplitude factor ξ_0 from Eqs. (2.37) and (2.38), we obtain an equation for the maximum load $\left(\frac{N_0^*}{Eh}\right)_{cr}$ an imperfect spherical shell can sustain, as a function of the imperfection parameter $\bar{\xi}_0$

$$\left[A_2\left(\left(\frac{N_0^*}{Eh}\right)_{cr}\right)\right]^3 + \frac{27}{8}{\bar{\xi}_0}^2 A_4\left(\left(\frac{N_0^*}{Eh}\right)_{cr}\right)\left[A_1\left(\left(\frac{N_0^*}{Eh}\right)_{cr}\right)\right]^2 = 0 \tag{2.39}$$

The diagrammatic sketch of the equilibrium state for perfect and imperfect spherical shells is illustrated in Fig. 2.2. Stable branch is indicated by a solid curve, while unstable branch by a dotted curve.

Therefore, for specific given parameters $k_s, \mu, R/h, G^*/G, h/h_0$, we can get the value of the maximum load $\left(\frac{N_0^*}{Eh}\right)_{cr}$ of an imperfect biopolymer spherical shell determined by the nondimensional imperfection parameter $\bar{\xi}_0$ by Eq. (2.39), and then calculate the so-called "knockdown factor" λ defined by

$$\lambda = \left(\frac{N_0^*}{Eh}\right)_{cr} \Big/ \left(\frac{N_0}{Eh}\right)_{cr} \tag{2.40}$$

where $\left(\frac{N_0}{Eh}\right)_{cr}$ given by Eq. (2.13) is the actual maximum load a prefect shell can sustain. Therefore, the dependence of the knockdown factor λ on the imperfection parameter $\bar{\xi}_0$ can be obtained based on Eqs. (2.13), (2.39) and (2.40).

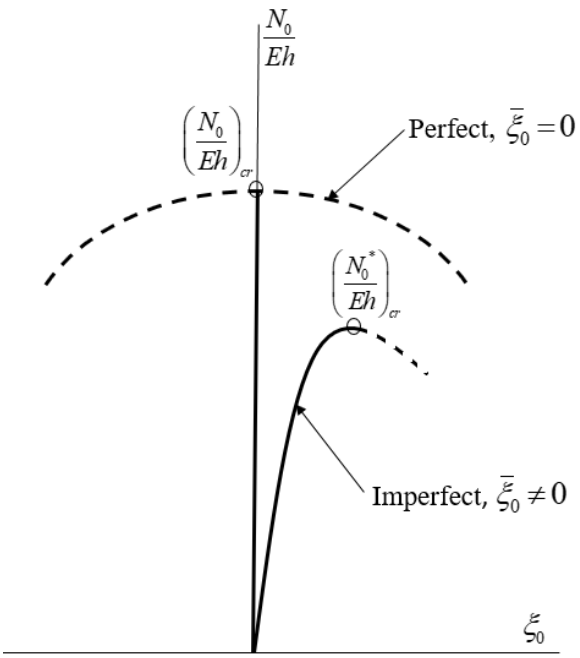

Fig. 2.2 The configuration of equilibrium path for perfect and imperfect spherical shells

To validate the present model and formulation, for example, with $\mu = 0.3$, $k_s = 5/6$, let us examine the classical case which is given by the present refined model with $h_0 = h$ and $G^*/G = \infty$. For the classical case, Koiter's result of imperfection sensitivity for axisymmetric buckling mode is given with the notation used in the present chapter (see Eq. (10.9) in (Koiter, 1969))

$$(1-\lambda)^{\frac{3}{2}}=9\sqrt{\frac{1-\mu}{2n+1}}\lambda\left|\bar{\xi}_0\right|\left[-\frac{1}{8}-\frac{1+3\mu}{2\pi^2}+\frac{1+\mu}{2\pi^2}(1-\lambda)\ln(17-8\lambda)\right.$$
$$\left.+\frac{1+\mu}{\pi^2}\left(\frac{27}{8}-(1-\lambda)^2\right)\frac{1}{\sqrt{1-\lambda^2}}\left(\arctan\frac{4-\lambda}{\sqrt{1-\lambda^2}}+\arctan\frac{\lambda}{\sqrt{1-\lambda^2}}\right)\right]^{\frac{1}{2}} \tag{2.41}$$

where the integer n is determined by

$$2\sqrt{3(1-\mu^2)}\,\frac{R}{h}\approx n(n+1)>>1 \tag{2.42}$$

It is readily seen that our condition (2.15) reduces to (2.42) if $h_0=h$ and $G^*/G=\infty$.

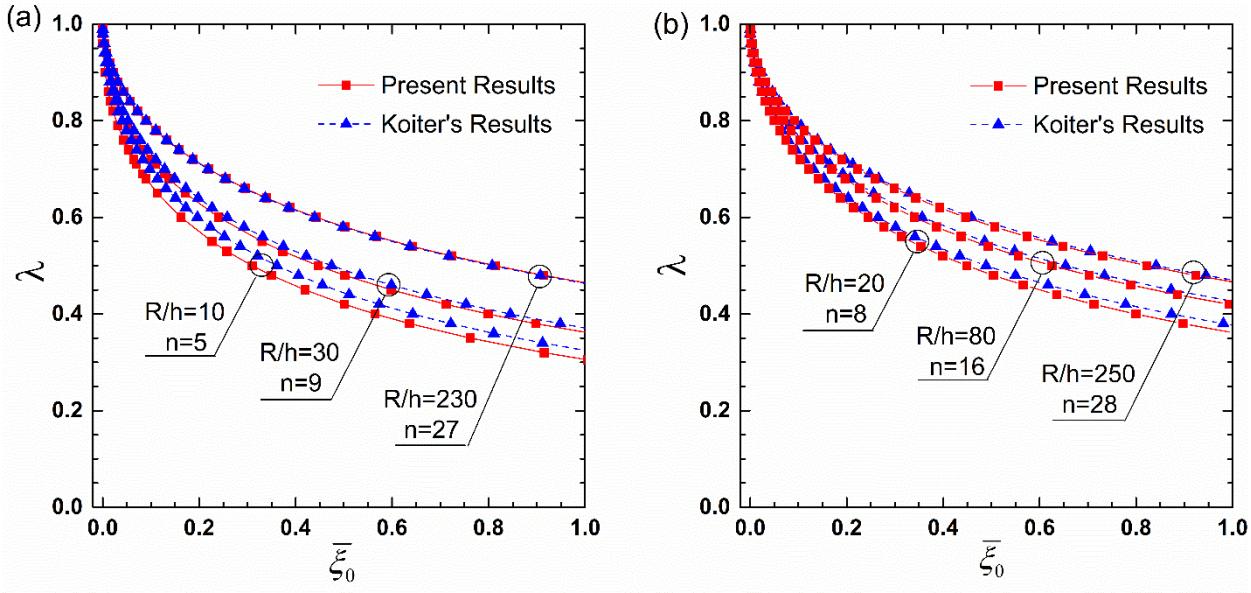

Fig. 2.3 The comparison between Koiter's results and our results with $h_0/h=1$, $G^*/G=\infty$ for different R/h for (a) buckling modes of odd degree and (b) buckling modes of even degree

The comparison of the present results with Koiter's data for the classical case (with $h_0=h$ and $G^*/G=\infty$) is shown in Fig. 2.3 for buckling modes of an even or odd degree n. It is seen from Fig. 2.3 that the results given by the present model are very close to Koiter's ones (Koiter, 1969) and both become even closer when n increase. We can also conclude that our results are more accurate

according to comments in (Koiter, 1969) that there is a relative error of order n^{-1} when calculating the quartic terms $A_4\left(\frac{N_0}{Eh}\right)$. This offers a verification of the present formulations and methods.

2.3.2 The influence of key parameters on imperfection sensitivity

The major goal of this chapter is to examine how the high structural heterogeneity, defined by the key parameters $R/h, G^*/G, h_0/h$ in the present refined shell model, affects the imperfection sensitivity of pressured biopolymer spherical shells. Therefore, let us investigate how the above-mentioned three key parameters influence the imperfection sensitivity with physically realistic imperfections.

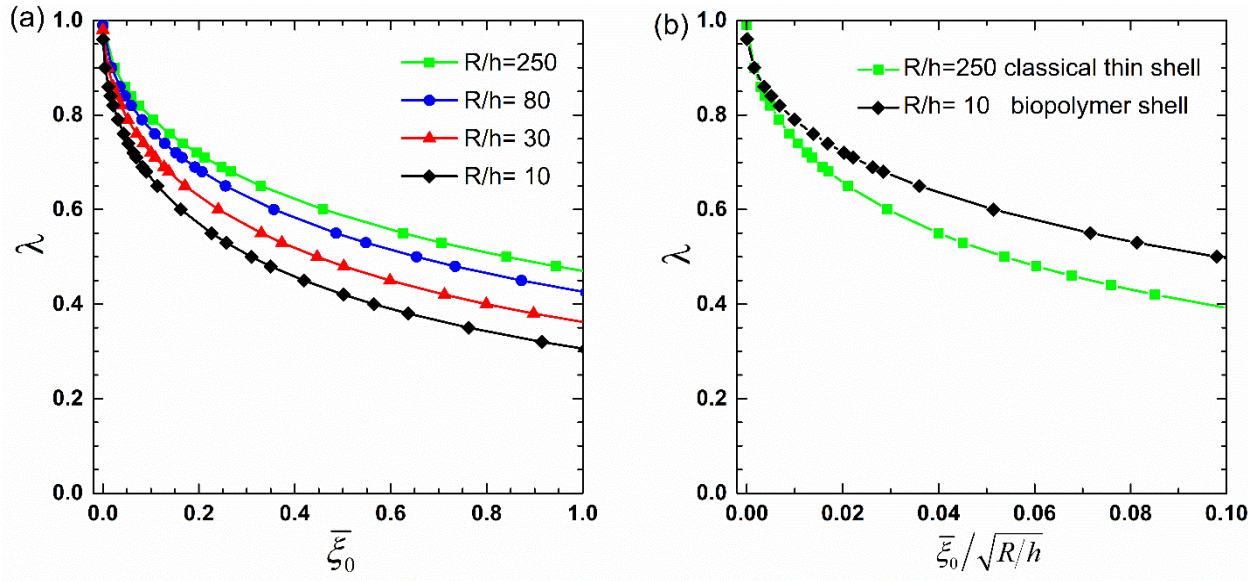

Fig. 2.4 Numerical results with fixed $G^*/G=\infty$ and $h_0/h=1$. (a) The influence of R/h on the imperfection sensitivity and (b) The influence of realistic imperfection on the knockdown factor

We firstly investigate how the parameter R/h influences the imperfection sensitivity and compare the predicted imperfection sensitivity of biopolymer spherical shells with classical elastic thin shells

of much larger R/h. We fix the values $k_s = 5/6$ and $\mu = 0.3$, and the classical case is defined by $h_0/h = 1$, $G^*/G = \infty$ with varying value of R/h. The dependence of the knockdown factor λ given by (2.40) on the imperfection parameter $\bar{\xi}_0$ (normalized by average thickness) is shown in Fig. 2.4(a) for a range of R/h between 10 and 250, which well agrees with Koiter's results (see Fig. 10.1 in (Koiter, 1969)). The physically realistic normalized imperfection parameter $\bar{\xi}_0$ for spherical viruses (see table 2.2) is very low (typically not bigger than 0.23) as compared to the normalized imperfection parameter $\bar{\xi}_0$ of classical elastic thin shells (typically not lower than 1.2-1.5, see e.g. (Koiter, 1969) and Hutchinson, 1960)). For majority of viral capsids having radius between 10 and 50 nm with a thickness of a few nanometers (typically 2-3nm, corresponding to a single protein layer), we find that the parameter R/h has little effect on the imperfection sensitivity. More specifically, let us compare a biopolymer spherical shell of $R/h = 10$ with a classical elastic thin shell of $R/h = 250$, as shown in Fig. 2.4(b). Since realistic imperfection amplitude depends on both radius and thickness, it is reasonable to assume that physically realistic imperfection amplitude scales with $\bar{\xi}_0/\sqrt{R/h}$. Thus, the dependence of the knockdown factor λ on $\bar{\xi}_0/\sqrt{R/h}$ is shown in Fig. 2.4(b) where the horizontal axis is denoted by $\bar{\xi}_0/\sqrt{R/h}$. It is seen from Fig. 2.4(b) that, over the range [0, 0.1] of $\bar{\xi}_0/\sqrt{R/h}$ (which means that the range of the normalized imperfection parameter $\bar{\xi}_0$ is [0, 0.3] for biopolymer shells and [0, 1.5] for the classical elastic thin shells), the biopolymer spherical shell of smaller R/h is actually less-sensitive to physically realistic imperfection as compared to the classical elastic thin shells of much larger R/h, because the realistic normalized imperfection parameter $\bar{\xi}_0$ of biopolymer spherical shells are much smaller than the normalized imperfection parameter $\bar{\xi}_0$ of classical elastic thin shells.

Let us examine the effect of G^*/G on the imperfection sensitivity. Then, we choose $h_0/h=1$ and $R/h=15$, the influence of different G^*/G (within the range (0.07, ∞) defined by the condition (2.18)) on the imperfection sensitivity is illustrated in Fig. 2.5. It is seen from Fig. 2.5 that the knockdown factor λ given by (2.40) remains almost unchanged from $G^*/G=\infty$ to $G^*/G=0.07$. Therefore, it is concluded that the effect of G^*/G on the imperfection sensitivity is negligible when G^*/G varies within a physically realistic range for biopolymer spherical shells.

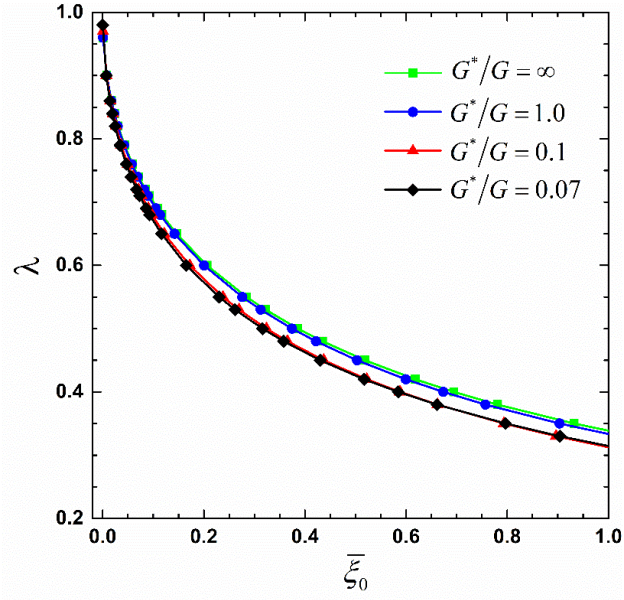

Fig. 2.5 The influence of G^*/G on the imperfection sensitivity with fixed $R/h=15$ and $h_0/h=1$

Lastly, let us examine the effect of h_0/h on the imperfection sensitivity. For this end, let us choose $R/h=15$ and $G^*/G=\infty$, we investigate the imperfection sensitivity for different h_0/h. As shown in Fig. 2.6, with h_0/h decrease from 1.45 to 0.4, the knockdown factor λ decreases substantially, which indicates that the parameter h_0/h has a greater impact on the imperfection sensitivity. Therefore, it is concluded that effective bending thickness has a greater effect on the imperfection sensitivity and therefore the thickness non-uniformity of biopolymer spherical shells could be mainly responsible for the imperfection sensitivity.

From Figs. 2.4, 2.5 and 2.6, we can see the slopes of all curves tend to infinite when the imperfection amplitudes $\bar{\xi}_0$ go to zero, which means that the pressued buckling load is extremely sensitive to vanishingly small imperfections. Here it should be stated that our results shown in Figs. 2.4, 2.5 and 2.6 (the knockdown factor monotonically decreases with increasing amplitude of imperfection) are qualitatively consistent with those of (Lee et al., 2016) (e.g. see their figures 4 and 6), (Hutchinson, 2016) (e.g. see his figure 7) and (Jimenez et al., 2017) (e.g. see their figure 2) for small-amplitude imperfections. Since the present weakly nonlinear initial post-buckling analysis with small-amplitude imperfection/deflection cannot be applied to arbitrarily large imperfections, our results shown in Figs. 2.4, 2.5 and 2.6 cannot be compared to those of Lee et al. (Lee et al., 2016), Hutchinson (Hutchinson, 2016) and Jimenez et al. (Jimenez et al., 2017) for sufficiently large amplitude of imperfections (where it is found that the knockdown factor approaches a constant limit value for sufficiently large amplitude of imperfections).

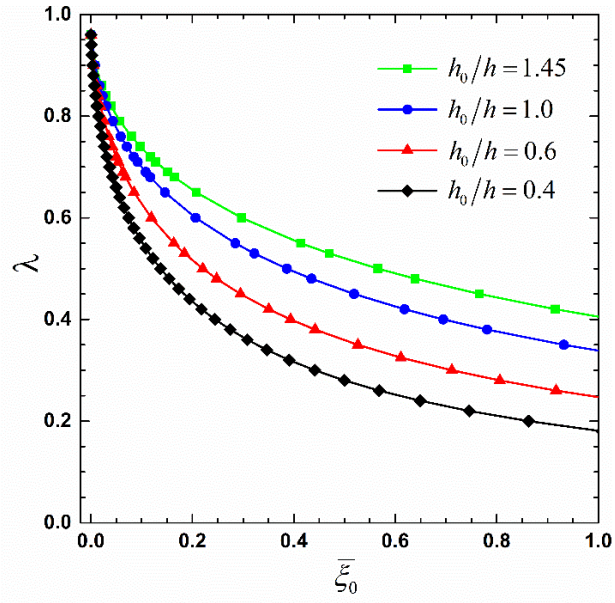

Fig. 2.6 The influence of h_0/h on the imperfection sensitivity with fixed $R/h=15$ and $G^*/G=\infty$

2.3.3 Imperfection sensitivity of specific biopolymer spherical shells

In this section, the combined effect of the three key parameters ($R/h, G^*/G, h_0/h$) on the imperfection sensitivity is studied based on physically realistic parameters of two typical biopolymer spherical shells: UCAs and spherical viruses, with reasonable imperfection amplitude parameter $\bar{\xi}_0$. The actual maximum pressure an imperfect biopolymer spherical shell can sustain will be predicted and compared to the critical pressure of a prefect spherical biopolymer shell.

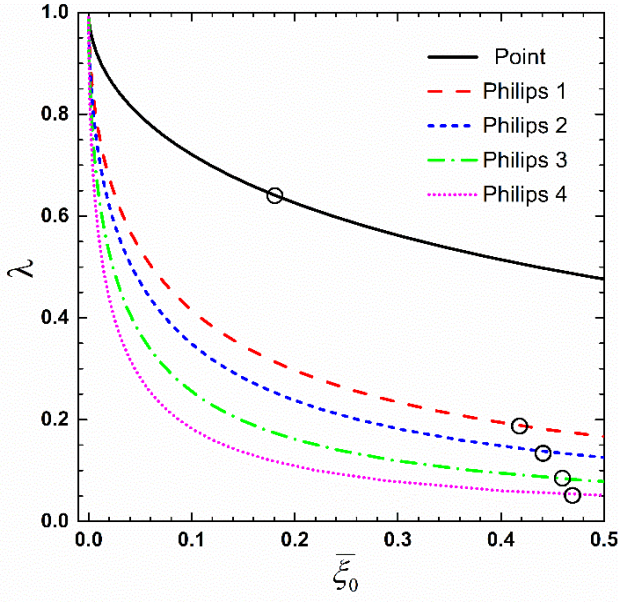

Fig. 2.7 The imperfection sensitivity of polymer-shelled UCAs with the relevant parameters in table 2.1

First, let us examine polymer-shelled UCAs, with the relevant parameters (shown in table 2.1) suggested by Chitnis et al. (Chitnis et al., 2013) for the present refined shell model. Two varieties of polymer-shelled UCAs, named by two manufacturers (Point and Philips), are employed in their study. The effective bending thickness used by Chitnis et al. (Chitnis et al., 2013), obtained by fitting experimental rupture data to the refined model with the shell parameters ($E = 1.35GPa$, $G^* = 0.4G$, $k_s = 5/6$, $\mu = 0.4$) is employed. Figure 2.7 shows the imperfection sensitivity for these two varieties

of UCAs by using these parameters. From Fig. 2.7, it is seen that the actual maximum external pressure keeps not lower than 60% of that of a prefect spherical Point UCAs shell with the reasonable nondimensional amplitude $\bar{\xi}_0 = |h - h_0|/(2h)$ (see the marker in Fig. 2.7). However, for the Philips type, which has much lower value of h_0/h than the Point type, the value of actual maximum load an imperfect shell can sustain can drop to as low as only 5%-20% (see the markers in Fig. 2.7) of the critical loading for a prefect spherical UCAs shell, which suggests that the thickness non-uniformity has the greatest effect on the imperfection sensitivity, and high non-uniformity of shell thickness can make the actual maximum buckling load more sensitive to even minor imperfection and lead to a maximum pressure much lower than that of a prefect spherical shell.

Table 2.1 Relevant parameters for two varieties of polymer-shelled UCAs

UCA type	R(nm)	h(nm)	h_0(nm)	R/h	h_0/h	G^*/G	$\bar{\xi}_0 = \|h - h_0\|/(2h)$
Point	1900	14.5	9.4	130	0.65	0.4	0.18
Philips 1	1000	31.6	4.8	30	0.15	0.4	0.42
Philips 2	1100	40.2	4.7	25	0.12	0.4	0.44
Philips 3	1300	82.2	6.4	15	0.08	0.4	0.46
Philips 4	1200	121.5	6.6	10	0.05	0.4	0.47

Next, we examine the imperfection sensitivity with relevant parameters for some typical spherical viruses. Table 2.2 shows the relevant parameters obtained from (May and Brooks, 2012) for some typical imperfect spherical virus shells which are divided into four groups based on the parameters ($R/h, G^*/G, h_0/h$) and the nondimensional imperfection amplitude $\bar{\xi}_0 = |h - h_0|/(2h)$. In (May and Brooks, 2012), the Foppl-von Kanman number γ, which is a ratio of the two-dimensional Young's modulus Y and the common bending modulus κ, is obtained by calculating Y and κ with a multiscale method developed by (May and Brooks, 2011). Therefore, the effective bending thickness is calculated through Foppl-von Kanman number from the relationship (Landau and Lifshitz,1986)

$$\gamma = \frac{YR^2}{\kappa} = \frac{EhR^2}{\frac{Eh_0^{\,3}}{12(1-\mu^2)}} = 12\left(1-\mu^2\right)\left(\frac{R}{h}\right)^2\left(\frac{h}{h_0}\right)^3 \tag{2.43}$$

The results shown in Fig. 2.8 are obtained based on the data in table 2.2. From Fig. 2.8, it is concluded that with the relevant parameters for some typical spherical virus shells, the maximum pressure of an imperfect spherical virus shell could reduce to 55-65% (see the markers in Fig. 2.8) of the maximum pressure for a perfect spherical virus shell with the ratio R/h ranging from 3 to 6, h_0/h ranging from 1.15 to 1.45, and the nondimensional imperfection amplitude $\bar{\xi}_0$ ranging from 0.07 to 0.23. As stated above, the ratio G^*/G, whose range is limited by the condition (2.18), has negligible effect on the imperfection sensitivity when it varies within a physically realistic range.

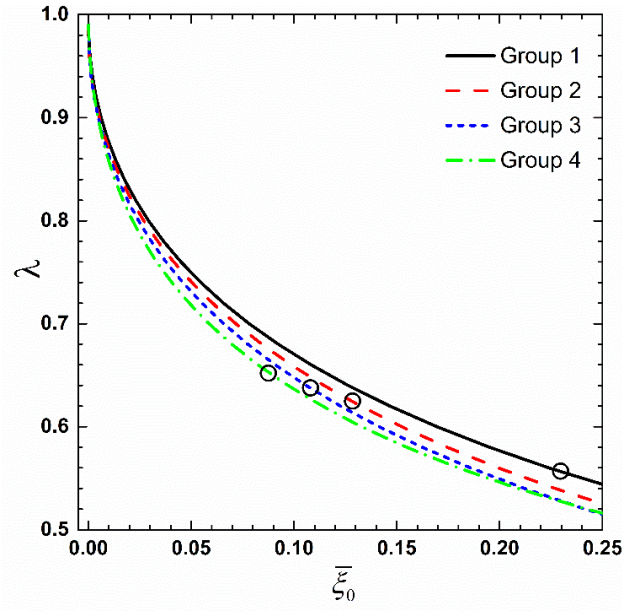

Fig. 2.8 The imperfection sensitivity of spherical virus shells with the relevant parameters in table 2.2

Table 2.2 Relevant parameters for some typical spherical viruses

Group	Virus	R(nm)	h(nm)	h_0(nm)	R/h	h_0/h	G^*/G	$\bar{\xi}_0 = \lvert h - h_0 \rvert/(2h)$
1	cowpea chlorotic mottle virus	11.8	2.9	4.2	4	1.45	0.5	0.23
	turnip yellow mosaic virus	12.7	2.6	3.6	5	1.38	0.5	0.20
2	tobacco necrosis virus	12.9	2.5	3.1	5	1.25	0.5	0.12
	cocksfoot mottle virus	13.0	2.7	3.4	5	1.26	0.5	0.13
	sesbania mosaic virus	13.0	2.6	3.1	5	1.20	0.5	0.10
	southern bean mosiac virus	13.1	2.7	3.3	5	1.22	0.5	0.11
	VLP	16.2	2.6	3.1	6	1.20	0.5	0.10
3	flockhouse virus	13.7	4.3	5.2	3	1.21	0.5	0.11
	simian virus 40	21.2	5.3	6.7	4	1.26	0.5	0.13
4	bovine papilloma virus	24.5	6.3	7.4	4	1.17	0.5	0.09
	norwalk virus	15.8	6.2	7.1	3	1.15	0.5	0.07

2.4 Conclusions

Imperfection sensitivity of pressured buckling of structurally heterogeneous biopolymer spherical shells is analyzed based on a recently developed refined elastic shell model. The formulas and solution procedure used in this chapter are validated by comparing the predicted results with the known classical data when the structural heterogeneity vanish and thus the present refined model reduces to the classical shell model. For structurally heterogeneous biopolymer spherical shells, the present analysis predicts that the effective bending thickness could be mainly responsible for the imperfection sensitivity of imperfect biopolymer spherical shells, although the effect of transvers shear

modulus is usually negligible. Based on physically relevant data available in literature for polymer-shelled UCAs and spherical viruses, the present model predicts that actual maximum external pressure could be reduced to 60% of that of a prefect UCA shell or to 55-65% of that of a prefect spherical virus shell, respectively. A major conclusion of the present chapter is that, because biopolymer shells are relatively thicker (defined by smaller radius-to-thickness ratio, e.g. 3-6 for spherical viruses and 10-130 for polymer-shelled UCAs) and the realistic imperfection amplitude normalized by thickness is relatively low, typical biopolymer spherical shells are only moderately sensitive to geometrical imperfections, as compared to classical elastic thin shells of much thinner thickness (defined by much larger radius-to-thickness ratio, say >>100) which can be extremely sensitive to geometrical imperfections.

Chapter 3: Non-axisymmetric imperfection sensitivity on pressured buckling of a biopolymer spherical shell

3.1 Introduction

The aim of this chapter is to study the imperfection sensitivity of pressured biopolymer spherical shells based on non-axisymmetric buckling modes and the associated mode interaction. The methods for imperfection sensitivity of classical elastic spherical shells developed in previous seminal works, e.g. by Hutchinson (Hutchinson, 1967), Koiter (Koiter, 1945, 1963, 1969) and Budiansky and Hutchinson (Budiansky and Hutchinson, 1964), will be employed. In section 3.2, the refined shell model formulated in (Ru, 2009) originally for linearized axisymmetric buckling is further developed to study initial post-buckling of a biopolymer spherical shell with non-axisymmetric buckling modes and the mode interaction. In section 3.3, the developed formulation is used to study the non-axisymmetric imperfection sensitivity, and the results are compared to the results obtained in chapter 2 based on axisymmetric assumption with an emphasis on the influence of key parameters on the non-axisymmetric imperfection sensitivity. Furthermore, the non-axisymmetric imperfection sensitivity is detailed in section 3.4 for two specific types of biopolymer spherical shells (ultrasound contrasts agents UCAs and spherical viruses). Finally, main conclusions are summarized in section 3.5.

3.2 Post-buckling of a biopolymer spherical shell with the mode interaction

In this section, weakly-nonlinear, non-axisymmetric initial post-buckling of a biopolymer spherical shell is studied based on the refined elastic spherical shell model proposed in (Ru, 2009) initially for linearized axisymmetric buckling of biopolymer spherical shells without mode interaction.

Spherical coordinates φ ($0 \le \varphi \le \pi$), θ ($0 \le \theta \le 2\pi$) and z ($-h/2 \le z \le h/2$) are used to describe a biopolymer spherical shell of middle surface radius R and average shell thickness h, where the radial coordinate z, whose sign is taken positive outward, indicates the distance of a point in the shell to the middle surface. Based on Sanders' nonlinear kinematic relations (Sanders,1963) and the shear deformation theory of Reddy and Liu (Reddy and Liu, 1985), for non-axisymmetric large-deflection post-buckling of an elastic spherical shell, the non-linear mid-face strains (including 2 transverse shear strains $e_{\theta z}$, $e_{\varphi z}$ and the change in curvatures k_φ, k_θ and $k_{\varphi\theta}$) of a spherical shell are given in terms of the displacements of the middle surface u, v, w and the rotations α, β of the normal of the middle surface in φ, θ directions by

$$
\begin{aligned}
e_\varphi &= \frac{1}{R}\frac{\partial u}{\partial \varphi} + \frac{w}{R} + \frac{1}{2}\left(\frac{\partial w}{R\partial \varphi}\right)^2, \quad e_\theta = \frac{u}{R}\cot\varphi + \frac{1}{R\sin\varphi}\frac{\partial v}{\partial \theta} + \frac{w}{R} + \frac{1}{2}\left(\frac{\partial w}{R\sin\varphi\partial \theta}\right)^2, \\
e_{\varphi\theta} &= \frac{1}{R\sin\varphi}\frac{\partial u}{\partial \theta} + \frac{1}{R}\frac{\partial v}{\partial \varphi} - \frac{v}{R}\cot\varphi + \left(\frac{\partial w}{R\partial \varphi}\right)\left(\frac{\partial w}{R\sin\varphi\partial \theta}\right), \\
e_{\varphi z} &= \frac{1}{R}\frac{\partial w}{\partial \varphi} + \alpha, \quad e_{\theta z} = \frac{1}{R\sin\varphi}\frac{\partial w}{\partial \theta} + \beta, \quad k_\varphi = \frac{1}{R}\frac{\partial \alpha}{\partial \varphi}, \quad k_\theta = \frac{\alpha}{R}\cot\varphi + \frac{1}{R\sin\varphi}\frac{\partial \beta}{\partial \theta}, \\
k_{\varphi\theta} &= \frac{1}{R\sin\varphi}\frac{\partial \alpha}{\partial \theta} + \frac{1}{R}\frac{\partial \beta}{\partial \varphi} - \frac{\beta}{R}\cot\varphi.
\end{aligned}
\tag{3.1}
$$

Based on the isotropic linear plane-stress stress-strain relation, the in-plane resultant membrane forces, bending moments and transverse shear forces are given by (Ru, 2009)

$$
\begin{aligned}
&\begin{bmatrix} N_\varphi \\ N_\theta \end{bmatrix} = \frac{Eh}{1-\mu^2}\begin{bmatrix} 1 & \mu \\ \mu & 1 \end{bmatrix}\begin{bmatrix} e_\varphi \\ e_\theta \end{bmatrix}, \quad N_{\varphi\theta} = Ghe_{\varphi\theta}, \\
&\begin{bmatrix} M_\varphi \\ M_\theta \end{bmatrix} = D\begin{bmatrix} 1 & \mu \\ \mu & 1 \end{bmatrix}\begin{bmatrix} \kappa_\varphi \\ \kappa_\theta \end{bmatrix}, \quad M_{\varphi\theta} = D_{12}\kappa_{\varphi\theta}, \\
&Q_\varphi = k_s G^* h e_{\varphi z}, \quad Q_\theta = k_s G^* h e_{\theta z},
\end{aligned}
\tag{3.2}
$$

where E is Young's modulus, μ is Poisson's ratio of the biopolymer shell, k_s is the shear coefficient (e.g. 5/6 in (Kraus, 1967)), G^* is the transverse shear modulus, G is the common in-plane shear modulus determined by (E, μ), and the bending stiffnesses of a biopolymer spherical shell are assumed to be determined by an effective bending thickness h_0 as

$$D = \frac{Eh_0^3}{12\left(1-\mu^2\right)}, \qquad D_{12} = \frac{Gh_0^3}{12}. \tag{3.3}$$

For a specific isotropic biopolymer shell, the average thickness h can be defined based on its non-uniform geometrical thickness, and then the Young's modulus can be defined based on its actual in-plane elastic modulus. Furthermore, the effective bending thickness h_0 can be calculated by the Young's modulus and its actual bending rigidity measured from experiments or calculated from micro/molecular simulations, as seen Eq. (2.43) and in (May and Brooks, 2011). Thus, with the present refined model, bending behavior of a biopolymer shell of high structural heterogeneity can be modeled with the single parameter h_0. For biopolymer spherical shells, it is assumed that the transverse shear modulus G^* could be different, or even much lower, than the in-plane shear modulus G. Also, the effective bending thickness h_0 can be considerably different from the average shell thickness h (Ru, 2009). It is the two additional parameters (G^*, h_0) which distinguish a biopolymer shell of high structural heterogeneity and thickness non-uniformity from a classical elastic shell defined by (E, μ, h).

The nonlinear deformation field of the spherical shell in initial post-buckled state is written as (Budiansky and Hutchinson, 1964; Hutchinson, 1967)

$$
\begin{aligned}
u &= u_0 + u_1^* + u_2^* + \ldots, \\
v &= v_0 + v_1^* + v_2^* + \ldots, \\
w &= w_0 + w_1^* + w_2^* + \ldots, \\
\alpha &= \alpha_0 + \alpha_1^* + \alpha_2^* + \ldots, \\
\beta &= \beta_0 + \beta_1^* + \beta_2^* + \ldots,
\end{aligned}
\tag{3.4}
$$

where the displacements ($u_0, v_0, w_0, \alpha_0, \beta_0$) are pre-buckling deformations prior to buckling. For a prefect spherical shell under a uniform applied external pressure q, this is just a uniform radial displacement ($u_0 = v_0 = \alpha_0 = \beta_0 = 0, w_0 = -(1-\mu)qR^2/(2Eh)$). Here, ($u_1^*, v_1^*, w_1^*, \alpha_1^*, \beta_1^*$) are the deviations from the pre-buckling state expanded in the linear buckling modes, ($u_2^*, v_2^*, w_2^*, \alpha_2^*, \beta_2^*$) are the deviations expanded in the second-order buckling modes which are orthogonal to ($u_1^*, v_1^*, w_1^*, \alpha_1^*, \beta_1^*$) (defined by $\int_0^{2\pi}\int_0^{\pi}\left(\frac{\partial w_1^*}{\partial \varphi}\right)\left(\frac{\partial w_2^*}{\partial \varphi}\right)R^2 \sin\varphi d\varphi d\theta = 0$), and the omitted terms in the present initial post-buckling analysis are higher-order mode terms which are orthogonal to both ($u_1^*, v_1^*, w_1^*, \alpha_1^*, \beta_1^*$) and ($u_2^*, v_2^*, w_2^*, \alpha_2^*, \beta_2^*$).

Substituting the displacements (3.4) into the midface strains (3.1) and then into Eq. (3.2), and considering that the spherical shell under uniform external pressure q prior to buckling is in a uniform membrane state of stress ($N_{\varphi 0} = N_{\theta 0} = N_0 - qR/2$), the in-plane resultant membrane forces, bending moments, and transverse shear forces have the expansions (Budiansky and Hutchinson, 1964; Hutchinson, 1967)

$$\begin{bmatrix} N_\varphi \\ N_\theta \\ N_{\varphi\theta} \\ M_\varphi \\ M_\theta \\ M_{\varphi\theta} \\ Q_\varphi \\ Q_\theta \end{bmatrix} = \begin{bmatrix} N_{\varphi 0} \\ N_{\theta 0} \\ 0 \\ 0 \\ 0 \\ 0 \\ 0 \\ 0 \end{bmatrix} + \begin{bmatrix} N^*_{\varphi 1} \\ N^*_{\theta 1} \\ N^*_{\varphi\theta 1} \\ M^*_{\varphi 1} \\ M^*_{\theta 1} \\ M^*_{\varphi\theta 1} \\ Q^*_{\varphi 1} \\ Q^*_{\theta 1} \end{bmatrix} + \begin{bmatrix} N^*_{\varphi 2} + \frac{1}{2}\frac{Eh}{1-\mu^2}\left(\left(\frac{\partial w^*_1}{R\partial\varphi}\right)^2 + \mu\left(\frac{\partial w^*_1}{R\sin\varphi\partial\theta}\right)^2\right) \\ N^*_{\theta 2} + \frac{1}{2}\frac{Eh}{1-\mu^2}\left(\mu\left(\frac{\partial w^*_1}{R\partial\varphi}\right)^2 + \left(\frac{\partial w^*_1}{R\sin\varphi\partial\theta}\right)^2\right) \\ N^*_{\varphi\theta 2} + Gh\left(\frac{\partial w^*_1}{R\partial\varphi}\right)\left(\frac{\partial w^*_1}{R\sin\varphi\partial\theta}\right) \\ M^*_{\varphi 2} \\ M^*_{\theta 2} \\ M^*_{\varphi\theta 2} \\ Q^*_{\varphi 2} \\ Q^*_{\theta 2} \end{bmatrix} + \ldots, \tag{3.5}$$

where $N^*_{\varphi i}$, $N^*_{\theta i}$, $N^*_{\varphi\theta i}$, $M^*_{\varphi i}$, $M^*_{\theta i}$, $M^*_{\varphi\theta i}$, $Q^*_{\varphi i}$ and $Q^*_{\theta i}$ $(i = 1, 2)$ represent forces and moments with linear strains.

The potential energy criterion can be applied to analyze the buckling and post-buckling behavior of spherical shells. The potential energy for a biopolymer spherical shell can be given by (Hutchinson, 1967; Kraus, 1967)

$$\begin{aligned} P = {} & \frac{1}{2}\int_0^\pi\int_0^{2\pi}(N_\varphi e_\varphi + N_\theta e_\theta + N_{\varphi\theta}e_{\varphi\theta} + M_\varphi k_\varphi + M_\theta k_\theta + M_{\varphi\theta}k_{\varphi\theta} + Q_\varphi e_{\varphi z} + Q_\theta e_{\theta z})R^2\sin\varphi d\varphi d\theta \\ & -\frac{1}{2}\int_0^\pi\int_0^{2\pi}\left[N_{\varphi 0}\left(\frac{1}{R}\frac{\partial u}{\partial\varphi} + \frac{w}{R}\right) + N_{\theta 0}\left(\frac{u}{R}\cot\varphi + \frac{1}{R\sin\varphi}\frac{\partial v}{\partial\theta} + \frac{w}{R}\right)\right]R^2\sin\varphi d\varphi d\theta \end{aligned} \tag{3.6}$$

where the first integral on the right side of Eq. (3.6) is the strain energy, and the second integral is the energy of the applied pre-buckling membrane forces, and $\left(\frac{1}{R}\frac{\partial u}{\partial\varphi} + \frac{w}{R}\right)$ and $\left(\frac{u}{R}\cot\varphi + \frac{1}{R\sin\varphi}\frac{\partial v}{\partial\theta} + \frac{w}{R}\right)$ are the linear parts of e_φ and e_θ respectively, because the pre-buckling state is described by linear membrane theory.

3.2.1 Non-axisymmetric buckling and post-buckling modes

First, let us carry out the linearized buckling analysis. Unlike Ru (Ru, 2009) and Zhang and Ru (Zhang and Ru, 2016) (i.e. chapter 2) which were limited to axisymmetric buckling (with $v=\beta=0$ and $\partial(\ )/\partial\theta=0$), we are now dealing with non-axisymmetric deformation of a spherical shell. With the use of Eq. (3.6), the equilibrium equations of a spherical shell can be derived from the variational principle on the basis of the potential energy criterion (Hutchinson, 1967)

$$\begin{aligned}&\frac{1}{2}\int_0^{\pi}\int_0^{2\pi}(N_{\varphi}\delta e_{\varphi}+N_{\theta}\delta e_{\theta}+N_{\varphi\theta}\delta e_{\varphi\theta}+M_{\varphi}\delta k_{\varphi}+M_{\theta}\delta k_{\theta}+M_{\varphi\theta}\delta k_{\varphi\theta}+Q_{\varphi}\delta e_{\varphi z}+Q_{\theta}\delta e_{\theta z})\\&R^2\sin\varphi d\varphi d\theta=\frac{1}{2}\int_0^{\pi}\int_0^{2\pi}\left[N_{\varphi 0}\delta\left(\frac{1}{R}\frac{\partial u}{\partial\varphi}+\frac{w}{R}\right)+N_{\theta 0}\delta\left(\frac{u}{R}\cot\varphi+\frac{1}{R\sin\varphi}\frac{\partial v}{\partial\theta}+\frac{w}{R}\right)\right]R^2\sin\varphi d\varphi d\theta.\end{aligned}\tag{3.7}$$

The mid-face strains (3.1), the displacement w given in (3.4) and the expansions (3.5) are then substituted into Eq. (3.7), which gives, on using the integration by parts and collecting the coefficients of $\delta u,\delta v,\delta w,\delta\alpha$ and $\delta\beta$ separately (Hutchinson, 1967) (all boundary terms vanish owing to the continuity of all displacements in a closed spherical shell (Zhang and Ru, 2016)).

$$
\begin{aligned}
0=\Bigg\{\int_0^{\pi}\int_0^{2\pi}\Bigg[&\left(-\frac{\partial}{\partial\varphi}(N^*_{\varphi 1}R\sin\varphi)+N^*_{\theta 1}R\cos\varphi-\frac{\partial}{\partial\theta}(N^*_{\varphi\theta 1}R)\right)\delta u+\left(-\frac{\partial}{\partial\varphi}(N^*_{\varphi\theta 1}R\sin\varphi)-N^*_{\varphi\theta 1}R\cos\varphi-\frac{\partial}{\partial\theta}(N^*_{\theta 1}R)\right)\delta v\\
&+\left(-\frac{\partial}{\partial\varphi}(N_{\varphi 0}\sin\varphi\frac{\partial w_1^*}{\partial\varphi})-\frac{\partial}{\partial\theta}(\frac{N_{\theta 0}}{\sin\varphi}\frac{\partial w_1^*}{\partial\theta})+N^*_{\varphi 1}R\sin\varphi+N^*_{\theta 1}R\sin\varphi-\frac{\partial}{\partial\varphi}(Q^*_{\varphi 1}R\sin\varphi)-\frac{\partial}{\partial\theta}(Q^*_{\theta 1}R)\right)\delta w\\
&+\left(-\frac{\partial}{\partial\varphi}(M^*_{\varphi 1}R\sin\varphi)+M^*_{\theta 1}R\cos\varphi-\frac{\partial}{\partial\theta}(M^*_{\varphi\theta 1}R)+Q^*_{\varphi 1}R^2\sin\varphi\right)\delta\alpha\\
&+\left(-\frac{\partial}{\partial\varphi}(M^*_{\varphi\theta 1}R\sin\varphi)-\frac{\partial}{\partial\theta}(M^*_{\theta 1}R)-M^*_{\varphi\theta 1}R\cos\varphi+Q^*_{\theta 1}R^2\sin\varphi\right)\delta\beta\Bigg]d\varphi d\theta\Bigg\}\\
+\Bigg\{\int_0^{\pi}\int_0^{2\pi}\Bigg[&\left(-\frac{\partial}{\partial\varphi}(N^*_{\varphi 2}R\sin\varphi)+N^*_{\theta 2}R\cos\varphi-\frac{\partial}{\partial\theta}(N^*_{\varphi\theta 2}R)+\frac{Eh}{2R(1-\mu^2)}\left(-\frac{\partial}{\partial\varphi}\left(\sin\varphi\left(\frac{\partial w_1^*}{\partial\varphi}\right)^2+\mu\sin\varphi\left(\frac{\partial w_1^*}{\sin\varphi\partial\theta}\right)^2\right)\right.\right.\\
&\left.-(1-\mu)\frac{\partial}{\partial\theta}\left(\left(\frac{\partial w_1^*}{\partial\varphi}\right)\left(\frac{\partial w_1^*}{\sin\varphi\partial\theta}\right)\right)+\mu\left(\frac{\partial w_1^*}{\partial\varphi}\right)^2\cos\varphi+\left(\frac{\partial w_1^*}{\sin\varphi\partial\theta}\right)^2\cos\varphi\right)\Bigg)\delta u\\
&+\left(-\frac{\partial}{\partial\varphi}(N^*_{\varphi\theta 2}R\sin\varphi)-N^*_{\varphi\theta 2}R\cos\varphi-\frac{\partial}{\partial\theta}(N^*_{\theta 2}R)+\frac{Eh\sin\varphi}{2R(1-\mu^2)}\left(-\frac{\partial}{\partial\theta}\left(\mu\left(\frac{\partial w_1^*}{\partial\varphi}\right)^2+\left(\frac{\partial w_1^*}{\sin\varphi\partial\theta}\right)^2\right)\right.\right.\\
&\left.\left.-\frac{\partial}{\partial\varphi}\left((1-\mu)\sin\varphi\left(\frac{\partial w_1^*}{\partial\varphi}\right)\left(\frac{\partial w_1^*}{\sin\varphi\partial\theta}\right)\right)-(1-\mu)\left(\frac{\partial w_1^*}{\partial\varphi}\right)\left(\frac{\partial w_1^*}{\sin\varphi\partial\theta}\right)\cos\varphi\right)\right)\delta v\\
&+\left(N^*_{\varphi 2}R\sin\varphi+N^*_{\theta 2}R\sin\varphi-\frac{\partial}{\partial\varphi}(Q^*_{\varphi 2}R\sin\varphi)-\frac{\partial}{\partial\theta}(Q^*_{\theta 2}R)+N_{\varphi 0}\left(-\frac{\partial}{\partial\varphi}\left(\sin\varphi\frac{\partial w_2^*}{\partial\varphi}\right)\right)\right.\\
&\left.+N_{\theta 0}\left(-\frac{\partial}{\partial\theta}\left(\frac{1}{\sin\varphi}\frac{\partial w_2^*}{\partial\theta}\right)\right)-\frac{\partial}{\partial\varphi}\left(N^*_{\varphi 1}\sin\varphi\frac{\partial w_1^*}{\partial\varphi}+N^*_{\varphi\theta 1}\frac{\partial w_1^*}{\partial\theta}\right)-\frac{\partial}{\partial\theta}\left(N^*_{\theta 1}\frac{1}{\sin\varphi}\frac{\partial w_1^*}{\partial\theta}+N^*_{\varphi\theta 1}\frac{\partial w_1^*}{\partial\varphi}\right)\right.\\
&\left.+\frac{Eh}{2R(1-\mu)}\left(\left(\frac{\partial w_1^*}{\partial\varphi}\right)^2\sin\varphi+\left(\frac{\partial w_1^*}{\sin\varphi\partial\theta}\right)^2\sin\varphi\right)\right)\delta w\\
&+\left(-\frac{\partial}{\partial\varphi}(M^*_{\varphi 2}R\sin\varphi)+M^*_{\theta 2}R\cos\varphi-\frac{\partial}{\partial\theta}(M^*_{\varphi\theta 2}R)+Q^*_{\varphi 2}R^2\sin\varphi\right)\delta\alpha\\
&+\left(-\frac{\partial}{\partial\varphi}(M^*_{\varphi\theta 2}R\sin\varphi)-\frac{\partial}{\partial\theta}(M^*_{\theta 2}R)-M^*_{\varphi\theta 2}R\cos\varphi+Q^*_{\theta 2}R^2\sin\varphi\right)\delta\beta\Bigg]d\varphi d\theta\Bigg\}\\
&+\ldots
\end{aligned}
\tag{3.8}
$$

where $N_{\varphi 0}=N_{\theta 0}=N_0$, the first brace on the right side of Eq. (3.8) contains all linear buckling modes and the second brace contains all second-order buckling modes. For the linearized buckling analysis, only the linear buckling modes in the first brace are retained. Since δu, δv, δw, $\delta\alpha$ and $\delta\beta$ are arbitrary and independent, we have the Euler equations (equilibrium equations) for five unknowns

$u_1^*, v_1^*, w_1^*, \alpha_1^*, \beta_1^*$, which are valid for linear non-axisymmetric buckling of biopolymer spherical shells (Hutchinson, 1967; Kraus, 1967)

$$\begin{gathered}
\frac{\partial N_{\varphi 1}^*}{\partial \varphi}+\frac{1}{\sin \varphi} \frac{\partial N_{\varphi \theta 1}^*}{\partial \theta}+\left(N_{\varphi 1}^*-N_{\theta 1}^*\right) \frac{\cos \varphi}{\sin \varphi}=0, \\
\frac{\partial N_{\varphi \theta 1}^*}{\partial \varphi}+\frac{1}{\sin \varphi} \frac{\partial N_{\theta 1}^*}{\partial \theta}+2 N_{\varphi \theta 1}^* \frac{\cos \varphi}{\sin \varphi}=0, \\
\frac{\partial Q_{\varphi 1}^*}{\partial \varphi}+\frac{1}{\sin \varphi} \frac{\partial Q_{\theta 1}^*}{\partial \theta}+Q_{\varphi 1}^* \frac{\cos \varphi}{\sin \varphi}-\left(N_{\varphi 1}^*+N_{\theta 1}^*\right)+N_0 R \nabla^2 w_1^*=0, \\
R Q_{\varphi 1}^*=\frac{\partial M_{\varphi 1}^*}{\partial \varphi}+\frac{1}{\sin \varphi} \frac{\partial M_{\varphi \theta 1}^*}{\partial \theta}+\left(M_{\varphi 1}^*-M_{\theta 1}^*\right) \frac{\cos \varphi}{\sin \varphi}, \\
R Q_{\theta 1}^*=\frac{\partial M_{\varphi \theta 1}^*}{\partial \varphi}+\frac{1}{\sin \varphi} \frac{\partial M_{\theta 1}^*}{\partial \theta}+2 M_{\varphi \theta 1}^* \frac{\cos \varphi}{\sin \varphi}.
\end{gathered} \tag{3.9}$$

In a similar way as Prasad (Prasad, 1964), let us define u_1^*, v_1^* and $Q_{\varphi 1}^*, Q_{\theta 1}^*$ in terms of two new functions $f_1^*(\varphi, \theta)$ and $g_1^*(\varphi, \theta)$ as

$$\begin{gathered}
u_1^*=\frac{\partial f_1^*}{\partial \varphi}, \quad v_1^*=\frac{\partial f_1^*}{\partial \theta} \csc \varphi, \\
Q_{\varphi 1}^*=\frac{\partial g_1^*}{\partial \varphi}, \quad Q_{\theta 1}^*=\frac{\partial g_1^*}{\partial \theta} \csc \varphi,
\end{gathered} \tag{3.10}$$

and then substituting Eq. (3.10) into Eq. (3.9), the five equilibrium equations will reduce to three equations for (f_1^*, w_1^*, g_1^*), which is valid for linear non-axisymmetric buckling of biopolymer spherical shells

$$\begin{gathered}
\left[R^2 \nabla^2+(1-\mu)\right] f_1^*+(1+\mu) w_1^*=0, \\
R \nabla^2 g_1^*-\frac{E h}{1-\mu}\left(\nabla^2 f_1^*+\frac{2 w_1^*}{R^2}\right)+N_0 \nabla^2 w_1^*=0, \\
\left(R \nabla^2+\frac{1-\mu}{R}-\frac{R}{D} k_s G^* h\right) g_1^*-\left(k_s G^* h \nabla^2+k_s G^* h \frac{1-\mu}{R^2}\right) w_1^*=0.
\end{gathered} \tag{3.11}$$

Following the procedure given in (Ru, 2009) for axisymmetric case, eliminating f_1^* and g_1^* in (3.11) leads to a decoupled equation for w_1^* for non-axisymmetric case as follows

$$\begin{aligned}
&R\left[R^2\nabla^2+(1-\mu)\right]\left[k_sG^*h\nabla^4w_1^*+k_sG^*h\frac{(1-\mu)}{R^2}\nabla^2w_1^*\right]\\
&+\frac{Eh}{1-\mu}\left\{R\nabla^2+\left[\frac{(1-\mu)}{R}-\frac{R}{D}k_sG^*h\right]\right\}(1+\mu)\nabla^2w_1^*\\
&=\left[R^2\nabla^2+(1-\mu)\right]\left\{R\nabla^2+\left[\frac{(1-\mu)}{R}-\frac{R}{D}k_sG^*h\right]\right\}\left(-N_0\nabla^2w_1^*+\frac{Eh}{1-\mu}\frac{2w_1^*}{R^2}\right)
\end{aligned}\tag{3.12}$$

It is known (Kraus, 1967; Victor et al., 2009) that the Legendre functions solve the following eigenvalue problem:

$$\nabla^2w_1^*(\varphi,\theta)=\frac{1}{R^2\sin\varphi}\left[\frac{\partial}{\partial\varphi}\left(\frac{\partial w_1^*}{\partial\varphi}\sin\varphi\right)+\frac{1}{\sin\varphi}\frac{\partial^2w_1^*}{\partial\theta^2}\right]=\chi w_1^*=-\frac{n(n+1)}{R^2}w_1^*,\tag{3.13}$$

where the nth eigenvalue χ_n is determined by $-\chi_nR^2=n(n+1)>>1$ (n is a natural number). Thus, for non-axisymmetric deformation with condition $-\chi_nR^2>>1$, Eq. (3.12) is reduced to the eigenvalue problem

$$\chi^2R^4\left(N_0+k_sG^*h\right)-\chi R^2\left(Eh+N_0\frac{R^2}{D}k_sG^*h\right)+Eh\frac{R^2}{D}k_sG^*h=0.\tag{3.14}$$

The critical value of N_0 is determined by the stationary condition $dN_0/d\chi=0$. It follows from Eq. (3.14) that

$$2\chi R^4\left(N_0+k_sG^*h\right)=R^2\left(Eh+N_0\frac{R^2}{D}k_sG^*h\right).\tag{3.15}$$

Eliminating χ from Eqs. (3.14) and (3.15), the linearized critical value of the external pressure, as given in the form of $\left(\frac{N_0}{Eh}\right)_{cr}$, is given by

$$\left(\frac{N_0}{Eh}\right)_{cr} = -\left(\frac{1}{\sqrt{3(1-\mu^2)}}\right)\left(\frac{h_0}{h}\right)^{\frac{3}{2}}\left(\frac{h}{R}\right)+\left(\frac{1}{6(1-\mu)k_s}\right)\left(\frac{h_0}{h}\right)^3\left(\frac{h}{R}\right)^2\left(\frac{G}{G^*}\right). \tag{3.16}$$

Clearly, the critical value (3.16) is same with the formula (2.13) developed based on the axisymmetric assumption, and reduces to the classical formula (1.1) when transverse shear strains are neglected ($G^*/G=\infty$) and $h_0 = h$, as shown in (Ru, 2009).

In particular, the corresponding value of χ_n is given by

$$-\chi_n R^2 = \frac{\frac{R^2}{D}k_s G^* h}{\sqrt{\frac{R^2}{EhD}k_s G^* h - 1}} = \frac{6(1-\mu)k_s \frac{G^*}{G}(\frac{R}{h})^2(\frac{h}{h_0})^3}{\frac{k_s\sqrt{3(1-\mu^2)}}{1+\mu}\frac{G^*}{G}\frac{R}{h}(\frac{h}{h_0})^{\frac{3}{2}}-1} \approx n(n+1) >> 1. \tag{3.17}$$

Likewise, Eq. (3.17) is same with the formula (2.15) based on the axisymmetric assumption. It is proved in (Ru, 2009) that the inequality condition [$n(n+1) >> 1$] is met as long as the following condition is satisfied

$$\frac{G^*}{G} > \frac{h(1+\nu)}{Rk_s\sqrt{3(1-\nu^2)}}(\frac{h_0}{h})^{3/2} \tag{3.18}$$

In particular, all physically realistic parameters of biopolymer shells studied in the present chapter well satisfy the condition (3.18).

Let us now derive the expression of ($u_1^*, v_1^*, w_1^*, \alpha_1^*, \beta_1^*$). Actually, w_1^* is the *n*th eigenfunction of the eigenvalue problem (3.13) with *n* determined by (3.17). To obtain the eigenfunction $w_1^*(\varphi,\theta)$

corresponding the nth eigenvalue χ_n determined by $-\chi_n R^2 = n(n+1)$, one can solve Eq. (3.13) by using Legendre polynomials and the separation of variables (Victor et al., 2009). The general form of the linear combination of buckling modes (i.e. the eigenfunction $w_1^*(\varphi,\theta)$) is given by (see also (Koiter, 1969)

$$w_1^*(\varphi,\theta) = -h\left[\xi_0 P_n(\cos\varphi) + \sum_{m=1}^{n}\left(\xi_m \cos m\theta + \kappa_m \sin m\theta\right)\bar{P}_n^m(\cos\varphi)\right], \tag{3.19}$$

where $P_n(\cos\varphi)$ is the Legendre-polynomial of degree n, $\bar{P}_n^m(\cos\varphi)$ is the associated normalized Legendre-polynomial of degree n and order m, and ξ_0, ξ_m, κ_m denote total $(2n+1)$ independent nondimensional amplitude factors normalized by the average thickness h. The integer n can be determined as the nearest natural number by Eq. (3.17). Here, it is seen from the representation (3.19) that there are in general $(2n+1)$ independent and mutually orthogonal linear buckling modes (one of which is axisymmetric, while other $2n$ are non-axisymmetric) at the same value of the critical buckling load (3.16), although chapter 2 (Zhang and Ru, 2016) only considered the axisymmetric linear mode $\xi_0 w_1 = -\xi_0 h P_n(\cos\varphi)$ (with $\xi_m = \kappa_m = 0$) (see Eq. (2.14)).

To derive formulas of u_1^*, v_1^*, α_1^* and β_1^*, it follows from the first and third equations of (3.11) that the expressions of f_1^* and g_1^* have a similar form as Eq. (3.19). Therefore, combined with Eq. (3.13), the first Laplacian of f_1^* and g_1^* gives

$$\nabla^2 f_1^* = \frac{-n(n+1)}{R^2} f_1^*, \qquad \nabla^2 g_1^* = \frac{-n(n+1)}{R^2} g_1^* \tag{3.20}$$

Subsequently, introducing Eqs. (3.13) and (3.20) into the first and third formulas of Eq. (3.11), we can get specific expression of f_1^* and g_1^*. Then substituting f_1^* and g_1^* into Eq. (3.10), the expressions of u_1^*, v_1^*, α_1^* and β_1^*, are determined in terms of w_1^* as

$$\begin{aligned} u_1^* &= \frac{-(1+\mu)}{n(n+1)-(1-\mu)}\frac{\partial w_1^*}{\partial \varphi}, \qquad v_1^* = \frac{-(1+\mu)}{n(n+1)-(1-\mu)}\frac{\partial w_1^*}{\partial \theta}\csc\varphi, \\ \alpha_1^* &= \frac{1}{R}\left[\frac{H}{-n(n+1)+(1-\mu)-H}\right]\frac{\partial w_1^*}{\partial \varphi}, \quad \beta_1^* = \frac{1}{R}\left[\frac{H}{-n(n+1)+(1-\mu)-H}\right]\frac{\partial w_1^*}{\partial \theta}\csc\varphi, \end{aligned} \tag{3.21}$$

where $H = 6(1-\mu)k_s\dfrac{G^*}{G}\left(\dfrac{h}{h_0}\right)^3\left(\dfrac{R}{h}\right)^2$. Therefore, (3.19) and (3.21) give the deviations based on the (2*n*+1) independent and mutually orthogonal linear buckling modes shown in (3.19) which are all associated with the same critical load (3.16), where the integer *n* is determined by (3.17).

Next, to determine $(u_2^*, v_2^*, w_2^*, \alpha_2^*, \beta_2^*)$, retaining only the second-order buckling modes in the second brace of Eq. (3.8), the rearranged equations give the second-order Euler equations for $(u_2^*, v_2^*, w_2^*, \alpha_2^*, \beta_2^*)$ (Hutchinson, 1967; Kraus, 1967)

$$\frac{\partial N_{\varphi 2}^*}{\partial \varphi}+\frac{1}{\sin\varphi}\frac{\partial N_{\varphi\theta 2}^*}{\partial \theta}+(N_{\varphi 2}^*-N_{\theta 2}^*)\frac{\cos\varphi}{\sin\varphi}+\frac{Eh}{2\left(1-\mu^2\right)\sin\varphi}\left\{\frac{\partial}{\partial\varphi}\left[\left(\left(\frac{\partial w_1^*}{R\partial\varphi}\right)^2+\mu\left(\frac{\partial w_1^*}{R\sin\varphi\partial\theta}\right)^2\right)\sin\varphi\right]\right.$$
$$\left.+\frac{\partial}{\partial\theta}\left[(1-\mu)\left(\frac{\partial w_1^*}{R\partial\varphi}\right)\left(\frac{\partial w_1^*}{R\sin\varphi\partial\theta}\right)\right]-\left[\mu\left(\frac{\partial w_1^*}{\partial\varphi}\right)^2+\left(\frac{\partial w_1^*}{\sin\varphi\partial\theta}\right)^2\right]\cos\varphi\right\}=0$$

$$\frac{\partial N_{\varphi\theta 2}^*}{\partial \varphi}+\frac{1}{\sin\varphi}\frac{\partial N_{\theta 2}^*}{\partial \theta}+2N_{\varphi\theta 2}^*\frac{\cos\varphi}{\sin\varphi}+\frac{Eh}{2R\left(1-\mu^2\right)}\left\{\frac{\partial}{\partial\theta}\left[\mu\left(\frac{\partial w_1^*}{R\partial\varphi}\right)^2+\left(\frac{\partial w_1^*}{R\sin\varphi\partial\theta}\right)^2\right]\right.$$
$$\left.+\frac{\partial}{\partial\varphi}\left[(1-\mu)\sin\varphi\left(\frac{\partial w_1^*}{R\partial\varphi}\right)\left(\frac{\partial w_1^*}{R\sin\varphi\partial\theta}\right)\right]-\left[(1-\mu)\cos\varphi\left(\frac{\partial w_1^*}{R\partial\varphi}\right)\left(\frac{\partial w_1^*}{R\sin\varphi\partial\theta}\right)\right]\right\}=0$$

$$\frac{\partial Q_{\varphi 2}^*}{\partial \varphi}+\frac{1}{\sin\varphi}\frac{\partial Q_{\theta 2}^*}{\partial \theta}+Q_{\varphi 2}^*\frac{\cos\varphi}{\sin\varphi}-(N_{\varphi 2}^*+N_{\theta 2}^*)+N_0R\nabla^2w_2^*+\frac{1}{\sin\varphi}\frac{\partial}{R\partial\varphi}\left(N_{\varphi 1}^*\sin\varphi\frac{\partial w_1^*}{R\partial\varphi}+N_{\varphi\theta 1}^*\frac{\partial w_1^*}{R\partial\theta}\right)$$
$$+\frac{1}{\sin\varphi}\frac{\partial}{\partial\theta}\left(N_{\theta 1}^*\frac{1}{R\sin\varphi}\frac{\partial w_1}{\partial\theta}+N_{\varphi\theta 1}^*\frac{\partial w_1}{R\partial\varphi}\right)-\frac{Eh}{2(1-\mu)}\left[\left(\left(\frac{\partial w_1^*}{R\partial\varphi}\right)^2+\left(\frac{\partial w_1^*}{R\sin\varphi\partial\theta}\right)^2\right)\sin\varphi\right]=0$$

$$\frac{\partial M_{\varphi 2}^*}{\partial \varphi}+\frac{1}{\sin\varphi}\frac{\partial M_{\varphi\theta 2}^*}{\partial \theta}+(M_{\varphi 2}^*-M_{\theta 2}^*)\frac{\cos\varphi}{\sin\varphi}-RQ_{\varphi 2}^*=0 \tag{3.22}$$

$$\frac{\partial M_{\varphi\theta 2}^*}{\partial \varphi}+\frac{1}{\sin\varphi}\frac{\partial M_{\theta 2}^*}{\partial \theta}+2M_{\varphi\theta 2}^*\frac{\cos\varphi}{\sin\varphi}-RQ_{\theta 2}^*=0$$

By substituting ($u_1^*, v_1^*, w_1^*, \alpha_1^*, \beta_1^*$) into Eq. (3.22), the deviations ($u_2^*, v_2^*, w_2^*, \alpha_2^*, \beta_2^*$) expanded by second-order buckling modes can finally be determined as function of $\frac{N_0}{Eh}$ (See the detailed procedure in Appendix D).

3.2.2 Non-axisymmetric post-buckling

The nonlinear, non-axisymmetric initial post-buckling of a biopolymer spherical shell can be studied using Koiter's general nonlinear theory of elastic stability (Koiter, 1945) and the procedure developed in his work on post-buckling behavior of a complete spherical shell (Koiter, 1969). Thus, with the potential energy Eq. (3.6), the increment in the potential energy of the spherical shell due to

the transmission from pre-buckling equilibrium state I to an arbitrary state II in the neighborhood of state I, $P[\hat{u}]=P_{II}-P_I$, is a potential energy functional of the displacement field $\hat{u}=(u-u_0,v-v_0,w-w_0,\alpha-\alpha_0,\beta-\beta_0)$. Therefore, the increment in potential energy due to the transmission from state I to state II is obtained as

$$\begin{aligned}P[\hat{u}]=&\frac{1}{2}\int_0^{\pi}\int_0^{2\pi}\left[N_{\varphi}(e_{\varphi}-e_{\varphi 0})+N_{\theta}(e_{\theta}-e_{\theta 0})+N_{\varphi\theta}e_{\varphi\theta}\right.\\&\left.+M_{\varphi}k_{\varphi}+M_{\theta}k_{\theta}+M_{\varphi\theta}k_{\varphi\theta}+Q_{\varphi}e_{\varphi z}+Q_{\theta}e_{\theta z}\right]R^2\sin\varphi d\varphi d\theta\\&-\frac{1}{2}\int_0^{\pi}\int_0^{2\pi}\left[N_{\varphi 0}\left(\frac{1}{R}\frac{\partial(u-u_0)}{\partial\varphi}+\frac{(w-w_0)}{R}\right)\right.\\&\left.+N_{\theta 0}\left(\frac{(u-u_0)}{R}\cot\varphi+\frac{1}{R\sin\varphi}\frac{\partial(v-v_0)}{\partial\theta}+\frac{(w-w_0)}{R}\right)\right]R^2\sin\varphi d\varphi d\theta\end{aligned}\tag{3.23}$$

Eqs.(3.1), (3.4) and (3.5) are then substituted into Eq. (3.23) to give in the form

$$\begin{aligned}P[\hat{u}]=&Eh^3\left\{\left(P_2\left[\left(u_1^*,v_1^*,w_1^*,\alpha_1^*,\beta_1^*\right);\frac{N_0}{Eh}\right]\right)\right.\\&+\left(P_3\left[u_1^*,v_1^*,w_1^*,\alpha_1^*,\beta_1^*\right]+P_{11}\left[\left(u_1^*,v_1^*,w_1^*,\alpha_1^*,\beta_1^*\right),\left(u_2^*,v_2^*,w_2^*,\alpha_2^*,\beta_2^*\right);\frac{N_0}{Eh}\right]\right)\\&\left.+\left(P_4\left[u_1^*,v_1^*,w_1^*,\alpha_1^*,\beta_1^*\right]+P_{21}\left[\left(u_1^*,v_1^*,w_1^*,\alpha_1^*,\beta_1^*\right),\left(u_2^*,v_2^*,w_2^*,\alpha_2^*,\beta_2^*\right)\right]+P_2\left[\left(u_2^*,v_2^*,w_2^*,\alpha_2^*,\beta_2^*\right);\frac{N_0}{Eh}\right]\right)\right\}\end{aligned}\tag{3.24}$$

where the subscript denotes the order of the term in the bracket and the first number of a double subscript denotes the order of the first term in the bracket, and the second number denotes the order of the second term in the bracket. The specific expressions of these terms are given in Appendix E.

Firstly, the orthogonality condition (D.6) ensures $P_{11}\left[\left(u_1^*,v_1^*,w_1^*,\alpha_1^*,\beta_1^*\right),\left(u_2^*,v_2^*,w_2^*,\alpha_2^*,\beta_2^*\right);\frac{N_0}{Eh}\right]$ vanish for any value of the load N_0, which can also be confirmed by introducing the deviations $u_1^*,v_1^*,w_1^*,\alpha_1^*,\beta_1^*$ ((3.19) and (3.21)) and $(u_2^*,v_2^*,w_2^*,\alpha_2^*,\beta_2^*)$ ((D.1) and (D.4)) into the third equation

in Appendix E and calculating with *Mathematica* when all parameters $(k_s, \mu, R/h, G^*/G, h_0/h)$ are given and the integer n is obtained by (3.17). Also, by doing this, the other expressions in Appendix E are given by

$$A_2^*\left(\frac{N_0}{Eh}\right) = P_2\left[\left(u_1^*, v_1^*, w_1^*, \alpha_1^*, \beta_1^*\right); \frac{N_0}{Eh}\right] = \left(A_{20}^* + B_{20}^*\frac{N_0}{Eh}\right)\left[\left(\xi_0\right)^2 + \frac{1}{2}\sum_{i=1}^{n}\left(\left(\xi_i\right)^2 + \left(\kappa_i\right)^2\right)\right], \tag{3.25}$$

$$\begin{aligned} A_3^* &= P_3\left[u_1^*, v_1^*, w_1^*, \alpha_1^*, \beta_1^*\right] \\ &= A_{30}^*\left(\xi_0\right)^3 + \sum_{i=1}^{n} A_{30i}^*\xi_0\left[\left(\xi_i\right)^2 + \left(\kappa_i\right)^2\right] + \sum_{i,j,k=1}^{n}\delta\left(i+j-k\right)A_{3ijk}^*\left(\xi_i\xi_j\xi_k + 2\xi_i\kappa_j\kappa_k - \kappa_i\kappa_j\xi_k\right), \end{aligned} \tag{3.26}$$

$$\begin{aligned} A_4^*\left(\frac{N_0}{Eh}\right) &= P_4\left[u_1^*, v_1^*, w_1^*, \alpha_1^*, \beta_1^*\right] + P_{21}\left[\left(u_1^*, v_1^*, w_1^*, \alpha_1^*, \beta_1^*\right), \left(u_2^*, v_2^*, w_2^*, \alpha_2^*, \beta_2^*\right)\right] + P_2\left[\left(u_2^*, v_2^*, w_2^*, \alpha_2^*, \beta_2^*\right); \frac{N_0}{Eh}\right] \\ &= A_{40}^*\left(\frac{N_0}{Eh}\right)\left(\xi_0\right)^4 + \sum_{i=1}^{n} A_{40i}^*\left(\frac{N_0}{Eh}\right)\left(\xi_0\right)^2\left(\left(\xi_i\right)^2 + \left(\kappa_i\right)^2\right) \\ &\quad + \sum_{i,j,k=1}^{n}\delta\left(i+j-k\right)A_{40ijk}^*\left(\frac{N_0}{Eh}\right)\left(\xi_0\xi_i\xi_j\xi_k + 2\xi_0\xi_i\kappa_j\kappa_k - \xi_0\kappa_i\kappa_j\xi_k\right) \\ &\quad + \sum_{i,j,k,l=1}^{n}\delta\left(i+j+k-l\right)B_{4ijkl}^*\left(\frac{N_0}{Eh}\right)\left(\xi_i\xi_j\xi_k\xi_l - \kappa_i\kappa_j\kappa_k\kappa_l + 3\xi_i\xi_j\kappa_k\kappa_l - 3\kappa_i\kappa_j\xi_k\xi_l\right) \\ &\quad + \sum_{i,j,k,l=1}^{n}\delta\left(i+l-j-k\right)C_{4ijkl}^*\left(\frac{N_0}{Eh}\right)\left(\xi_i\xi_j\xi_k\xi_l + \kappa_i\kappa_j\kappa_k\kappa_l + 2\xi_i\xi_j\kappa_k\kappa_l + 2\kappa_i\kappa_j\xi_k\xi_l\right) \\ &\quad - \sum_{i,j,k,l=1}^{n}\delta\left(i+j-k-l\right)C_{4ijkl}^*\left(\frac{N_0}{Eh}\right)\left(\xi_i\xi_j\kappa_k\kappa_l + \kappa_i\kappa_j\xi_k\xi_l\right), \end{aligned} \tag{3.27}$$

where coefficients $A_{20}^*, B_{20}^*, A_{30}^*, A_{30i}^*, A_{3ijk}^*$ are real numbers, $A_{40}^*\left(\frac{N_0}{Eh}\right), A_{40i}^*\left(\frac{N_0}{Eh}\right), \quad A_{40ijk}^*\left(\frac{N_0}{Eh}\right)$, $B_{4ijkl}^*\left(\frac{N_0}{Eh}\right)$ and $C_{4ijkl}^*\left(\frac{N_0}{Eh}\right)$ are functions of $\frac{N_0}{Eh}$ and can be calculated easily through *Mathematica*, and δ is the Dirac's delta symbol. Here, it is noted that Eqs. (3.25) and (3.26) are identical to Koiter's formulas for second and third order terms (see Eq. 4.24 and Eq.5.15 in (Koiter, 1969)), and the third-order term A_3^* vanishes for buckling modes of an odd degree *n*. Thus, similar as the axisymmetric case

based on the axisymmetric mode without mode interaction (Koiter, 1969; Zhang and Ru, 2016), the fourth-order term $A_4^*\left(\frac{N_0}{Eh}\right)$ is essential for non-axisymmetric post-buckling. Therefore, based on Koiter's (Koiter, 1945, 1969) general nonlinear theory of elastic stability, the potential energy functional (3.24), which describes the initial post-buckling behavior of a pressured perfect biopolymer spherical shell, is given by

$$P[\hat{u}] = Eh^3\left[A_2^*\left(\frac{N_0}{Eh}\right) + A_3^* + A_4^*\left(\frac{N_0}{Eh}\right)\right] \tag{3.28}$$

for both cases when the integer n is an even or odd number.

3.3 Non-axisymmetric imperfection sensitivity of an imperfect biopolymer spherical shell

Based on the formulation of non-axisymmetric post-buckling behavior of a pressured perfect biopolymer spherical shell, let us now study the non-axisymmetric imperfection sensitivity of an imperfect biopolymer spherical shell.

3.3.1 Formulation of imperfection sensitivity with the mode interaction

Similar as Koiter (Koiter, 1969) and Hutchinson (Hutchinson, 1967) for a classical homogeneous spherical shell, the general form of geometric imperfection is given in the form of the linear combination of buckling modes by

$$\bar{w}_1^* = -h\left[\bar{\xi}_0 P_n(\cos\varphi) + \sum_{m=1}^{n}\left(\bar{\xi}_m \cos m\theta + \bar{\kappa}_m \sin m\theta\right)\bar{P}_n^m(\cos\varphi)\right] \tag{3.29}$$

where $\bar{\xi}_0, \bar{\xi}_m$ and $\bar{\kappa}_m$ are the nondimensional axisymmetric and non-axisymmetric imperfection amplitudes normalized by average thickness *h*, respectively.

With the imperfection (3.29), the nonlinear strain-displacement relations (3.1) becomes to

$$\begin{aligned} e_\varphi &= \frac{1}{R}\frac{\partial u}{\partial \varphi} + \frac{w}{R} + \frac{1}{2}\left(\frac{\partial w}{R\partial \varphi}\right)^2 + \frac{\partial w}{R\partial \varphi}\frac{\partial \bar{w}_1^*}{R\partial \varphi}, \\ e_\theta &= \frac{u}{R}\cot\varphi + \frac{1}{R\sin\varphi}\frac{\partial v}{\partial \theta} + \frac{w}{R} + \frac{1}{2}\left(\frac{\partial w}{R\sin\varphi\partial \theta}\right)^2 + \frac{\partial w}{R\sin\varphi\partial \theta}\frac{\partial \bar{w}_1^*}{R\sin\varphi\partial \theta}, \\ e_{\varphi\theta} &= \frac{1}{R\sin\varphi}\frac{\partial u}{\partial \theta} + \frac{1}{R}\frac{\partial v}{\partial \varphi} - \frac{v}{R}\cot\varphi + \left(\frac{\partial w}{R\partial \varphi}\right)\left(\frac{\partial w}{R\sin\varphi\partial \theta}\right) + \frac{\partial w}{R\partial \varphi}\frac{\partial \bar{w}_1^*}{R\sin\varphi\partial \theta} + \frac{\partial \bar{w}_1^*}{R\partial \varphi}\frac{\partial w}{R\sin\varphi\partial \theta}, \end{aligned} \tag{3.30}$$

In the presence of the imperfection (3.29), the expression (3.5) for membrane forces (N_φ, N_θ) are augmented by terms involving the order $\xi_0\bar{\xi}_0, \xi_i\bar{\xi}_i, \kappa_i\bar{\kappa}_i$ and higher; similarly, the term $Eh^3\left\{A_{10}^*\frac{N_0}{Eh}\left[\xi_0\bar{\xi}_0 + \frac{1}{2}\sum_{i=1}^{n}\left(\xi_i\bar{\xi}_i + \kappa_i\bar{\kappa}_i\right)\right]\right\}$ together with other higher orders than $\xi_0\bar{\xi}_0$, $\xi_i\bar{\xi}_i$ and $\kappa_i\bar{\kappa}_i$ are added to Eq. (3.24). Following Koiter (Koiter, 1969), we now limit ourselves to the first-order approximation by neglecting all terms of higher orders than $\xi_0\bar{\xi}_0$, $\xi_i\bar{\xi}_i$ and $\kappa_i\bar{\kappa}_i$, thus the potential energy functional which describes the post-buckling behavior of a pressured biopolymer spherical shell with the imperfection (3.29) is given by

$$P[\hat{u}] = Eh^3\left[A_2^*\left(\frac{N_0}{Eh}\right) + A_3^* + A_4^*\left(\frac{N_0}{Eh}\right) + A_1^*\left(\frac{N_0}{Eh}\right)\right] \tag{3.31}$$

where the specific expression of $A_1^*\left(\frac{N_0}{Eh}\right)$ is given by

$$A_1^*\left(\frac{N_0}{Eh}\right) = \int_0^{2\pi}\int_0^{\pi}\left\{\frac{N_0}{Eh}\left[\left(\frac{\partial w_1^*}{h\partial \varphi}\right)\left(\frac{\partial \bar{w}_1^*}{h\partial \varphi}\right) + \left(\frac{1}{h\sin\varphi}\frac{\partial w_1^*}{\partial \theta}\right)\left(\frac{1}{h\sin\varphi}\frac{\partial \bar{w}_1^*}{\partial \theta}\right)\right]\right\}\sin\varphi d\varphi d\theta \tag{3.32}$$

By introducing the deviation w_1^* (3.19) and geometric imperfection (3.29) into Eq. (3.32) and calculating with *Mathematica* with given parameters ($k_s, \mu, R/h, G^*/G, h_0/h$) and the integer n determined by (3.17), we have

$$A_1^*\left(\frac{N_0}{Eh}\right) = A_{10}^*\frac{N_0}{Eh}\left[\xi_0\overline{\xi}_0 + \frac{1}{2}\sum_{i=1}^{n}\left(\xi_i\overline{\xi}_i + \kappa_i\overline{\kappa}_i\right)\right] \tag{3.33}$$

where the value of A_{10}^* can be obtained easily through *Mathematica*.

In chapter 2 (Zhang and Ru, 2016), the imperfection sensitivity for an axisymmetric imperfection without considering non-axisymmetric buckling modes and the mode interaction ($\xi_i = \overline{\xi}_i = \kappa_i = \overline{\kappa}_i = 0, i = 1,2,3,...,n$) has been studied, and the dependence of the actual maximum load an imperfect biopolymer spherical shell can sustain on the axisymmetric imperfection amplitude $\overline{\xi}_0$ is given as Eq. (2.39). Now, let us investigate the role of non-axisymmetric buckling modes and associated mode interaction by using Hutchinson's method (Hutchinson, 1967). Interaction between the axisymmetric and non-axisymmetric modes will occur only if the nonlinear coupling coefficients in the third and fourth order terms (Eqs. (3.26) and (3.27)) are nonzero (i.e. the argument in Dirac's delta symbol equals 0) (Hutchinson, 1967). Therefore, as we can see from Eqs. (3.26) and (3.27), two or three or four of these linear buckling modes will interact. Also, it can be verified by *Mathematica* that the order of the subscript i, j, k or i, j, k, l does not affect the values of these coupling coefficients (e.g. $A_{40246}^*\left(\frac{N_0}{Eh}\right) = A_{40426}^*\left(\frac{N_0}{Eh}\right)$), which implies that the terms like $\xi_0\xi_2\xi_4\xi_6$ and $\xi_0\xi_2\kappa_4\kappa_6$ have same coefficients, and this also applies to other terms in Eqs. (3.26) and (3.27). Therefore the effect of mode interaction on the imperfection sensitivity between ξ_0, ξ_2, ξ_4 and ξ_6 is same with that between ξ_0, ξ_2, κ_4 and κ_6. Therefore, we shall focus on non-axisymmetric buckling modes ξ_i $(i = 1,2,3,...,n)$

and the associated mode interaction. For the sake of brevity, similar to the case discussed in Hutchinson (Hutchinson, 1967), we take two-mode interaction as an example to show this procedure. The interaction between three or four modes follows the similar procedure as shown numerically in Fig. 3.2 (the number of the mode interaction can be seen from the legends of Fig. 3.2).

Let us firstly consider the axisymmetric imperfection $-h\bar{\xi}_0 P_n(\cos\varphi)$ and the mode interaction between the axisymmetric mode $\xi_0 P_n(\cos\varphi)$ and a non-axisymmetric mode $\xi_m \cos m\theta \bar{P}_n^m(\cos\varphi)$ ($m = 1,2,3,...,n$). In this case, the potential energy functional (3.31) becomes

$$\begin{aligned} P[\hat{u}] = Eh^3 \Bigg[& \left(A_{20}^* + B_{20}^* \frac{N_0}{Eh} \right) \left(\xi_0{}^2 + \frac{1}{2} \xi_m{}^2 \right) + A_{30}^* (\xi_0)^3 + A_{30m}^* \xi_0 (\xi_m)^2 + A_{40}^* \left(\frac{N_0}{Eh} \right) \xi_0{}^4 \\ & + A_{40m}^* \left(\frac{N_0}{Eh} \right) (\xi_0 \xi_m)^2 + C_{4mmmm}^* \left(\frac{N_0}{Eh} \right) \xi_m{}^4 + A_{10}^* \frac{N_0}{Eh} \xi_0 \bar{\xi}_0 \Bigg] \end{aligned} \tag{3.34}$$

The two equilibrium equations obtained by the first variation of (3.34) with respect to ξ_0 and ξ_m, respectively, in terms of $\frac{N_0}{Eh}$, are given by

$$\frac{\partial P[\hat{u}]}{\partial \xi_0} = 2\left(A_{20}^* + B_{20}^* \frac{N_0}{Eh} \right) \xi_0 + 3A_{30}^* (\xi_0)^2 + 4A_{40}^* \left(\frac{N_0}{Eh} \right) (\xi_0)^3 + 2A_{40m}^* \left(\frac{N_0}{Eh} \right) \xi_0 \xi_m{}^2 + A_{10}^* \frac{N_0}{Eh} \bar{\xi}_0 = 0 \tag{3.35}$$

$$\frac{\partial P[\hat{u}]}{\partial \xi_m} = \left(A_{20}^* + B_{20}^* \frac{N_0}{Eh} \right) \xi_m + 2A_{40m}^* \left(\frac{N_0}{Eh} \right) \xi_0{}^2 \xi_m + 4C_{4mmmm}^* \left(\frac{N_0}{Eh} \right) \xi_m{}^3 = 0. \tag{3.36}$$

Before the maximum load is reached, the load increases with the amplitude of the axisymmetric mode (with $\xi_m = 0$) (Hutchinson, 1967). Then Eq. (3.35) has three solutions and only one of them reduces to the undeformed shell $\xi_0 = 0$ at $\frac{N_0}{Eh} = 0$ and therefore is the physically most significant branch of

the solutions (called "natural branch", (Koiter, 1945, 1969)), which is given as an implicit function X_0 determined by solving Eq. (3.35) with $\xi_m = 0$

$$\xi_0 = X_0\left(\frac{N_0}{Eh}, \bar{\xi}_0\right) \tag{3.37}$$

The nature branch loses its stability at the critical value of the load $\frac{N_0}{Eh}$ where a bifurcation occurs. For this case, a bifurcation develops when a non-zero ξ_m increases, which is determined by solving equilibrium equations (3.35) and (3.36) for ξ_0 and ξ_m with $\bar{\xi}_0 = 0$ (i.e. the equilibrium path for the perfect spherical shell) (Hutchinson, 1967), and the solution is given by the implicit expressions Y_0 and Y_m as

$$\xi_0 = Y_0\left(\frac{N_0}{Eh}\right), \qquad \xi_m = Y_m\left(\frac{N_0}{Eh}\right). \tag{3.38}$$

Following the bifurcation, the load the shell can sustain falls with a deflection consisted of both the axisymmetric and the non-axisymmetric modes. The post-buckling behavior of such a biopolymer spherical shells is illustrated by Fig. 3.1, where stable branch is indicated by a solid curve, and the unstable branch by a dashed curve.

Thus, the maximum load the imperfect shell can sustain, denoted by $\left(\frac{N_0^*}{Eh}\right)_{cr}$, is the bifurcation pressure determined by canceling out ξ_0 through Eqs. (3.37) and the first equation of (3.38) and is determined by

$$X_0\left(\left(\frac{N_0^*}{Eh}\right)_{cr}, \bar{\xi}_0\right) - Y_0\left(\left(\frac{N_0^*}{Eh}\right)_{cr}\right) = 0 \tag{3.39}$$

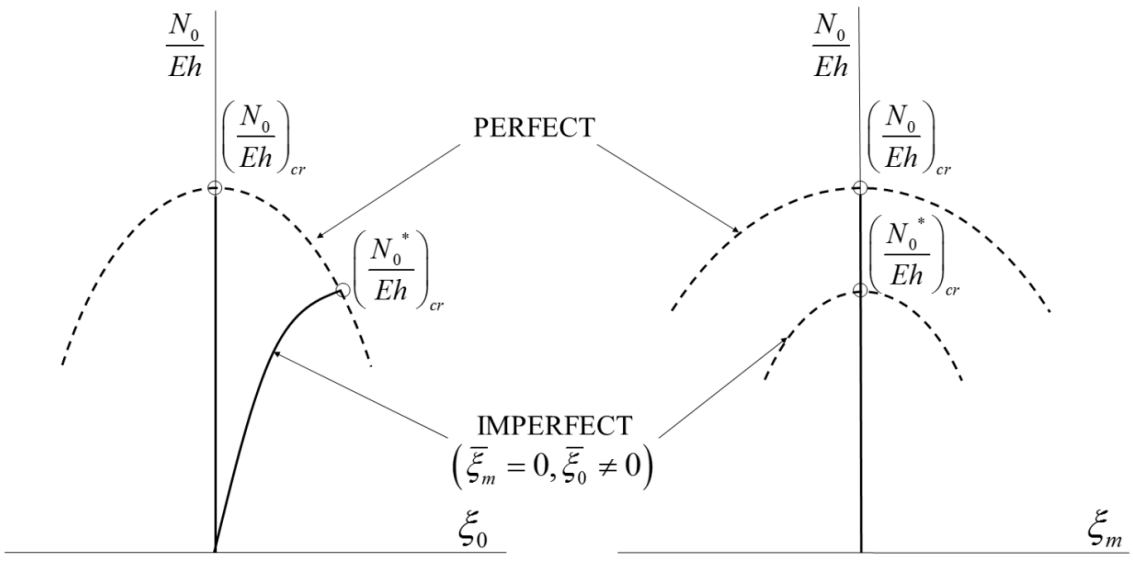

Fig. 3.1 Post-buckling equilibrium path in terms of the two amplitudes ξ_0 and ξ_m for the case of an axisymmetric imperfection

Let us now consider a non-axisymmetric imperfection $-h\bar{\xi}_i \cos i\theta \bar{P}_n^i(\cos\varphi)(i \neq 0)$ and the mode interaction between two non-axisymmetric modes $h\xi_i \cos i\theta \bar{P}_n^i(\cos\varphi)(i \neq 0)$ and $h\xi_j \cos j\theta \bar{P}_n^j(\cos\varphi)$ ($j \neq i$ and $j \neq 0$). In this case, the potential energy functional (3.31) becomes

$$P[\hat{u}] = Eh^3 \left\{ \left(A_{20}^* + B_{20}^* \frac{N_0}{Eh} \right) \left[\frac{1}{2}\left(\xi_i^{\,2} + \xi_j^{\,2} \right) \right] + C_{iiii}^* \left(\frac{N_0}{Eh} \right) \xi_i^{\,4} + A_{4jjjj}^* \left(\frac{N_0}{Eh} \right) \xi_j^{\,4} + A_{4ijij}^* \left(\frac{N_0}{Eh} \right) \left(\xi_i \xi_j \right)^2 + \frac{1}{2} A_{10}^* \frac{N_0}{Eh} \xi_i \bar{\xi}_i \right\} \tag{3.40}$$

The two equilibrium equations obtained by the first variation of (3.40) with respect to ξ_i and ξ_j in terms of $\frac{N_0}{Eh}$, are given by

$$\frac{\partial P[\hat{u}]}{\partial \xi_i} = \left(A_{20}^* + B_{20}^* \frac{N_0}{Eh} \right) \xi_i + 4C_{4iiii}^* \left(\frac{N_0}{Eh} \right) \xi_i^3 + 2C_{4ijij}^* \left(\frac{N_0}{Eh} \right) \xi_i \xi_j^2 + \frac{1}{2} A_{10}^* \frac{N_0}{Eh} \bar{\xi}_i = 0 \tag{3.41}$$

$$\frac{\partial P[\hat{u}]}{\partial \xi_j} = \left(A_{20}^* + B_{20}^* \frac{N_0}{Eh} \right) \xi_j + 4C_{4jjjj}^* \left(\frac{N_0}{Eh} \right) \xi_j^3 + 2C_{4ijij}^* \left(\frac{N_0}{Eh} \right) \xi_i^2 \xi_j = 0 \tag{3.42}$$

Before the maximum load is reached, the load increases with the amplitude of the non-axisymmetric mode $h\xi_i \cos i\theta \bar{P}_n^i (\cos\varphi)(i \neq 0)$ (with $\xi_j = 0$) (Hutchinson, 1967). Then Eq. (3.41) has three solutions and only one of them represents the natural branch and is given by an implicit function X_i

$$\xi_i = X_i \left(\frac{N_0}{Eh}, \bar{\xi}_i \right) \tag{3.43}$$

Bifurcation occurs when a non-zero ξ_j develops, which is determined by solving equilibrium equations (3.41) and (3.42) with $\bar{\xi}_i = 0$ (i.e. the equilibrium path for the perfect spherical shell) (Hutchinson, 1967) and the solution is given by the implicit expressions Y_i and Y_j as

$$\xi_i = Y_i \left(\frac{N_0}{Eh} \right), \qquad \xi_j = Y_j \left(\frac{N_0}{Eh} \right). \tag{3.44}$$

Following the bifurcation, the load the shell can sustain falls with a deflection consisted of the two non-axisymmetric modes. Thus, the maximum load the imperfect shell can sustain, denoted by $\left(\frac{N_0^*}{Eh} \right)_{cr}$, is the bifurcation pressure determined by canceling out ξ_i through Eqs. (3.43) and the first equation of (3.44) and is determined by

$$X_i \left(\left(\frac{N_0^*}{Eh} \right)_{cr}, \bar{\xi}_i \right) - Y_i \left(\left(\frac{N_0^*}{Eh} \right)_{cr} \right) = 0 \tag{3.45}$$

Therefore, with the mode interaction, we can determine the actual maximum load an imperfect biopolymer spherical shell can sustain $\left(\frac{N_0^*}{Eh}\right)_{cr}$ as a function of the nondimensional imperfection amplitude $\overline{\xi}_0$ or $\overline{\xi}_i$. Thus, one can calculate the so-called "knockdown factor" λ defined by Hutchinson (Hutchinson, 2010)

$$\lambda = \left(\frac{N_0^*}{Eh}\right)_{cr} \Big/ \left(\frac{N_0}{Eh}\right)_{cr} \tag{3.46}$$

where $\left(\frac{N_0}{Eh}\right)_{cr}$ given by Eq. (3.16) is the linear critical load, which is also actually the maximum load a prefect shell can sustain. Therefore, the dependence of the knockdown factor λ on the imperfection amplitude $\overline{\xi}_0$ or $\overline{\xi}_i$ can be obtained based on Eqs. (3.16), (3.39) and (3.46) for an axisymmetric geometric imperfection and Eqs. (3.16), (3.45) and (3.46) for a non-axisymmetric geometric imperfection, respectively.

3.3.2 Non-axisymmetric imperfection sensitivity of an imperfect biopolymer spherical shell

One major goal of this work is to study how the non-axisymmetric buckling mode and the mode interaction affect the imperfection sensitivity. For this end, let us compare the result obtained in chapter 2 (Eq. (2.39)) based on the axisymmetric assumption to either Eq. (3.39) for an axisymmetric imperfection with mode interaction or Eq. (3.45) for a non-axisymmetric imperfection with mode interaction, respectively. From Fig. 3.2, it can be seen that the effect is quite similar for different sets of values of the key parameters $R/h, G^*/G, h_0/h$.

Firstly, it is seen from Figs. 3.2a, 3.2c and 3.2e that, by comparing Eq. (3.39) with our previous results (Eq. (2.39)), the mode interaction has a significant effect on imperfection sensitivity of even a biopolymer spherical shell of an axisymmetric imperfection. Furthermore, the effect is more significant with more modes interacted each other. Figures 3.2b, 3.2d and 3.2f show how the non-axisymmetric geometric imperfection affects the imperfection sensitivity with the same four-mode interaction. It is seen that the non-axisymmetric imperfection with large wave number in θ direction (see Eq. (3.29)) has a greater effect on imperfection sensitivity. Therefore, to compare the mode interaction effect among different key parameters $R/h, G^*/G, h_0/h$, we consider the combination of the mode interaction and the non-axisymmetric imperfection that has the greatest influence on imperfection sensitivity with the results shown in Fig. 3.3. With fixed values of $k_s = 5/6$, $\mu = 0.3$ and the other parameters, the dependence of the knockdown factor λ defined by (3.16), (3.39), (3.45) and (3.46) on the imperfection parameter $\bar{\xi}_0$ or $\bar{\xi}_i$ (normalized by average thickness) is shown, respectively, in Figs. 3.3a, 3.3b and 3.3c for a range of R/h between 10 and 80, in Figs. 3.3d, 3.3e and 3.3f for a range of G^*/G between 0.1 and ∞, and in Figs. 3.3g, 3.3h and 3.3i for a range of h_0/h between 0.2 and 2.0. From Fig. 3.3, it can be seen that for most cases of biopolymer spherical shells characterized by different key parameters $R/h, G^*/G, h_0/h$ (which are physically realistic for typical biopolymer spherical shells) shown in Figs. 3a-3h, the difference between the knockdown factor based on the mode interaction and non-axisymmetric imperfection and that predicted by chapter 2 (Eq. (2.39)) based on axisymmetric mode without the mode interaction is around 30%. However, for the case of biopolymer spherical shells characterized by $R/h = 30, G^*/G = \infty, h_0/h = 0.2$ shown in Fig. 3.3i, the difference is less than 10% or even smaller when the key parameters R/h and h_0/h are smaller. Therefore, we can conclude that:

1) If a relative error less than 10% is acceptable, the imperfection sensitivity based on the simplified axisymmetric analysis as given in chapter 2 (Zhang and Ru, 2016) is practically useful under reasonably mild conditions that biopolymer spherical shells have relatively thicker average thickness (defined by moderate radius-to-thickness ratio, say, <30) and higher thickness non-uniformity (defined by smaller effective bending thickness-to-average shell thickness ratio, say, <0.2).
2) However, in other more general cases, the relative errors between the results based on the present non-axisymmetric analysis with the mode interaction and that predicted by the simplified axisymmetric analysis can be significant (typically around 30% or even larger). In such cases, a more accurate non-axisymmetric analysis with the mode interaction is required.

For some cases considered here, the non-axisymmetric modes and the associated mode interaction can have a significant effect, in a non-trivial way, on imperfection sensitivity of pressured biopolymer spherical shells. This justifies the relevance of the present non-axisymmetric analysis of imperfection sensitivity.

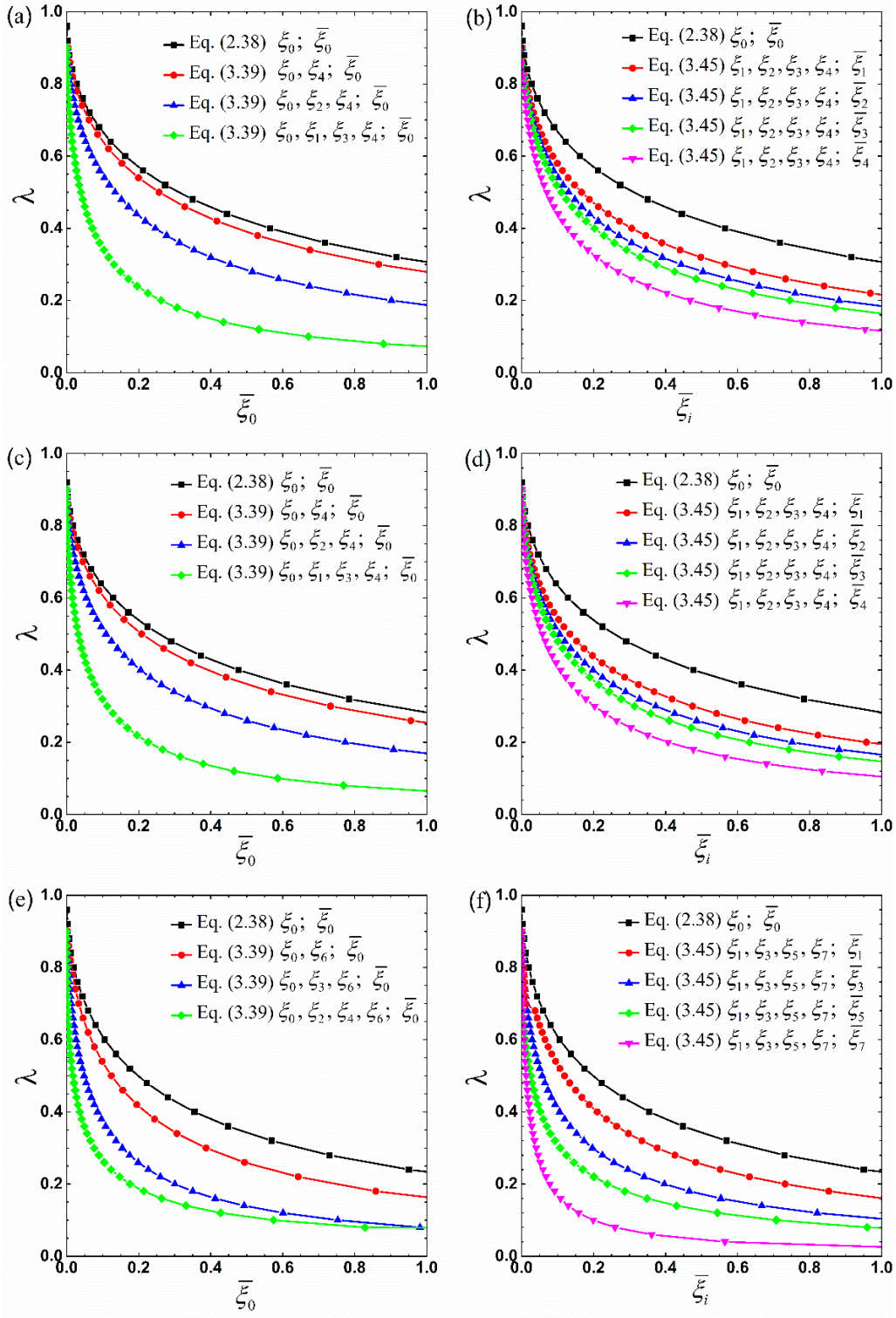

Fig. 3.2 The effect of the non-axisymmetric buckling mode and the mode interaction on imperfection sensitivity. (a) (b) $R/h=10, G^*/G=\infty, h_0/h=1; n=5$ (c) (d) $R/h=10, G^*/G=1.0, h_0/h=1; n=5$ (e) (f) $R/h=10, G^*/G=\infty, h_0/h=0.6; n=7$

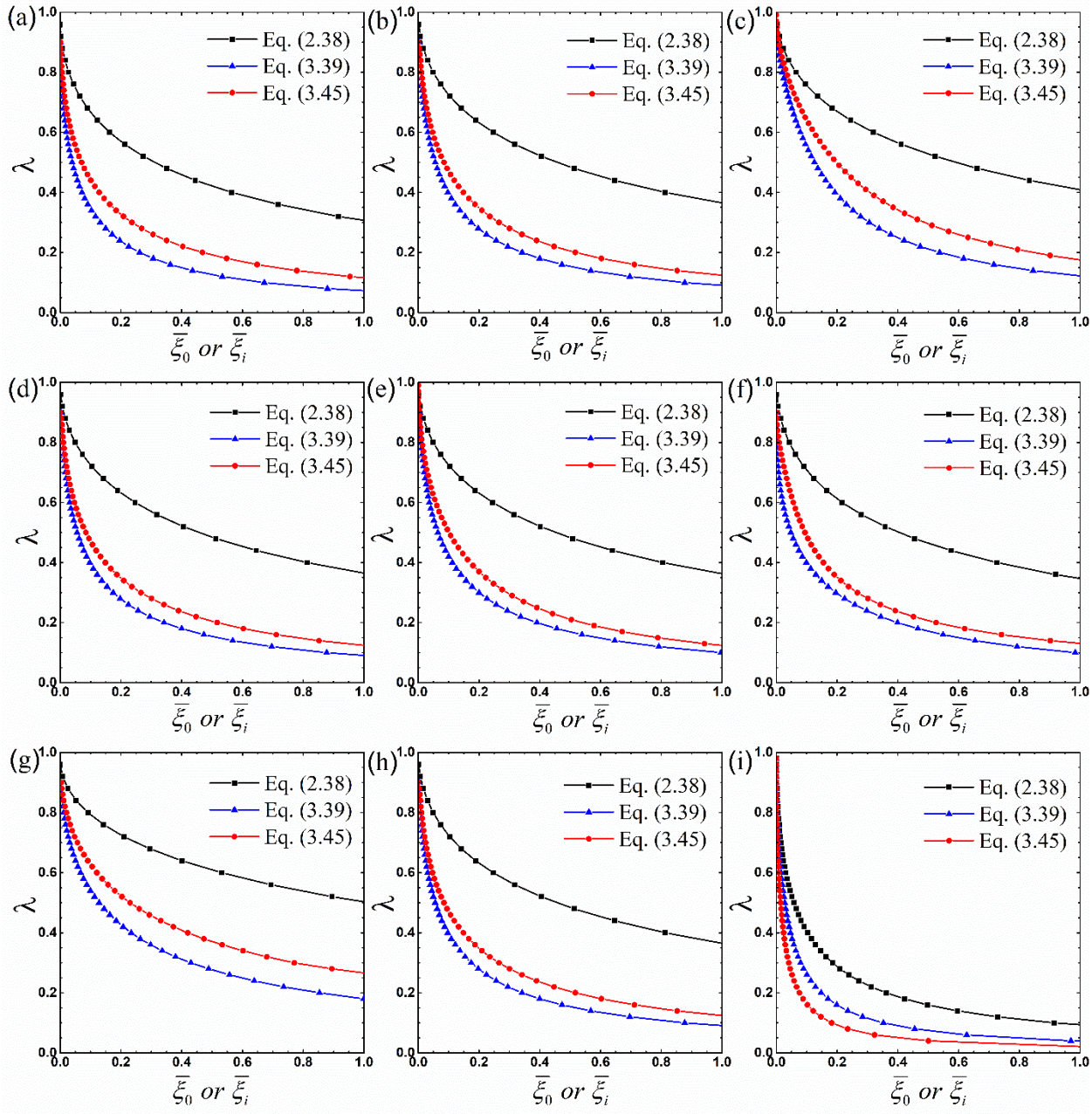

Fig. 3.3 (a) (b) (c) The influence of R/h on the imperfection sensitivity with fixed $G^*/G=\infty$ and $h_0/h=1$. (a) $n=5; R/h=10$ (b) $n=9; R/h=30$ (c) $n=16; R/h=80$. (d) (e) (f) The influence of G^*/G on the imperfection sensitivity with fixed $R/h=30$ and $h_0/h=1$. (d) $n=9; G^*/G=\infty$. (e) $n=9; G^*/G=1.0$ (f) $n=12; G^*/G=0.1$ (g) (h) (i)The influence of h_0/h on the imperfection sensitivity with fixed $R/h=30$ and $G^*/G=\infty$ (g) $n=5; h_0/h=2.0$. (h) $n=9; h_0/h=1.0$ (i) $n=44; h_0/h=0.2$

3.3.3 The influence of key parameters on imperfection sensitivity

With the refined model, it is the two additional parameters (G^*, h_0) which distinguish a biopolymer shell of high structural heterogeneity and thickness non-uniformity from a classical elastic spherical shell defined by (*E,* μ *, h, R*). Therefore, it is worth investigating how the high structural heterogeneity, defined by the key parameters $R/h, G^*/G, h_0/h$ in the refined shell model, affects the non-axisymmetric imperfection sensitivity of a pressured biopolymer spherical shell. As shown in Fig. 3.3, it can be concluded that

1) Within the range of R/h between 10 to 80 (which is realistic for typical biopolymer spherical shells), the parameter R/h has only a moderate effect on the non-axisymmetric imperfection sensitivity.
2) The effect of G^*/G on the non-axisymmetric imperfection sensitivity is negligible when G^*/G varies within a physically realistic range (say, between 0.1 to ∞) for biopolymer spherical shells.
3) The parameter h_0/h has a greater impact on the imperfection sensitivity. Therefore, the thickness non-uniformity of biopolymer spherical shells could be mainly responsible for the non-axisymmetric imperfection sensitivity.

These conclusions are qualitatively similar to those obtained in chapter 2 on axisymmetric buckling of biopolymer spherical shells with axisymmetric imperfections. Again, it should also be stated that results shown in Figs. 3.2 and 3.3 (in which the knockdown factor is extremely sensitive to vanishingly small imperfections and monotonically decreases with increasing amplitude of imperfection) are qualitatively consistent with those of (Lee et al., 2016) (e.g. see their figures 4 and 6), (Hutchinson,

2016) (e.g. see his figure 7) and (Jimenez et al., 2017) (e.g. see their figure 2) for small-amplitude imperfections and cannot be applied to arbitrarily large imperfections.

3.4 Imperfection sensitivity of specific biopolymer spherical shells

In this section, the effect of the non-axisymmetric buckling mode and mode interaction on imperfection sensitivity is studied for two typical biopolymer spherical shells: UCAs and spherical viruses. The physically relevant parameters for UCAs and spherical viruses are shown in table 2.1 and table 2.2, respectively. The actual maximum load an imperfect biopolymer spherical shell can sustain will be evaluated and compared to the prediction obtained in chapter 2 based on axisymmetric mode without mode interaction.

First, let us examine polymer-shelled UCAs, with the relevant parameters shown in table 2.1 suggested by (Chitnis et al., 2013) for the refined shell model (also see details in chapter 2). Two kinds of polymer-shelled UCAs, named by two manufacturers (Point and Philips), are employed in their study. Figure 3.4 shows the imperfection sensitivity based on the present non-axisymmetric analysis for polymer-shelled UCAs of an axisymmetric imperfection (figure 3.4a) and a non-axisymmetric imperfection (figure 3.4b), respectively. From Fig. 3.4, it is seen that the present non-axisymmetric analysis makes the maximum load reduced to approximately 40% (see the marked in the Fig. 3.4 and table 3.1) of that of a prefect spherical Point UCAs shell, or to approximately 2%-15% (see the marked in the Fig. 3.4 and table 3.1) of that of a prefect spherical Philips UCAs shell, respectively, which is around 25% or 5% lower than the prediction obtained in our previous work (see Fig. 2.6 in chapter 2 and table 3.1) based on axisymmetric mode without mode interaction, respectively.

Next, let us examine the imperfection sensitivity with physically relevant parameters shown in table 2.2 for some typical spherical viruses which are divided into four groups based on the parameters

($R/h, G^*/G, h_0/h$) and the nondimensional imperfection amplitude $\overline{\xi}_0$ or $\overline{\xi}_i$. The results shown in Fig. 3.5 are obtained based on the data in table 2.2. From Fig. 3.5, it is concluded that the present non-axisymmetric analysis makes the actual maximum load reduced to 25-40% (see the marked in the Fig. 3.5 and table 3.2) of that of a perfect spherical virus shell, which is around 30% lower than the prediction obtained in our previous work (see Fig. 2.7 in chapter 2 and table 3.2) based on axisymmetric mode without mode interaction.

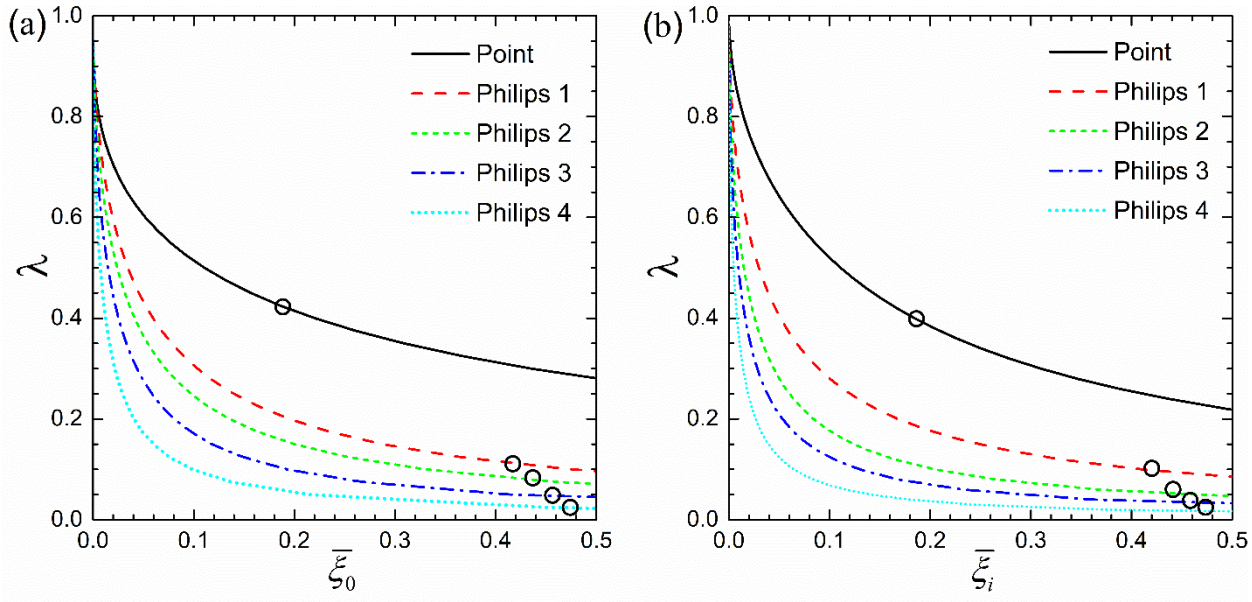

Fig. 3.4 The imperfection sensitivity of polymer-shelled UCAs with the relevant parameters listed in table 2.1 (a) axisymmetric geometric imperfection (b) non-axisymmetric geometric imperfection

Table 3.1 The comparison the reduction of the maximum load between the axisymmetric analysis in chapter 2 and the present non-axisymmetric analysis for two varieties of polymer-shelled UCAs.

UCA type	Axisymmetric analysis	Non-axisymmetric analysis (Axisymmetric imperfection)	Non-axisymmetric analysis (Non-axisymmetric imperfection)
Point	65%	40%	40%
Philips 1	20%	15%	13%
Philips 2	15%	10%	8%
Philips 3	10%	5%	4%
Philips 4	5%	2%	2%

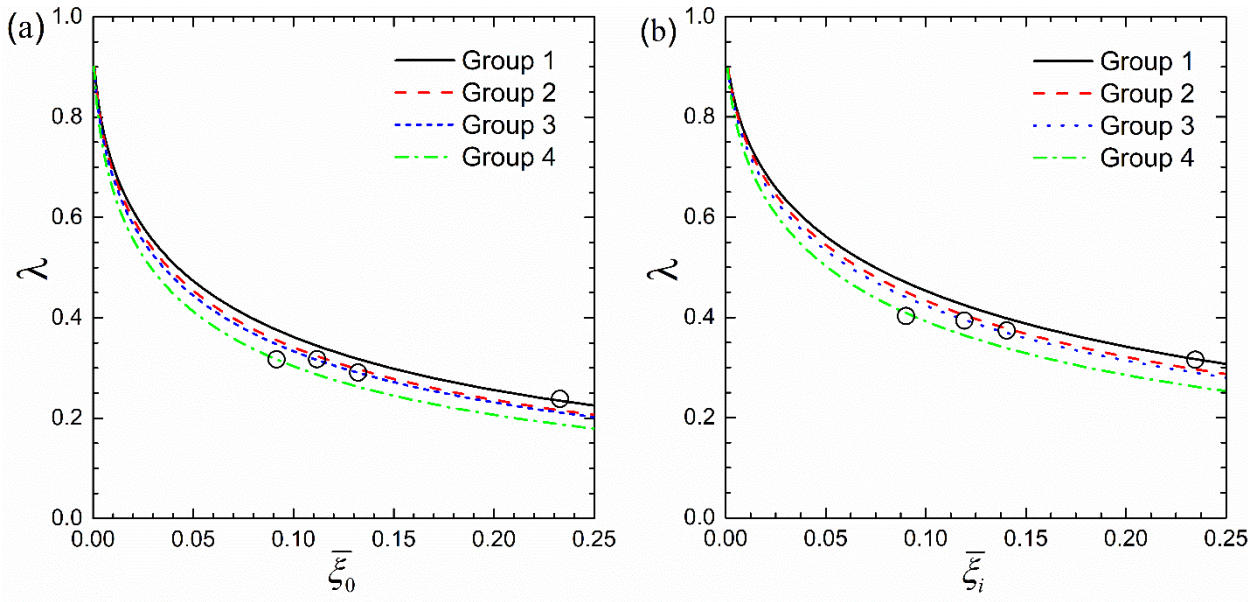

Fig. 3.5 The imperfection sensitivity of spherical virus shells with the relevant parameters listed in table 2.2 (a) axisymmetric geometric imperfection (b) non-axisymmetric geometric imperfection

Table 3.2 The comparison of the reduction of the maximum load between the axisymmetric analysis in chapter 2 and the present non-axisymmetric analysis for some typical spherical viruses.

Group	Axisymmetric analysis	Non-axisymmetric analysis (Axisymmetric imperfection)	Non-axisymmetric analysis (Non-axisymmetric imperfection)
1	55%	25%	30%
2	62%	30%	35%
3	64%	32%	37%
4	65%	31%	38%

3.5 Conclusions

The present chapter studies the effect of non-axisymmetric buckling modes and the associated mode interaction (up to four-mode interaction considered) on imperfection sensitivity of pressured buckling of structurally heterogeneous biopolymer spherical shells. Our results show that the maximum load (or the so-called "knockdown factor") predicted based on the present non-axisymmetric buckling modes with the mode interaction can be significantly lower than those predicted based on the axisymmetric mode without the mode interaction. For example, with physically realistic parameters for typical imperfect biopolymer spherical shells, the maximum load predicted by the present non-axisymmetric analysis drops to approximately 25%-40% of that of a prefect spherical virus shell, which is about 30% lower than the previous estimation based on axisymmetric mode without the mode interaction. Therefore, imperfection sensitivity of pressured buckling of biopolymer spherical shells can be significantly influenced by non-axisymmetric imperfections and non-axisymmetric modes with the mode interaction, although this influence can be relatively small (say, with a relative error less than 10%) for those biopolymer spherical shells with moderate radius-to-thickness ratio (say, less than 30) and smaller effective bending thickness (say, less than 0.2 times average shell thickness). This justifies the relevance of non-axisymmetric imperfection sensitivity with the mode interaction for biopolymer spherical shells of high geometric heterogeneity.

Chapter 4: Free vibration of biopolymer spherical shells of high structural heterogeneity

4.1 Introduction

This chapter aims to investigate the role of high structural heterogeneity and thickness nonuniformity on free vibration of biopolymer spherical shells. For this purpose, a refined shell model originally proposed in (Ru, 2009) for pressured buckling of biopolymer spherical shells (also employed by (Chitnis et al., 2011) to study rupture of ultrasound contrast agents) is employed, in which two additional parameters (called "effective bending thickness" and "transverse shear modulus") are added to the classical elastic homogeneous shell model to define the high structural heterogeneity and thickness nonuniformity. In section 4.2, using the analysis procedure for free vibration of a classical elastic spherical shell developed in several previous works, e.g. by (Wilkinson and Kalnins, 1965) and (Wilkinson, 1965, 1966), the refined shell model is used to study natural frequencies and associated vibration modes of a biopolymer spherical shell, for both axisymmetric and non-axisymmetric modes, respectively. Furthermore, in section 4.3, the role of high structural heterogeneity and thickness non-uniformity on free vibration of a biopolymer spherical shell is investigated by examining the effects of effective bending thickness and transverse shear modulus on natural frequencies and the associated vibration modes, with detailed comparison to the predictions given by the classical homogeneous shell model. Finally, main conclusions are summarized in section 4.4.

4.2 Basic equations for free vibration of a biopolymer spherical shell

In this section, linear axisymmetric and non-axisymmetric free vibration of a biopolymer spherical shell of high structure heterogeneity and thickness nonuniformity is studied based on the refined shell model proposed in (Ru, 2009). To this purpose, we shall adopt an analysis procedure similar to that developed in (Wilkinson and Kalnins, 1965) and (Wilkinson, 1965, 1966), on axisymmetric and non-axisymmetric vibration of a classical homogeneous spherical shell.

Consider a biopolymer spherical shell defined by the spherical coordinates φ ($0 \le \varphi \le \pi$), θ ($0 \le \theta \le 2\pi$) and z ($-h/2 \le z \le h/2$) (taken positive outward) and having middle surface radius R and average shell thickness h. The linear mid-face strains (including 2 transverse shear strains $e_{\theta z}$, $e_{\varphi z}$ and the change in curvatures k_φ, k_θ and $k_{\varphi\theta}$) of a spherical shell are given in terms of the displacements of the middle surface (u, v, w) and the rotations (α, β) of the normal of the middle surface in φ, θ directions by (Ru, 2009)

$$
\begin{gathered}
e_\varphi = \frac{1}{R}\frac{\partial u}{\partial \varphi} + \frac{w}{R}, \quad e_\theta = \frac{u}{R}\cot\varphi + \frac{1}{R\sin\varphi}\frac{\partial v}{\partial \theta} + \frac{w}{R}, \\
e_{\varphi\theta} = \frac{1}{R\sin\varphi}\frac{\partial u}{\partial \theta} + \frac{1}{R}\frac{\partial v}{\partial \varphi} - \frac{v}{R}\cot\varphi, \quad e_{\varphi z} = \frac{1}{R}\frac{\partial w}{\partial \varphi} - \frac{u}{R} + \alpha, \quad e_{\theta z} = \frac{1}{R\sin\varphi}\frac{\partial w}{\partial \theta} - \frac{v}{R} + \beta, \\
k_\varphi = \frac{1}{R}\frac{\partial \alpha}{\partial \varphi}, \quad k_\theta = \frac{\alpha}{R}\cot\varphi + \frac{1}{R\sin\varphi}\frac{\partial \beta}{\partial \theta}, \quad k_{\varphi\theta} = \frac{1}{R\sin\varphi}\frac{\partial \alpha}{\partial \theta} + \frac{1}{R}\frac{\partial \beta}{\partial \varphi} - \frac{\beta}{R}\cot\varphi.
\end{gathered}
\tag{4.1}
$$

Furthermore, based on the isotropic linear plane-stress stress-strain relation, the in-plane resultant membrane forces, bending moments and transverse shear forces are given by (Ru, 2009)

$$
\begin{gathered}
\begin{bmatrix} N_\varphi \\ N_\theta \end{bmatrix} = \frac{Eh}{1-\mu^2}\begin{bmatrix} 1 & \mu \\ \mu & 1 \end{bmatrix}\begin{bmatrix} e_\varphi \\ e_\theta \end{bmatrix}, \quad N_{\varphi\theta} = Ghe_{\varphi\theta}, \\
\begin{bmatrix} M_\varphi \\ M_\theta \end{bmatrix} = D\begin{bmatrix} 1 & \mu \\ \mu & 1 \end{bmatrix}\begin{bmatrix} \kappa_\varphi \\ \kappa_\theta \end{bmatrix}, \quad M_{\varphi\theta} = D_{12}\kappa_{\varphi\theta}, \\
Q_\varphi = k_s G^* h e_{\varphi z}, \quad Q_\theta = k_s G^* h e_{\theta z},
\end{gathered}
\tag{4.2}
$$

where E is Young's modulus, μ is Poisson's ratio of the biopolymer shell, k_s is the shear coefficient (e.g. 5/6 in (Kraus, 1967)), G^* is the transverse shear modulus, G is the common in-plane shear modulus determined by (E, μ), and the bending stiffnesses of a biopolymer spherical shell are assumed to be determined by an effective bending thickness h_0 as

$$D = \frac{Eh_0^3}{12\left(1-\mu^2\right)}, \qquad D_{12} = \frac{Gh_0^3}{12}. \tag{4.3}$$

Likewise, for biopolymer shells, it is assumed that transverse shear modulus G^* can be much lower than the in-plane shear modulus G, and the effective bending thickness h_0 can be considerably different from the average shell thickness h (Ru, 2009). It is the two additional parameters (G^*, h_0) which distinguish a biopolymer shell of high structural heterogeneity and thickness non-uniformity from a classical elastic shell defined by (E, μ, h).

Finally, five equations of motion for five unknowns u, v, w, α, β of linearized free vibration of a spherical shell are given as follows (Kraus, 1967; Ru, 2009; Wilkinson and Kalnins, 1965)

$$\begin{aligned}
&\frac{\partial N_\varphi}{\partial \varphi} + \frac{\partial N_{\varphi\theta}}{\partial \theta}\csc\varphi + (N_\varphi - N_\theta)\cot\varphi + Q_\varphi = R\rho h\left(k_1\frac{\partial^2 u}{\partial t^2} + Rk_2\frac{\partial^2 \alpha}{\partial t^2}\right),\\
&\frac{\partial N_{\varphi\theta}}{\partial \varphi} + \frac{\partial N_\theta}{\partial \theta}\csc\varphi + 2N_{\varphi\theta}\cot\varphi + Q_\theta = R\rho h\left(k_1\frac{\partial^2 v}{\partial t^2} + Rk_2\frac{\partial^2 \beta}{\partial t^2}\right),\\
&\frac{\partial Q_\varphi}{\partial \varphi} + \frac{\partial Q_\theta}{\partial \theta}\csc\varphi + Q_\varphi\cot\varphi - (N_\varphi + N_\theta) = R\rho h k_1\frac{\partial^2 w}{\partial t^2},\\
&\frac{\partial M_\varphi}{\partial \varphi} + \frac{\partial M_{\varphi\theta}}{\partial \theta}\csc\varphi + (M_\varphi - M_\theta)\cot\varphi - RQ_\varphi = \frac{R\rho h^3}{12}\left(\frac{c_r}{R}\frac{\partial^2 u}{\partial t^2} + k_r\frac{\partial^2 \alpha}{\partial t^2}\right),\\
&\frac{\partial M_{\varphi\theta}}{\partial \varphi} + \frac{\partial M_\theta}{\partial \theta}\csc\varphi + 2M_{\varphi\theta}\cot\varphi - RQ_\theta = \frac{R\rho h^3}{12}\left(\frac{c_r}{R}\frac{\partial^2 v}{\partial t^2} + k_r\frac{\partial^2 \beta}{\partial t^2}\right),
\end{aligned} \tag{4.4}$$

where the tracers are given by $k_1 = 1 + \frac{1}{12}\left(\frac{h}{R}\right)^2$, $k_2 = \frac{1}{6}\left(\frac{h}{R}\right)^2$, $k_r = 1 + \frac{3}{20}\left(\frac{h}{R}\right)^2$, $c_r = 2$ (Kraus, 1967; Wilkinson and Kalnins, 1965), t is time, and ρ denotes the mass density of the shell.

4.2.1 Axisymmetric free vibration of a biopolymer spherical shell

First, let us investigate axisymmetric free vibration of a biopolymer spherical shell. For this case, we set all θ-variations in Eqs. (4.1) and (4.4) to zero, thus five equations (Eq. (4.4)) are reduced to three equations (the first, third and fourth equations of (4.4)) for u, w, α (spheroidal mode) and two equations (the second and fifth equations of (4.4)) for v, β (torsional mode), and the former is decoupled from the latter. Therefore, axisymmetric motions of a spherical shell are either of a spheroidal mode with no motion in the circumferential direction, or of a torsional mode in which the motion is exclusively in the circumferential direction (Wilkinson, 1966). This remains true for the refined shell model as confirmed in the present work. Now let us discuss the two cases separately.

4.2.1.1 Frequency equation for spheroidal vibration modes

The equations governing axisymmetric spheroidal deformations of a biopolymer spherical shell are written for three unknowns u, w, α as follows (the first, third and fourth equations of (4.4) with setting θ-variations to zero, and the other two unknowns v, β vanish) (Wilkinson, 1966)

$$\frac{\partial N_\varphi}{\partial \varphi}+(N_\varphi-N_\theta)\cot\varphi+Q_\varphi=R\rho h\left(k_1\frac{\partial^2 u}{\partial t^2}+Rk_2\frac{\partial^2 \alpha}{\partial t^2}\right),$$
$$\frac{\partial Q_\varphi}{\partial \varphi}+Q_\varphi\cot\varphi-(N_\varphi+N_\theta)=R\rho h k_1\frac{\partial^2 w}{\partial t^2}, \tag{4.5}$$
$$\frac{\partial M_\varphi}{\partial \varphi}+(M_\varphi-M_\theta)\cot\varphi-RQ_\varphi=\frac{R\rho h^3}{12}\left(\frac{c_r}{R}\frac{\partial^2 u}{\partial t^2}+k_r\frac{\partial^2 \alpha}{\partial t^2}\right),$$

In a similar way as (Wilkinson, 1966), let us define u and Q_φ in terms of two auxiliary functions f, g as

$$u=\frac{\partial f}{\partial \varphi},\qquad Q_\varphi=\frac{\partial g}{\partial \varphi} \tag{4.6}$$

Setting all θ-variations in Eq. (4.1) to zero, introducing Eqs. (4.1), (4.2) and (4.6) into Eqs. (4.5) and assuming that the time dependence of all shell variables (u, w, α) is of the form $\cos\omega t$, where ω is the angular frequency, we have three equations for (w, f, g)

$$\left(\nabla^2+A_1\right)f+\frac{R}{Eh}A_2 g+A_3 w=0,$$
$$B_1\nabla^2 f+\frac{R}{Eh}\left(B_2\nabla^2+B_3\right)g-\left(\nabla^2-B_4\right)w=0, \tag{4.7}$$
$$\frac{Eh}{R}C_1\nabla^2 f+\nabla^2 g+\frac{Eh}{R}C_2 w=0,$$

where

$$A_1=(1-\mu)+\Omega^2\left(k_1+k_2\right),\quad A_2=\left(1-\mu^2\right)+2\Omega^2\left(1+\mu\right)\frac{k_2}{k_s}\frac{G}{G^*},\quad A_3=(1+\mu)-\Omega^2 k_2,$$
$$B_1=(1-\mu)+\Omega^2\left(\frac{h}{h_0}\right)^3\left(c_r+k_r\right),\qquad B_2=\frac{2(1+\mu)}{k_s}\frac{G}{G^*},$$
$$B_3=\frac{2\left(1-\mu^2\right)}{k_s}\frac{G}{G^*}-12\left(1-\mu^2\right)\left(\frac{R}{h}\right)^2\left(\frac{h}{h_0}\right)^3+2\Omega^2\frac{(1+\mu)}{k_s}\frac{G}{G^*}\left(\frac{h}{h_0}\right)^3 k_r, \tag{4.8}$$
$$B_4=-(1-\mu)-\Omega^2\left(\frac{h}{h_0}\right)^3 k_r,\qquad C_1=\frac{-1}{1-\mu},\qquad C_2=\frac{-2}{1-\mu}+\frac{k_1}{1-\mu^2}\Omega^2,$$

and Ω^2 denotes the dimensionless natural frequency defined by

$$\Omega^2 = \frac{\rho R^2 \omega^2 (1-\mu^2)}{E}. \tag{4.9}$$

By treating the Laplacian operator as an algebraic quantity, we can derive from Eqs. (4.7) an uncoupled equation in the radial displacement w

$$\nabla^6 w + W_1 \nabla^4 w + W_2 \nabla^2 w + W_3 w = 0, \tag{4.10}$$

where Laplacian operator for the axisymmetric case takes the form $\nabla^2(\ ) = \frac{\partial^2(\ )}{\partial \varphi^2} + \cot\varphi \frac{\partial(\ )}{\partial \varphi}$ and

$$\begin{aligned} W_1 &= A_1 + A_3 - B_4 - A_2 C_1 - A_3 B_2 C_1 + B_2 C_2, \\ W_2 &= -A_1 B_4 + A_3 B_1 + A_2 B_4 C_1 - A_3 B_3 C_1 - A_2 C_2 + B_3 C_2 + A_1 B_2 C_2, \\ W_3 &= A_1 B_3 C_2 - A_2 B_1 C_2. \end{aligned} \tag{4.11}$$

In the case of axisymmetric motion of a complete closed spherical shell, the radial displacement w of the spheroidal modes is given by (Wilkinson, 1965)

$$w = \zeta_0 P_n(\cos\varphi)\cos\omega t, \tag{4.12}$$

where ζ_0 is arbitrary constant, n is any non-negative integer ($n = 0, 1, 2, 3, \ldots$), and $P_n(\cos\varphi)$ is the Legendre-polynomial of degree n. Introducing Eqs. (4.8), (4.11) and (4.12) into Eq. (4.10) and considering the identity $\nabla^2 P_n(\cos\varphi) = -n(n+1) P_n(\cos\varphi)$, the resulting frequency equation may be written as a cubic equation in Ω^2 as follows

$$\Omega^6\left[\frac{2k_1}{k_s(1-\mu)}(k_1k_r-k_2c_r)\frac{G}{G^*}\left(\frac{h}{h_0}\right)^3\right]-\Omega^4\left\{(k_1k_r-k_2c_r)\left[r\left(\frac{h}{h_0}\right)^3+\frac{4(1+\mu)}{k_s(1-\mu)}\frac{G}{G^*}\left(\frac{h}{h_0}\right)^3\right]\right.$$
$$\left.+k_1\left[\eta(k_1+k_2)+(c_r+k_r)\left(\frac{h}{h_0}\right)^3+\frac{2}{k_s}\left(k_1+k_r\left(\frac{h}{h_0}\right)^3\right)\frac{G}{G^*}\left(\frac{r}{1-\mu}-1\right)\right]\right\}$$
$$+\Omega^2\left\{(1+\mu)(2-r)\left(\eta k_2+\left(\frac{h}{h_0}\right)^3 c_r\right)+k_r\left[r(r-3-\mu)\left(\frac{h}{h_0}\right)^3+2(1+\mu)\right.\right. \tag{4.13}$$
$$\times\left(\frac{(r-2)}{k_s}\frac{G}{G^*}+1\right)\left(\frac{h}{h_0}\right)^3\Big]+k_1\left[\frac{2}{k_s(1-\mu)}r(r+4\mu)\frac{G}{G^*}+r(r+\eta+\mu)+(1+3\mu)\right.$$
$$\left.\left.\times\left(\eta-\frac{2}{k_s}\frac{G}{G^*}\right)-(1-\mu)\right]\right\}-(r-2)\left[r(r-2)+\frac{2(1+\mu)}{k_s}(r-1+\mu)\frac{G}{G^*}+(1-\mu^2)(\eta+1)\right]=0,$$

where $\eta=12\left(\frac{R}{h}\right)^2\left(\frac{h}{h_0}\right)^3$ and $r=n(n+1)$. It is noted that the frequency equation (4.13) given by the present refined model reduces to the classical formula (1.3) when $G^*=G$ and $h_0=h$, as expected.

It is confirmed by solving Eq. (4.13) with *Mathematica* that for the present refined model with physically realistic parameters of biopolymer spherical shells, there are always three positive roots $\Omega_1,\Omega_2,\Omega_3$ ($\Omega_1<\Omega_2<\Omega_3$) for $n=1,2,3,...$ and two positive roots Ω_2,Ω_3 for $n=0$, which give dimensionless natural frequencies. For example, the dimensionless natural frequencies for different values of *n* are plotted in Fig. 4.1 for the parameters $k_s=5/6$, $\mu=0.3$, $R/h=10$, $G^*/G=1.0$ and $h_0/h=1.0$, which is identical to figure 1 in (Wilkinson, 1965).

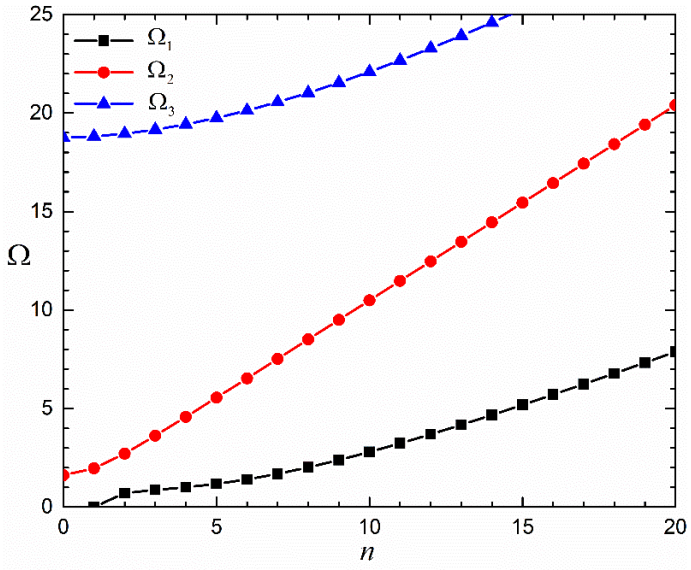

Fig. 4.1 The dimensionless natural frequencies corresponding to different values of n

The radial displacement w of the associated vibration mode is given by (4.12), while the associated tangential displacement u and rotation α can be obtained based on Eq. (4.6), in which the expressions of f and g can be derived from Eqs. (4.7) as

$$\begin{aligned} F_1 f &= F_2\nabla^4 w + F_3\nabla^2 w + F_4 w, \\ G_1 g &= \frac{Eh}{R}\left(G_2\nabla^4 w + G_3\nabla^2 w + G_4 w\right), \end{aligned} \tag{4.14}$$

where $F_1, F_2, F_3, F_4, G_1, G_2, G_3, G_4$, which are also used in the following non-axisymmetric analysis, are related to the parameters defined in (4.8), as given in Appendix F.

It is seen that because w given by (Eq. (4.12)) only depends on the value of n, the radial displacements w of different vibration modes corresponding to the same value of n are the same. However, because u and α given by Eq. (4.6) depend on the value of dimensionless natural frequency Ω, the tangential displacements u and rotations α of different vibration modes corresponding to the same value of n are different.

4.2.1.2 Frequency equation for torsional vibration modes

In the torsional case, axisymmetric motion of a biopolymer spherical shell is governed by the following two equations for two unknowns v,β (the second and fifth equations of (4.4)) with setting θ-variations to zero, and the other three unknowns u,w,α vanish) (Wilkinson, 1966)

$$\begin{aligned}
&\frac{\partial N_{\varphi\theta}}{\partial\varphi}+2N_{\varphi\theta}\cot\varphi+Q_\theta=R\rho h\left(k_1\frac{\partial^2 v}{\partial t^2}+Rk_2\frac{\partial^2\beta}{\partial t^2}\right),\\
&\frac{\partial M_{\varphi\theta}}{\partial\varphi}+2M_{\varphi\theta}\cot\varphi-RQ_\theta=\frac{R\rho h^3}{12}\left(\frac{c_r}{R}\frac{\partial^2 v}{\partial t^2}+k_r\frac{\partial^2\beta}{\partial t^2}\right).
\end{aligned}\tag{4.15}$$

Similarly, Setting all θ-variations in Eq. (4.1) to zero, introducing Eqs. (4.1), (4.2) into Eqs. (4.15) and assuming that the time dependence of all shell variables (v,β) is of the form $\cos\omega t$, we have two coupled equations in v and Q_θ

$$\begin{aligned}
\left(\nabla_1^{\,2}+\frac{2A_1}{1-\mu}\right)v+\frac{R}{Eh}\left(\frac{2A_2}{1-\mu}\right)Q_\theta=0,\\
\left(\nabla_1^{\,2}+\frac{2B_1}{1-\mu}\right)v+\frac{R}{Eh}\left(B_2\nabla_1^{\,2}+\frac{2B_3}{1-\mu}\right)Q_\theta=0,
\end{aligned}\tag{4.16}$$

where $\nabla_1^{\,2}(\ )=\dfrac{\partial^2(\ )}{\partial\varphi^2}+\cot\varphi\dfrac{\partial(\ )}{\partial\varphi}-(\ )\csc^2\varphi$. Then, by treating $\nabla_1^{\,2}$ as an algebraic quantity, one may obtain an uncoupled equation in the tangential displacement v

$$V_1\nabla_1^{\,4}v+V_2\nabla_1^{\,2}v+V_3v=0,\tag{4.17}$$

where

$$V_1=B_2(1-\mu)^2,\quad V_2=2(1-\mu)(-A_2+B_3+A_1B_2),\quad V_3=4A_1B_3-4A_2B_1.\tag{4.18}$$

In the case of axisymmetric motion of a complete closed spherical shell, the tangential displacement v of the torsional modes is given by (Wilkinson, 1965)

$$v = \zeta_1 P_k^1(\cos\varphi)\cos\omega t, \tag{4.19}$$

where ζ_1 is arbitrary constant, k is any non-negative integer ($k = 0,1,2,3,...$), and $P_k^1(\cos\varphi)$ is the associated Legendre-polynomial of degree k and order 1. Then introducing Eq. (4.19) into Eq. (4.17) and considering the identity $\nabla_1^2 P_k^1(\cos\varphi) = -k(k+1)P_k^1(\cos\varphi)$, we obtain the following quadratic frequency equation in Ω^2

$$\begin{aligned}\Omega^4\left[\frac{4}{k_s(1-\mu)}(k_1k_r - k_2c_r)\frac{G}{G^*}\left(\frac{h}{h_0}\right)^3\right] - 2\Omega^2\left[\eta(k_1+k_2)+(c_r+k_r)\left(\frac{h}{h_0}\right)^3\right.\\ \left.+\frac{1}{k_s}\left(k_1+k_r\left(\frac{h}{h_0}\right)^3\right)\frac{G}{G^*}(r-2)\right]+(1-\mu)(r-2)\left[\frac{r-2}{k_s}\frac{G}{G^*}+(\eta+1)\right]=0,\end{aligned} \tag{4.20}$$

where $\eta = 12\left(\frac{R}{h}\right)^2\left(\frac{h}{h_0}\right)^3$ and $r = k(k+1)$. It is also noted that the frequency equation (4.20) given by the present refined model reduces to the classical formula (1.4) when $G^* = G$ and $h_0 = h$, as expected.

Similarly, it is confirmed by solving Eq. (4.20) with *Mathematica* that for the refined model with physically realistic parameters of biopolymer spherical shells, there are always two positive roots Ω_4, Ω_5 ($\Omega_4 < \Omega_5$) for $k = 1,2,3,...$ and one positive root Ω_5 for $k = 0$, which give dimensionless natural frequencies. For example, the dimensionless natural frequencies for different values of *k* are plotted in Fig. 4.2 for the parameters $k_s = 5/6$, $\mu = 0.3$, $R/h = 10$, $G^*/G = 1.0$ and $h_0/h = 1.0$, which is identical to figure 2 in (Wilkinson, 1965).

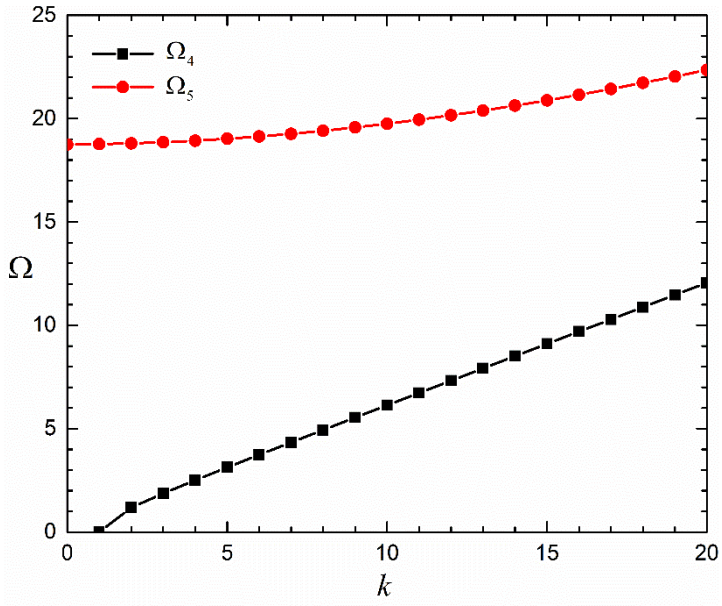

Fig. 4.2 The dimensionless natural frequencies corresponding to different values of k

The tangential displacement v in the θ (circumferential) direction of the associated vibration mode is given by (4.19), while the associated rotation β in the circumferential direction can be obtained based on the expression of Q_θ, which is derived from Eqs. (4.16) as

$$Q_\theta = -\frac{Eh}{R}\frac{1}{A_2}\left(\frac{1-\mu}{2}\nabla_1^2 v + A_1 v\right). \tag{4.21}$$

It is seen that because v given by (Eq. (4.19)) only depends on the value of k, the tangential displacements v of different vibration modes corresponding to the same value of k are the same. However, because β given by Eq. (4.21) depends on the valve of dimensionless natural frequency Ω, the rotations β of different vibration modes corresponding to the same value of k are different.

Therefore, for axisymmetric free vibration of a biopolymer spherical shell, for given parameters $(\mu, k_s, R/h, G^*/G, h_0/h)$, one can determine the dimensionless nature frequencies from Eq. (4.13) or Eq. (4.20) for each value of n or k, respectively. Thus, there are total five natural frequencies

associated with each pair (n, k). Three of them, determined by Eq. (4.13) for each value of n, are associated with the spheroidal modes (i.e. torsionless modes in (Wilkinson and Kalnins, 1965), or coupled bending-stretching modes in (Rochal et al., 2017)), and the other two, determined by Eq. (4.20) for each value of k, are associated with the torsional modes (i.e. toroidal modes in (Mcgee and Spry, 1997), or thickness-shear modes in (Kraus, 1967)). For the spheroidal modes, the radial displacement w is given by (4.12) while the tangential displacement u and the rotation α in φ direction are determined from (4.6) and (4.14). For the torsional modes, the tangential displacement v is given by (4.19) while the rotation β in θ direction is obtained from (4.21). Therefore, the spheroidal modes have radial and tangential components while the torsional modes have only a tangential component.

4.2.2 Non-axisymmetric free vibration of a biopolymer spherical shell

Next, let us investigate non-axisymmetric free vibration. In a similar way as (Wilkinson and Kalnins, 1965), let us define u, v and Q_φ, Q_θ in terms of four auxiliary functions f, g, ψ, Λ as

$$\begin{aligned} u &= \frac{\partial f}{\partial \varphi} - \psi \sin\varphi, \qquad v = \frac{\partial f}{\partial \theta}\csc\varphi, \\ Q_\varphi &= \frac{\partial g}{\partial \varphi} - \Lambda \sin\varphi, \quad Q_\theta = \frac{\partial g}{\partial \theta}\csc\varphi. \end{aligned} \tag{4.22}$$

Similar to the axisymmetric case, introducing Eqs.(4.1), (4.2) and (4.22) into Eqs. (4.4) and assuming that the time dependence of all shell variables (u, v, w, α, β) is of the form $\cos\omega t$, one gets two uncoupled equations (one is same as Eq. (4.10) and the other is similar to Eq. (4.17) with ψ in place of v) for (w, ψ) given by (for detailed procedure based on (Kalnins, 1961; Wilkinson and Kalnins, 1965), see Appendix F)

$$\nabla^6 w + W_1 \nabla^4 w + W_2 \nabla^2 w + W_3 w = 0 \tag{4.23}$$

and

$$V_1 \nabla^4 \psi + V_2 \nabla^2 \psi + V_3 \psi = 0, \tag{4.24}$$

where the Laplacian operator for the non-axisymmetric case takes the form $\nabla^2 (\ ) = \frac{\partial^2 (\ )}{\partial \varphi^2} + \cot\varphi \frac{\partial (\ )}{\partial \varphi} + \csc^2 \varphi \frac{\partial^2 (\ )}{\partial \theta^2}$. The remaining three auxiliary functions (f, g, Λ) are related to w and ψ by (see details in Appendix F)

$$\begin{aligned} \Lambda &= -\frac{Eh}{R}\frac{1}{A_2}\left(\frac{1-\mu}{2}\nabla^2 \psi + A_1 \psi\right), \\ F_1 f &= F_2 \nabla^4 w + F_3 \nabla^2 w + F_4 w + F_5 \frac{\partial \psi}{\partial \varphi}\sin\varphi + F_6 \frac{\partial \Lambda}{\partial \varphi}\sin\varphi, \\ G_1 g &= \frac{Eh}{R}\left(G_2 \nabla^4 w + G_3 \nabla^2 w + G_4 w + G_5 \frac{\partial \psi}{\partial \varphi}\sin\varphi + G_6 \frac{\partial \Lambda}{\partial \varphi}\sin\varphi\right) \end{aligned} \tag{4.25}$$

where the parameters $F_1, F_2, F_3, F_4, F_5, F_6, G_1, G_2, G_3, G_4, G_5, G_6$ are related to parameters in (4.8) as given in Appendix F. It is also proved that Eqs. (4.23), (4.24), (4.25) reduce to the classical formulas (see Eqs. (3)-(7) in (Wilkinson and Kalnins, 1965) for the non-axisymmetric vibration) when $G^* = G$ and $h_0 = h$, as expected.

In the non-axisymmetric case, for a complete spherical shell, the general solutions of (4.23) and (4.24) are a linear combination of solutions of the separable form (Bryan, 2017; Wilkinson and Kalnins, 1965)

$$w = \left[\sum_{m=-n}^{n} \tau_m \cos m\theta P_n^m (\cos\varphi)\right] \cos \omega t \tag{4.26}$$

and

$$\psi = \left[\sum_{m=-k}^{k} \overline{\tau}_m \cos m\theta P_k^m \left(\cos\varphi \right) \right] \cos \omega t, \tag{4.27}$$

where $\tau_m, \overline{\tau}_m$ are arbitrary constants, $P_n^m \left(\cos\varphi \right)$ is the associated Legendre-polynomial of degree n and order m, and the indexes n and k are two non-negative integers.

It can be easily verified that natural frequencies depend on the integer *n* or k but are independent of *m*. In view of the fact that the governing equations (4.23) and (4.24) for non-axisymmetric vibration are the same as the governing equations (4.10) and (4.17) for axisymmetric vibration, frequencies equations for non-axisymmetric vibration are identical to the frequencies equations Eqs. (4.13) and (4.20) for axisymmetric vibration. Thus it is concluded that for each non-negative integer value of *n* or *k*, the dimensionless natural frequencies for non-axisymmetric vibration are identical to the dimensionless natural frequencies for axisymmetric vibration and can be determined by the frequencies equations Eqs. (4.13) and (4.20) for axisymmetric vibration.

Therefore, for given parameters ($\mu, k_s, R/h, G^*/G, h_0/h$), the natural frequencies and the associated vibration modes (u, v, w, α, β) for non-axisymmetric vibration of a biopolymer spherical shell can be determined, as illustrated below for the case of the parameters ($k_s = 5/6$, $\mu = 0.3$, $R/h = 10$, $G^*/G = 1.0$ and $h_0/h = 1.0$) used in Figs. 4.1 and 4.2. First, for any non-negative integer *n* (say, *n*=5), the radial displacement w can be determined by Eq. (4.26), and the three dimensionless natural frequencies can be obtained through Eq. (4.13) (see Fig. 4.1). For example, it is seen from Fig. 4.1 that the lowest natural frequency for *n*=5 gives $\Omega = 1.0$. Next, to determine the corresponding tangential displacements u, v and rotations α, β from Eqs. (4.22) and (4.25)), the corresponding value of the non-negative integer *k* can be determined as the nearest natural number by introducing the natural

frequency $\Omega = 1.0$ into Eq. (4.20) (see Fig. 4.2, with $\Omega = 1.0$, the nearest natural number k=2). Thus, the four auxiliary functions f, g, ψ, Λ can be determined by (4.25) and (4.27), and the corresponding tangential displacements u, v and rotations α, β are obtained through Eq. (4.22). Therefore, for non-axisymmetric free vibration of biopolymer spherical shells, corresponding to a natural frequency, the values of n and k can be determined by Eqs. (4.13) and (4.20), respectively. Then, the corresponding vibration modes (u, v, w, α, β) can be obtained by Eqs. (4.22), (4.25), (4.26) and (4.27).

It is seen from the representation (4.26) that there are in general (2n+1) independent vibrational modes corresponding to each natural frequency (one of which is an axisymmetric mode, while all other 2n modes are non-axisymmetric), consistent with the conclusion made by (Silbiger, 1962) for classical spherical shells. Because of spherical symmetry, the frequencies of the non-axisymmetric modes are identical to the frequencies of the axisymmetric modes of the same integer n. The statements of Silbiger (Silbiger, 1962) regarding the number of independent modes, 2n+1, are confirmed by simulations (see figures 4 and 5 in (Duffey et al., 2007)) and theoretical verification (see figure 4 in (Bryan, 2017)) for classical homogeneous shell. As we shown here, all of these results remain valid for the present refined shell model for biopolymer spherical shells of high structural heterogeneity.

4.3 Influence of high structural heterogeneity on vibration of a biopolymer spherical shell

The major goal of this work is to examine how the high structural heterogeneity, defined by the key parameters ($R/h, G^*/G, h_0/h$), affects the natural frequencies and vibration modes of a biopolymer spherical shell. Now, let us investigate how these parameters influence free vibrational of a biopolymer spherical shell with their physically realistic values.

4.3.1 The influence on axisymmetric free vibration

For the axisymmetric case, the three frequencies of the spheroidal vibration modes determined by Eq. (4.13) are denoted by $\Omega_1, \Omega_2, \Omega_3$ ($\Omega_1 < \Omega_2 < \Omega_3$), while the two frequencies of the torsional vibration modes determined by Eq. (4.20) are denoted by Ω_4, Ω_5 ($\Omega_4 < \Omega_5$).

4.3.1.1 The influence of key parameters

Let us now investigate how the key parameters ($R/h, G^*/G, h_0/h$) influence the axisymmetric vibration frequencies and the associated vibrational modes. It is known that for biopolymer spherical shells, the low-lying frequencies and the associated vibration modes are usually involved in their biological functions, and one can gain insights into the collective motions relevant to biological function by examining the lowest frequency modes (Balandin and Fonoberov, 2005; Bergman and Lezon, 2017; Dykeman and Sankey, 2008, 2009, 2010; Ford, 2003; Ghavanloo and Fazelzadeh, 2015; Kahn et al., 2001; May et al., 2011; May and Brooks, 2011, 2012; May, 2014; Peeters and Taormina, 2008, 2009; Talati and Jha, 2006; Tama and Brooks, 2005; Tsen et al., 2006, 2007; Wells et al., 2015; Widom et al., 2007; Yang et al., 2009). Therefore, we shall focus on the dimensionless natural frequency Ω_1 and Ω_2 for spheroidal modes and Ω_4 for the torsional modes (see Figs. 4.1 and 4.2 that Ω_3 is much larger than Ω_1 and Ω_2, and Ω_5 is much larger than Ω_4 for same value of *n* and *k*, respectively).

Let us first investigate the influence of the parameter R/h, for fixed values $k_s = 5/6$, $\mu = 0.3$, $G^*/G = 1.0$ and $h_0/h = 1.0$. In this case, the present refined model reduces to the classical shell model (Eqs. (4.13) and (4.20) reduce to Eqs. (1.3) and (1.4)), and the effect of R/h on the natural frequencies of a classical spherical shell has been investigated (e.g. see (Bryan, 2017; Mcgee and Spry, 1997; Talati

and Jha, 2006)). For the present study, the dependence of the dimensionless natural frequency Ω given by Eq. (4.13) for the spheroidal modes and Eq. (4.20) for the torsional modes on the non-negative integer *n* or *k* is shown in Figs. 4.3a and 4.3b, respectively, for a range of R/h between 5 and 50. It is seen from Figs. 4.3a and 4.3b that the frequencies of the spheroidal modes decrease with increasing value of R/h, which is consistent with the known results (see e.g. table II in (Talati and Jha, 2006), table IV and figure 3 in (Mcgee and Spry, 1997), and figure 2 in (Bryan, 2017)). On the other hand, the frequencies of the torsional modes remain fairly unchanged when R/h varies from $R/h=5$ to $R/h=50$, which is consistent with known results (e.g. Table V and figure 4 in (Mcgee and Spry, 1997)).

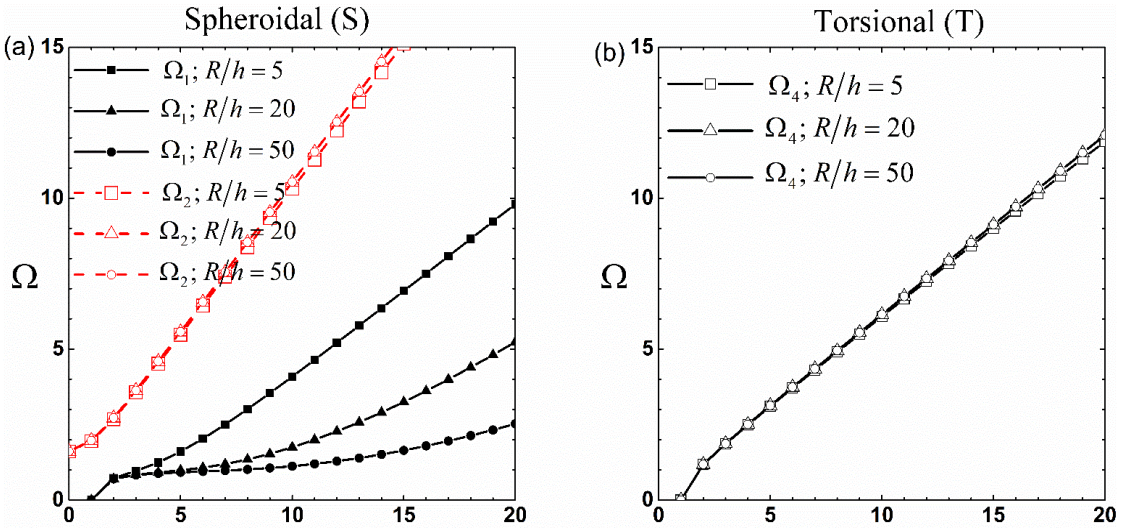

Fig. 4.3 The effect of R/h on natural frequencies

Next let us examine the effect of transverse shear modulus G^*/G and effective bending thickness h_0/h on the vibration frequencies and the associated modes for fixed values $k_s=5/6$ and $\mu=0.3$. The influence of varying G^*/G within the range [0.01, 1] (with fixed value $h_0/h=1.0$), and the influence of varying h_0/h within the range [0.2, 1] (with fixed value $G^*/G=1.0$) on the natural frequencies of a spherical shell are illustrated in Figs. 4.4 and 4.5 for three different values of R/h,

respectively. It is seen from Figs. 4.4 and 4.5 that when G^*/G decreases from 1.0 to 0.01, or when h_0/h decreases from 1.0 to 0.2, the frequencies of the spheroidal modes decrease substantially (especially for larger *n*) for thicker and small-radius spherical shells (defined by smaller value of R/h), while the decrease is negligible for thinner and larger-radius spherical shells. On the other hand, transverse shear modulus and effective bending thickness have almost no effect on the vibration frequencies of the torsional modes.

The Stick spectrum of the corresponding vibration modes for the cases illustrated in Figs. 4.4 and 4.5 are shown in Figs. 4.6 and 4.7, respectively, where the horizontal axis denotes the vibration modes ("S" denotes the spheroidal modes and "T" denotes the torsional modes) and the vertical axis denotes the corresponding dimensionless natural frequencies Ω. Similar stick spectrums of vibration of some spherical viruses can be seen in (Dykeman and Sankey, 2010) (see their figures 4, 7, 11). It can be seen from Figs. 4.6 and 4.7 that G^*/G and h_0/h have a significant effect on the vibration modes of thicker and small-radius spherical shells. Specifically, for thicker and small-radius spherical shells, if transverse shear modulus is much lower than the in-plane shear modulus or/and the effective bending thickness is considerably smaller than the average thickness, the spheroidal modes of shorter wavelength (corresponding to larger integer *n,* as seen in Figs. 4.4a and 4.5a) become the dominant modes in the low frequency range (say $0.5 < \Omega < 2$).

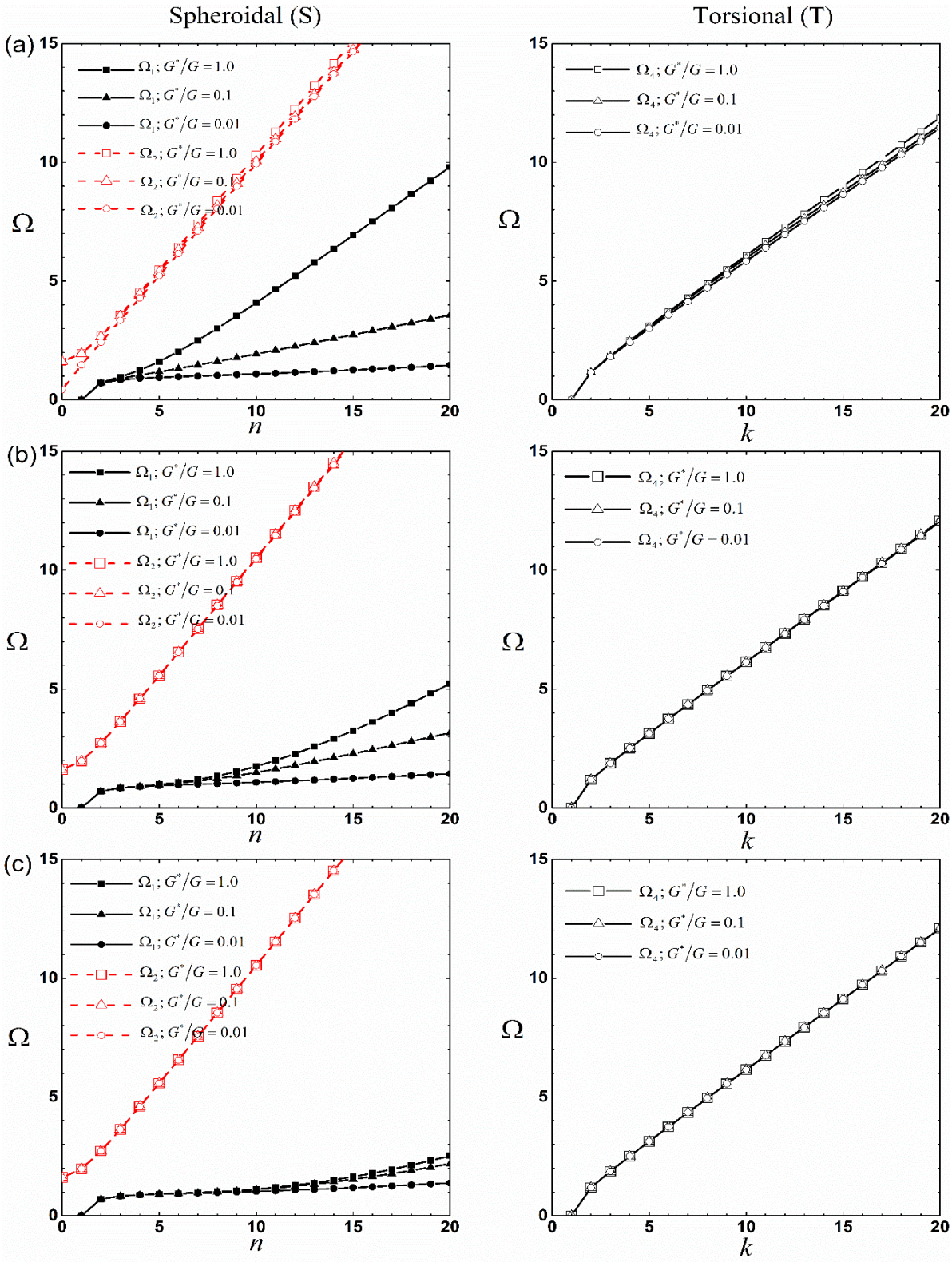

Fig. 4.4 The effect of G^*/G on natural frequencies for three values of R/h. (a) $R/h = 5$; (b) $R/h = 20$; (c) $R/h = 50$

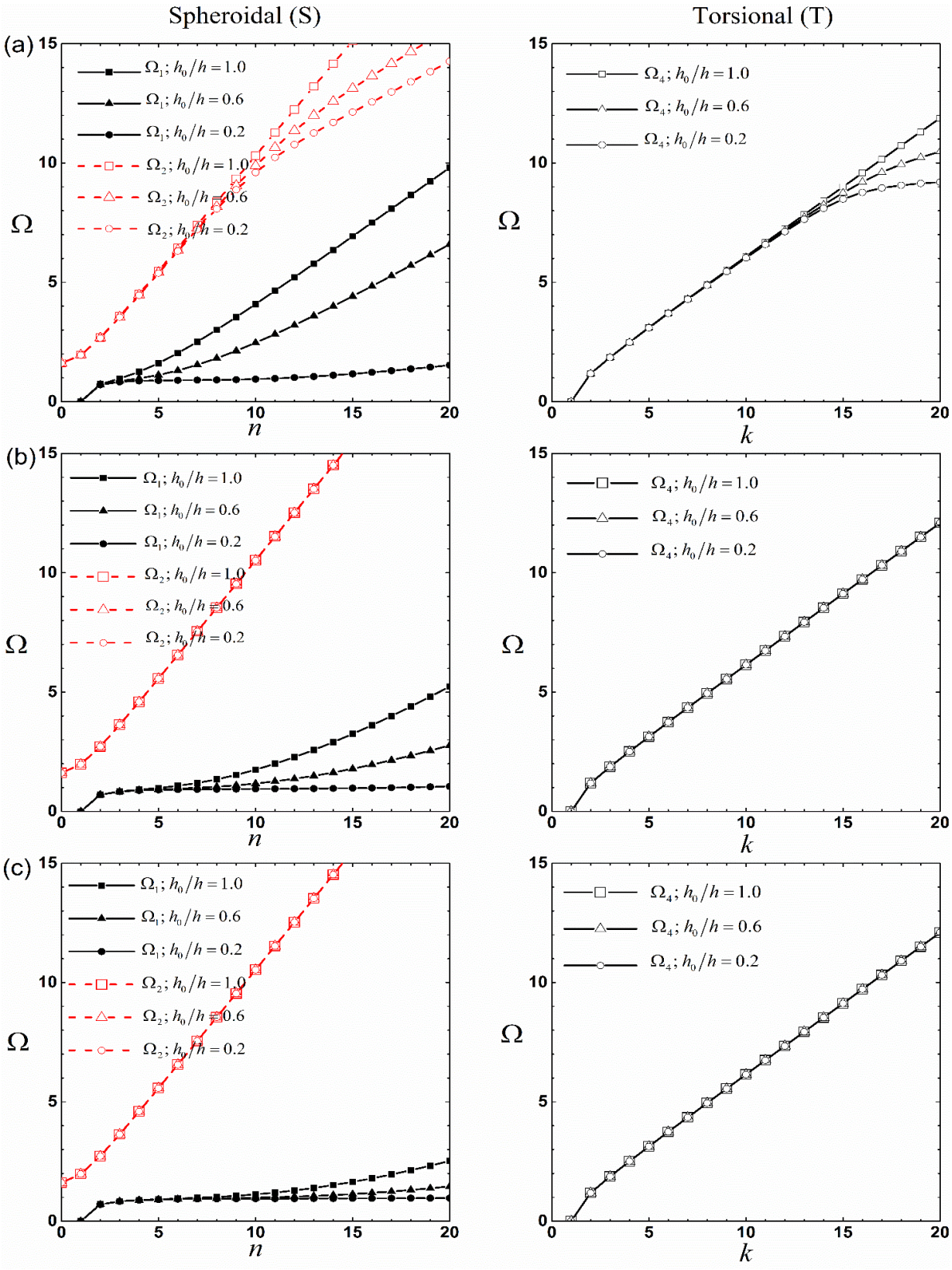

Fig. 4.5 The effect of h_0/h on natural frequencies for three values of R/h. (a) $R/h = 5$; (b) $R/h = 20$; (c) $R/h = 50$

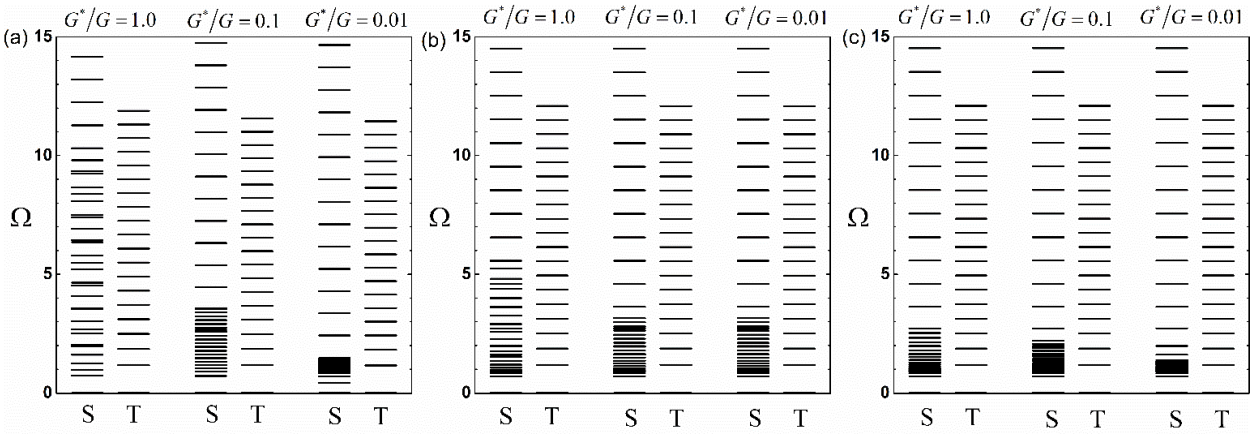

Fig. 4.6 The effect of G^*/G on the associated vibration modes for three values of R/h. (a) $R/h = 5$; (b) $R/h = 20$; (c) $R/h = 50$

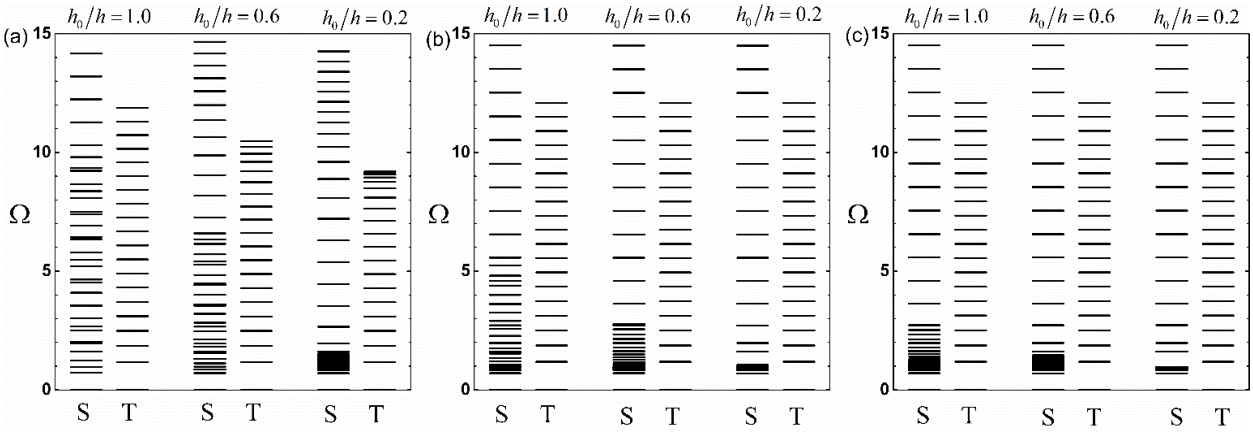

Fig. 4.7 The effect of h_0/h on the associated vibration modes for three values of R/h. (a) $R/h = 5$; (b) $R/h = 20$; (c) $R/h = 50$

Therefore, since biopolymer spherical shells are relatively thicker and smaller in radius (defined by smaller radius-to-thickness ratio, e.g. see R/h ranging from 3 to 6 in table 2.2 for several viral capsids, and figures 2 and 3 of (Yang et al., 2009) for Lumazine synthase and viral capsid STMV, respectively), and are of high structural heterogeneity and thickness non-uniformity (characterized by transverse shear modulus much lower than the in-plane shear modulus *G* and an effective bending thickness

significantly smaller from the average shell thickness), the actual frequencies of spheroidal modes of a biopolymer spherical shell could be much lower than those predicted by the classical homogeneous shell model (see Eqs. (1.3) and (1.4)), although the frequencies of torsional modes can be quite close to those predicted by the classical homogeneous shell model. For the vibration modes of biopolymer spherical shells, the spheroidal modes with shorter wavelength are more likely dominant in the low-frequency range, as confirmed using simulation methods (e.g. atomistic modeling (Dykeman and Sankey, 2010)). Indeed, as seen in figures 5, 8 and 12 of (Dykeman and Sankey, 2010), the displacement patterns of three types of spherical viruses in the lowest-frequency range are largely dominated by the spheroidal modes.

4.3.1.2 Comparison with the known results

In order to justifies the relevance of the present refined shell model for specific biopolymer spherical shells, let us compare our predicted results with some know data. First, let us compare the results given by the present refined model for the icosahedron with the known results obtained with the mass-and-spring model given in (Widom et al., 2007). The dependence of frequencies of the spheroidal modes ($\Omega_2; n=0$ (breathing mode), $\Omega_1; n=6,10,12$) and torsional modes ($\Omega_4; k=6$) on varying value of h_0/h (equivalently, varying value of the Foppl-von Karman number γ (defined by (2.43)) is shown in Fig. 4.8, with fixed values $k_s=5/6$, $\mu=0.3$, $R/h=4$ (Lidmar et al., 2003; Widom et al., 2007) and $G^*/G=1.0$. It is seen from Fig. 4.8 that the results given by the present model are qualitatively consistent with the known results shown in figure 4 of (Widom et al., 2007). As shown in Fig. 4.8 and figure 4 of (Widom et al., 2007), the frequencies of spheroidal modes (i.e. $\Omega_1; n=6,10,12$ in Fig. 4.8 and the mixing mode Y_{6m}, Y_{10m}, Y_{12m} in (Widom et al., 2007)) decrease with increasing Foppl-von

Karman number γ and the decrease is more significant for larger integer n (i.e. $\Omega_1; n = 12$ in Fig. 4.8 and Y_{12m} in (Widom et al., 2007)), while the frequencies of the torsional mode (i.e. $\Omega_4; k = 6$ in Fig. 4.8 and the tangent mode X_{6m} in (Widom et al., 2007)) and the breathing mode (i.e. $\Omega_2; n = 0$ in Fig. 4.8 and Y_{00} in (Widom et al., 2007)) remain almost unchanged with varying value of γ.

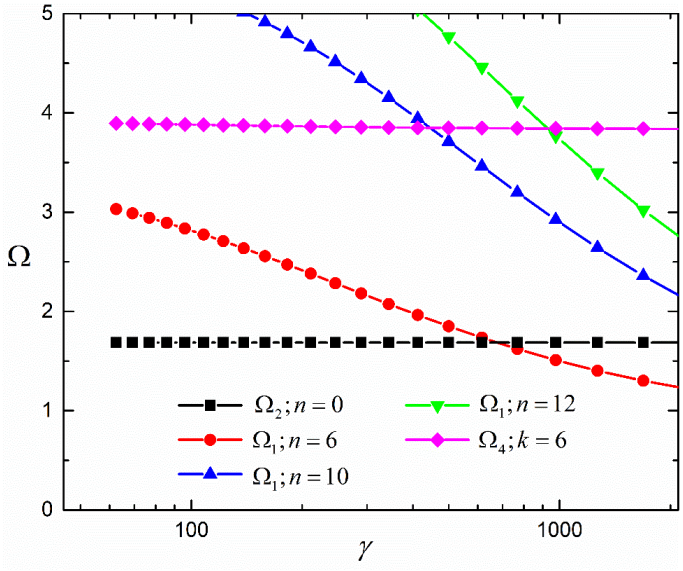

Fig. 4.8 The dependence of frequencies of the spheroidal modes ($\Omega_2; n = 0$ (breathing mode), $\Omega_1; n = 6,10,12$) and torsional modes ($\Omega_4; k = 6$) on the Foppl-von Karman number γ.

Table 4.1. Parameters used in the present refined shell model for biopolymer spherical shells of high structural heterogeneity, where the Young's modulus E is determined based on the relative Young's modulus in table 4 of (Yang et. al., 2009), which is in the reasonable range provided in (Yang et. al., 2009).

Types	k_s	$\rho\,(kg/m^3)$	μ	E (Gpa)	R (nm)	h (nm)	G^*/G	h_0/h
Lumazine synthase	5/6	987.60	0.30	6.4	6	3.6	1.0	0.8
Virus capsids STMV	5/6	823.82	0.24	3.7	7	3.1	1.0	0.75

Let us now compare the results given by the present model for two biopolymer spherical shells (Lumazine synthase and Virus capsids STMV) to those predicted by the classical shell model (1.3) and (1.4) (which can be obtained by the present model with $G^*/G=1.0$ and $h_0/h=1.0$) and simulation results of (Yang et. al., 2009) (see tables 2 and 3 in (Yang et. al., 2009)). Yang et. al. (Yang et. al., 2009) employed the coarse-grained elastic network to obtain discretized frequencies and associated vibration modes for the two specific spherical shell-like biomolecular assemblies (Lumazine synthase and Virus capsids STMV), and then to estimate the Young's modulus (E) Poisson's ratio (μ) by fitting them to the continuum shell model (based on the assumptions of axisymmetric motion and the transverse shear modulus equal to the in-plane shear modulus). The parameters R and h are calculated based on the inner and outer radii shown in figures 2 and 3 in (Yang et. al., 2009), and the parameters ρ, μ, E are obtained from table 4 in (Yang et. al., 2009). To apply the present refined shell model to biopolymer spherical shells of high structural heterogeneity, we have chosen $k_s=5/6$, $G^*/G=1.0$ (to be consistent with the assumption made in (Yang et. al., 2009)) for the two biomolecular assemblies with $h_0/h=0.8$ (for Lumazine synthase) and $h_0/h=0.75$ (for virus capsids STMV) determined by fitting the results in (Yang et. al., 2009), respectively, as given in table 4.1. For both cases, the results of the classical shell model shown in table 4.2 are obtained with $h_0/h=1.0$ and otherwise identical parameters as the refined shell model. As shown in table 4.2, the results given by the present refined shell model, for both natural frequencies and associated vibration modes, agree well with the simulation results in (Yang et. al., 2009), although the results given by the classical shell model show significant deviations from the simulation results of (Yang et. al., 2009). For example, it is seen from table 4.2 that, compared to Yang et al.'s simulations (Yang et. al., 2009), the classical shell model considerably overestimates the natural frequencies of spheroidal modes especially for larger *n* (see *n*=3,4,5 for Virus capsids STMV, for which the frequencies predicted by classical shell

model are about 30-50% higher than the simulation results of (Yang et. al., 2009), while the latter are very close to those predicted by the present refined shell model with the maximum relative errors not more than 5%). This offers an evidence of the physical relevance and usefulness of the present refined shell model over the classical shell model for biopolymer spherical shell of high structural heterogeneity.

Table 4.2. Comparison for two specific spherical shell-like biomolecular assemblies (Lumazine synthase and Virus capsids STMV), where $V_n + W_n$ and V_n refer to spheroidal modes with angular momentum index n, X_n refers to torsional modes with angular momentum index n, V_0 refers to breathing mode, (Ω_1, Ω_2) are the calculated frequencies correspond to spheroidal modes, and Ω_4 is the calculated frequencies correspond to torsional modes.

Lumazine synthase					
Results of table 2 in (Yang et. al., 2009)		Classical shell model		The refined shell model	
Frequency $\omega^2(ps^{-2})$	Vibration Mode	Frequency $\omega^2(ps^{-2})$	Vibration Mode	Frequency $\omega^2(ps^{-2})$	Vibration Mode
0.83817 0.84045	$V_2 + W_2$	0.99153	$\Omega_1(n=2)$	0.84248	$\Omega_1(n=2)$
1.41542 1.42215	X_2	1.52197	$\Omega_4(n=2)$	1.43243	$\Omega_4(n=2)$
1.98688 1.99022	$V_3 + W_3$	2.66892	$\Omega_1(n=3)$	2.15597	$\Omega_1(n=3)$
3.09788	V_0	2.99600	$\Omega_2(n=0)$	2.99600	$\Omega_2(n=0)$
3.26416	X_3	3.80491	$\Omega_4(n=3)$	3.52810	$\Omega_4(n=3)$
3.44217	V_1	4.01303	$\Omega_2(n=1)$	3.69429	$\Omega_2(n=1)$

Virus capsids STMV					
Results of table 3 in (Yang et. al., 2009)		Classical shell model		The refined shell model	
Frequency $\omega^2(ps^{-2})$	Vibration Mode	Frequency $\omega^2(ps^{-2})$	Vibration Mode	Frequency $\omega^2(ps^{-2})$	Vibration Mode
0.43242	V_2+W_2	0.45131	$\Omega_1(n=2)$	0.40445	$\Omega_1(n=2)$
0.73901 0.82876	V_3+W_3	1.05	$\Omega_1(n=3)$	0.79236	$\Omega_1(n=3)$
1.05426	X_2	0.94754	$\Omega_4(n=2)$	0.93702	$\Omega_4(n=2)$
1.22444 1.46058	V_4+W_4	2.05953	$\Omega_1(n=4)$	1.42567	$\Omega_1(n=4)$
1.81925	V_0	1.64603	$\Omega_2(n=0)$	1.64603	$\Omega_2(n=0)$
2.13790 2.28670	V_5+W_5	3.56305	$\Omega_1(n=5)$	2.42355	$\Omega_1(n=5)$
2.30968	V_1	2.23733	$\Omega_2(n=1)$	2.20857	$\Omega_2(n=1)$

4.3.2 The influence on non-axisymmetric vibration modes

Since axisymmetric and non-axisymmetric modes of the same index *n* or *k* correspond to exactly the same natural frequencies, as explained previously, here we shall focus on how the key parameters ($R/h, G^*/G, h_0/h$) affect the non-axisymmetric vibration modes.

As stated previously, there are in general (2*n*+1) independent vibrational modes corresponding to one natural frequency. Therefore, the number of the independent vibration modes corresponding to one natural frequency is determined by the value of the integer *n*, and then depends on the two key parameters (G^*/G, h_0/h) determined by the high structural heterogeneity. It is seen from Figs. 4.4

and 4.5 that when the key parameter G^*/G or /and h_0/h decreases, the integer *n*, and therefore the number of the independent vibration modes, increases in the low-frequency range (say $\Omega_1 < 2.0$) for thicker and smaller-radius spherical shells. Since biopolymer spherical shells, often characterized by low transverse shear modulus and smaller effective bending thickness, are relatively thicker and smaller in radius, the actual number of independent vibration modes corresponding to a lower frequency predicted by the present model could be much larger than that predicted by the classical homogeneous shell model. For example, let us compare two cases in Fig. 4.5a: one is $R/h = 5; G^*/G = 1.0; h_0/h = 1.0$ (the classical shell model), and the other is $R/h = 5; G^*/G = 1.0; h_0/h = 0.2$ (the present refined shell model). All independent vibration modes for $n \le 6$ and the corresponding frequencies are shown in Fig. 4.9 (Fig. 4.9a for the classical shell model, and Fig. 4.9b for the present refined shell model). It is seen from Fig. 4.9 that the number of independent vibration modes of a low frequency (say, around $\Omega = 1.0$) predicted by the present refined shell model is 37 (determined by $(3+4+5+6)\times 2+1$), which are considerably large than the number 7 (determined by $3\times 2+1$) predicted by the classical shell model, in qualitative agreement with known atomistic simulation results for several viral capsids (see e.g. figures 4 and 5 in (Peeters and Taormina, 2008) and figures 1-3, 6, 7, 10, 11 in (Peeters and Taormina, 2009)) which showed a low frequency plateau characterized by a large number of vibration modes (e.g. 24 vibration modes for STMV, and 40 vibration modes for RYMV).

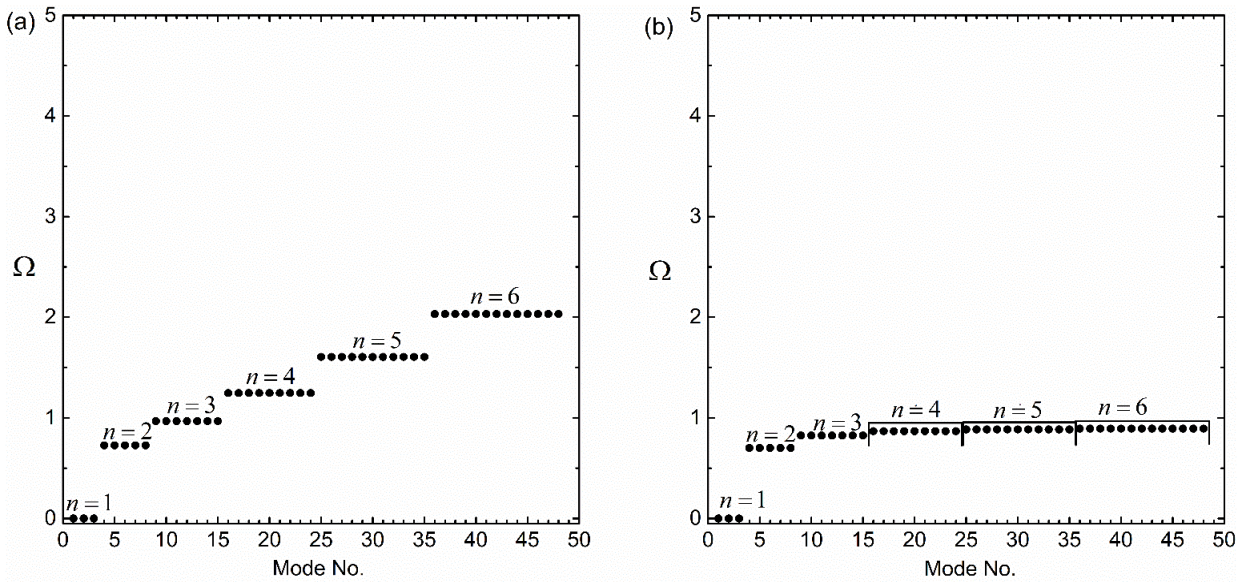

Fig. 4.9 All independent vibration modes for $n \le 6$ and the corresponding frequencies (a) the classical shell model; (b) the present refined shell model

4.4 Conclusions

Free-vibration frequencies and vibration modes of a biopolymer spherical shell of high structural heterogeneity are investigated with a refined shell model. Unlike the classical homogeneous shell model, this refined shell model of biopolymer spherical shells is characterized by an effective bending thickness (which can be quite different from the average thickness) and the transverse shear modulus (which can be much lower than the in-plane shear modulus). Our major results include

1). Two frequency equations are derived for axisymmetric spheroidal and torsional modes of a biopolymer spherical shell of high structural heterogeneity, and the effects of structural heterogeneity on natural frequencies can be investigated by studying the influence of the effective bending thickness and transverse shear modulus on natural frequencies.

2). For example, the natural frequencies of spheroidal modes of several specific virus capsids STMV predicted by the present model are about 30-50% lower than those predicted by the classical

homogeneous shell model, in good agreement with known simulation results. This offers an evidence of the physical relevance and usefulness of the present refined shell model for biopolymer spherical shell of high structural heterogeneity.

3). Also, the present refined shell model predicts that the spheroidal modes with shorter wavelength are dominant in the lowest frequency range, qualitatively consistent with the known displacement patterns in the lowest frequency range obtained by other researches using simulation methods.

4). In addition, in the low frequency range of several viral capsids, the number of independent vibration modes predicted by the present refined shell model is much larger than that predicted by the classical homogeneous shell model, in qualitative agreement with known atomistic simulation results.

All of these results suggest that the refined shell model could be used to simulate mechanical behaviors of biopolymer spherical shells of high structural heterogeneity.

Chapter 5: Conclusions and future works

5.1 Conclusions

The main conclusions of this research are summarized below:

1) A recently developed refined elastic shell model is employed to conduct an axisymmetric imperfection sensitivity of pressured buckling of biopolymer spherical shells. Results show that

1.1) the axisymmetric imperfection sensitivity of imperfect biopolymer spherical shells is mainly influenced by the effective bending thickness, but insensitive to the transverse shear modulus;

1.2) with the physically relevant parameters for polymer-shelled UCAs and spherical viruses, the maximum sustainable pressure of an imperfect UCA shell or an imperfect spherical virus shell could reduce to 60% or 55-65% of the maximum sustainable pressure for a perfect UCA shell or a spherical virus shell, respectively;

1.3) compared to classical elastic thin shells that can be extremely sensitive to geometrical imperfections, typical biopolymer spherical shells are only moderately sensitive to geometrical imperfections.

2) Furthermore, a non-axisymmetric imperfection sensitivity analysis is conducted. Results show that:

2.1) the present non-axisymmetric imperfection sensitivity analysis can predict much lower maximum pressure than those predicted based on axisymmetric imperfection sensitivity. For example, with physically realistic parameters for some typical imperfect biopolymer spherical shells, the maximum load predicted by the present non-axisymmetric analysis drops to approximately 25%–40% of that of a perfect spherical virus shell, which is about 30% lower than the predicted maximum load based on axisymmetric imperfection sensitivity;

2.2) for the biopolymer spherical shells of moderate radius-to-thickness ratio (say, less than 30) and smaller effective bending thickness (say, less than 0.2 times average shell thickness), the imperfection sensitivity based on the simplified axisymmetric analysis is practically useful, while a more accurate non-axisymmetric analysis with the mode interaction is required in other more general cases.

3) A refined shell model is presented to study free-vibration frequencies and vibration modes of a biopolymer spherical shell of high structural heterogeneity. Major results include:

3.1) two frequency equations are derived for axisymmetric spheroidal and torsional modes of a biopolymer spherical shell of high structural heterogeneity. With the frequency equations, the predicted natural frequencies of spheroidal modes of virus capsids STMV are about 30-50% lower than those predicted by the classical homogeneous shell model, in good agreement with known simulation results. This justifies the usefulness of the present refined shell model for biopolymer spherical shell of high structural heterogeneity;

3.2) the present refined shell model also shows that the shorter-wavelength spheroidal modes are the dominant vibration modes in the lowest frequency range, which is confirmed by other works using simulation methods;

3.3) the number of independent vibration modes corresponding to a lower frequency predicted by the present model is much larger than that predicted by the classical homogeneous shell, in qualitative agreement with known atomistic simulation results.

In summary, to study the axisymmetric and non-axisymmetric imperfection sensitivity of pressured buckling and free vibration of biopolymer spherical shells, a refined shell model is developed and employed in the present research. Compared with the classical homogeneous shell model, higher-order effects, caused by structural heterogeneity, thickness nonuniformity and geometric imperfection, on global mechanical response of biopolymer spherical shells are carefully examined. The main

achievements in the thesis are: 1) Axisymmetric and non-axisymmetric imperfection sensitivity analyses are conducted to study the effect of geometric imperfections on pressured buckling of biopolymer spherical shells; 2) clarify the cases in which the simplified axisymmetric analysis is practically useful and the cases in which a more accurate non-axisymmetric analysis with the mode interaction is required; 3) A refined shell model is developed to study free-vibration frequencies and vibration modes of a biopolymer spherical shell of high structural heterogeneity. As compared to the imperfection sensitivity in previous work done by Koiter (Koiter, 1969) and Hutchinson (Hutchinson, 1967), the axisymmetric and non-axisymmetric imperfection sensitivity analyses in the present work are done for biopolymer spherical shells characterized by structural heterogeneity (measured by transverse shear modulus) and thickness non-uniformity (measured by effective bending thickness). In particular, the present work investigates how the key parameters (transverse shear modulus and effective bending thickness) affect the imperfection sensitivity. With physically realistic parameters for some typical biopolymer spherical shells, the predictions of actual maximum pressure and natural frequencies and associated vibration modes given by the present model provide plausible comparisons and explanations for known simulations and experiments.

5.2 Future works

Based on research results achieved in the present thesis, the following topics are recommended for further studies:

1) <u>The effect of geometrical imperfection on the natural frequencies and vibration modes of free vibration of biopolymer spherical shells:</u>

In chapter 4, we study the effects of structural heterogeneity and thickness nonuniformity on the natural frequencies and vibration modes of biopolymer spherical shells. In the future, it is worthwhile to investigate the axisymmetric and non-axisymmetric imperfection sensitivity analyses of free

vibration of biopolymer spherical shells, as we did to the pressured buckling of biopolymer spherical shells.

2) Further explore the viscous effect on the high frequency vibration of biopolymer spherical shells:

In chapter 4, we only focus on the low frequency vibration of biopolymer spherical shells, therefore the viscous effects can be ignored reasonably. However, for the high frequency vibration of biopolymer spherical shells, such viscous effects may play a significant role and should be considered in the future study.

3) Further consider more general geometric imperfections and large imperfections:

In (Lee et al., 2016; Hutchinson, 2016), they considered more general geometric imperfections such as dimple-shaped undulations and sinusoidal-shaped equatorial undulations with larger imperfection amplitude for pressured buckling of classical homogeneous spherical shells, which is worthwhile to be studied for pressured buckling of biopolymer spherical shells

4) Further study on other mechanical behaviors of biopolymer spherical shells:

Based on the refined shell model employed in this thesis for biopolymer spherical shells of high structural heterogeneity and thickness nonuniformity, other mechanical behaviors such as indentation, adhesion and fracture of biopolymer spherical shells are worthy to be further studied.

References

Arani, A. G., Haghparast, E., Maraghi, Z. K., 2017. Vibrational response of coupled orthotropic protein microtubules immersed in cytosol considering small-scale and surface effects. Proc. IMechE Part N: J. Nanoengineering and Nanosystems. 23, 131-139.

Babincová, M., Sourivong, P., Babinec, P., 2000. Resonant absorption of ultrasound energy as a method of HIV destruction. Med. Hypotheses 55, 450-451.

Baker, W. E., 1961. Axisymmetric Modes of Vibration of Thin Spherical Shell," J. Acoust. Soc. Am., 33, 1749–1758.

Baker, T. S., Olson, N. H., Fuller, S. D., 1999. Adding the third dimension to virus life cycles: Three-dimensional reconstruction of icosahedral viruses from cryo-electron micrographs. Microbiol. Mol. Biol. Rev. 63, 862-922.

Balandin, A. A., Fonoberov, V. A., 2005. Vibrational modes of nano-template viruses. J. Biomed. Nanotechnol. 1, 90–95.

Baninajjaryan, A., Beni, Y. T., 2015. Theoretical study of the effect of shear deformable shell model, elastic foundation and size dependency on the vibration of protein microtubule. J. Theor. Biol. 382, 111–121.

Bealle, G., Jestinc, J., Carriere, D., 2011. Osmotically induced deformation of capsid-like icosahedral vesicles. Soft Matter. 7, 1084–1089.

Beni, Y. T., Zeverdejani, M. K., Mehralian, F., 2017. Buckling analysis of orthotropic protein microtubules under axial and radial compression based on couple stress theory. Math. Biosci. 292, 18-29.

Bergman, S., Lezon, T. R., 2017. Modeling global changes induced by local perturbations to the HIV-1 capsid. J. Mol. Graph. Model. 71, 218-226.

Bryan, A., 2017. Free Vibration of Thin Spherical Shells. ASME J. Vib. Acoust. 139, 061020.

Budiansky, B., Hutchinson, J. W., 1964. Dynamic buckling of imperfection-sensitivity structures. In: Henry G. (Ed.), Proceedings of the Eleventh International Congress of Applied Mechanics, Germany, pp. 636-651.

Carlson, R. L., Sendelbeck, R. L., Hoff, N. J., 1967. Experimental studies of the buckling of complete spherical shells. Exp. Mech., 7, pp. 281–288.

Caston, J. R., 2013. Conventional electron microscopy, cryo-electron microscopy and cryo-Electron tomography of viruses. in: Mateu, M. G. (Ed.), Structure and physics of viruses. Springer, Dordrecht, pp. 79-115.

Chitnis, P. V., Koppolu, S., Mamou, J., Chlon, C., Ketterling, J. A., 2013. Influence of shell properties on high-frequency ultrasound imaging and drug delivery using polymer-shelled microbubbles. IEEE Trans. Ultrason. Ferroelectr. Freq. Control 60, 53-64.

Chitnis, P. V., Lee, P., Mamou, J., Allen, J. S., Bohmer, M., Ketterling, J. A., 2011a. Rupture threshold characterization of polymer-shelled ultrasound contrast agents subjected to static overpressure. J. Appl. Phys. 109, 084906.

Chitnis, P. V., Lee, P., Mamou, J., Ketterling, J., 2010. Influence of shell properties on rupture of polymeric contrast agents in response to overpressure. In: 2010 IEEE International Ultrasonics Symposium Proceedings, San Diego, pp. 1720-1723.

Chitnis, P. V., Mamou, J., Koppolu, S., Ketterling, J. A., 2011b. Influence of shell parameters on response of polymer-shelled microbubbles to high-frequency ultrasound. in: 2011 IEEE International Ultrasonics Symposium Proceedings Orlando, pp. 644-647.

Chlon, C., Gudon, C., Verhaagen, B., Shi, W. T., Hall, C. S., Lub, J., B¨ohmer, M. R., 2009. Effect of Molecular Weight, Crystallinity, and Hydrophobicity on the Acoustic Activation of Polymer-Shelled Ultrasound Contrast Agents. Biomacromolecules 10, 1025-1031.

Civalek, O., Demir, C., Bending analysis of microtubules using nonlocal Euler–Bernoulli beam theory. Appl. Math. Model. 35, 2053–2067.

Daneshmand, F., Amabili, M., 2012. Coupled oscillations of a protein microtubule immersed in cytoplasm: an orthotropic elastic shell modeling. J. Biol. Phys. 38, 429–448.

Danielson, D. A., 1974. Theory of shell stability. In: Fung, Y. C., Sechler, E. E. (Ed.), Thin-shell structures-theory, experiment, and design, Prentice-Hall, Inc., Englewood Cliffs, NJ, pp. 45-58.

Duffey, T. A., Pepin, J. E., Robertson, A. N., Steinzig, M. L., Coleman, K., 2007. Vibrations of Complete Spherical Shells with imperfections. ASME J. Vib. Acoust. 129, 363-370.

Dykeman, E. C., Sankey, O. F., 2008. Low frequency mechanical modes of viral capsids: an atomistic approach. Phys. Rev. Lett. 100, 028101.

Dykeman, E. C., Sankey, O. F., 2009. Theory of the low frequency mechanical modes and Raman spectra of the M13 bacteriophage capsid with atomic detail. J. Phys.: Condens. Matter 21, 035116.

Dykeman, E. C., Sankey, O. F., 2010a. Normal mode analysis and applications in biological physics. J. Phys.: Condens. Matter 22, 423202.

Dykeman, E. C., Sankey, O. F., 2010b. Atomistic modeling of the low-frequency mechanical modes and raman spectra of icosahedral virus capsids. Phys. Rev. E 81, 021918.

Evkina, A. Y., Lykhachova, O. V., 2017. Energy barrier as a criterion for stability estimation of spherical shell under uniform external pressure. Int. J. Solids Struct. 118, 14–23.

Federhofer, K., 1937. Zur Berechnung der Eigenschwingungen der Kugelschale. Sitzber. Akad. Wiss. Wien, Math.-Naturw. KI. 2A, 146, 57-69 and 505-514.

Ford, L. H., 2003. Estimate of the vibrational frequencies of spherical virus particles. Phys. Rev. E 67, 051924.

Fu, Y. M., Zhang, J., 2010. Modeling and analysis of microtubules based on a modified couple stress theory. Physica E. 42, 1741–1745.

Ghavanloo E., Fazelzadeh, S. A., Nonlocal shell model for predicting axisymmetric vibration of spherical shell-like nanostructures. Mech. Adv. Mater. Struc. 22, 597-603.

Gibbons, M. M., Klug, W. S., 2007. Nonlinear finite-element analysis of nanoindentation of viral capsids. Phys. Rev. E 75, 031901.

Gibbons, M. M., Klug, W. S., 2007a. Mechanical modeling of viral capsids. J. Mater. Sci. 42, 8995–9004.

Gibbons, M. M., Klug, W. S., 2008. Influence of Nonuniform Geometry on Nanoindentation of Viral Capsids. Biophys. J. 95, 3640-3649.

Gibbons, M. M., Perotti, L. E., Klug, W. S., 2015. Computational Mechanics of Viral Capsids. in: Brendan, P. O. (Ed.), Protein Cages, Springer, London, pp. 139-188.

Gu, B., Mai, Y. W., Ru, C. Q., 2009. Mechanics of microtubules modeled as orthotropic elastic shells with transverse shearing. Acta. Mech. 207, 195–209.

Guo, G., Tu, J., Guo, X., Huang, P., Wu, J., Zhang, D., 2016. Characterization of mechanical properties of hybrid contrast agents by combining atomic force microscopy with acoustic/optic assessments. J. Biomech. 49, 319–325.

Heireche, H., Tounsi, A., Benhassaini, H., Benzair, A., Bendahmane, M., Missouri M., Mokadem, S., 2010. Nonlocal elasticity effect on vibration characteristics of protein microtubules. Physcia E. 42, 2375–2379.

Hernando-Perez, M., Pascual, E., Aznar, M., Ionel, A., Caston, J. R., Luque, A., Carrascosa, J. L., Reguera, D., de Pablo, P. J., 2014. The interplay between mechanics and stability of viral cages. Nanoscale 6, 2702–2709.

Homewood, R. H., Brine, A. C., Johnson, A. E., Jr., 1961. Experimental Investigation of the Buckling Instability of Monocoque Shells. Exp. Mech., 1, pp. 88–96.

Hutchinson, J. W., 1960. Imperfection Sensitivity of Externally Pressurized Spherical Shells. J. Appl. Mech. 34, 49-55.

Hutchinson, J. W., 2010. Knockdown factors for buckling of cylindrical and spherical shells subject to reduced biaxial membrane stress. Int. J. Solids Struct. 47, 1443–1448.

Hutchinson, J. W., 2016. Buckling of spherical shells revisited. Proc. R. Soc. A 472, 20160577.

Hutchinson, J. W., Thompson, J. M. T., 2017. Nonlinear buckling behavior of spherical shells: barriers and symmetry-breaking dimples. Phil. Trans. R. Soc. A 375, 20160154.

Jimenez, F. L., Marthelot, J., Lee, A., Hutchinson, J. W., Reis, P. M., 2017. Technical brief: knockdown factor for the buckling of spherical shells containing large-amplitude geometric defects. J. Appl. Mech. 84, 034501.

Kahn, D., Kim, K. W., Strascio, M. A., 2001. Quantized vibrational modes of nanospheres and nanotubes in the elastic continuum model. J. Appl. Phys. 89, 5107-5111.

Kalnins, A., 1961. On Vibrations of Shallow Spherical Shells. J. Acoust. Soc. Am. 33, 1102-1107.

Kalnins, A., 1964. Effect of Bending on Vibrations of Spherical Shells," J. Acoust. Soc. Am., 36, 74–81.

Kalnins, A., Biricikoglu, V., 1970. On the stability analysis of imperfect spherical shell. J. Appl. Mech. 37, 29-634.

Kaplan, A., and Fung, Y. C., 1954. A Nonlinear Theory of Bending and Buckling of Thin Elastic Shallow Spherical Shells. National Advisory Committee for Aeronautics, Washington, DC, Technical Note 3212.

Kis, A., Kasas, S., Babic, B., Kulik, A. J., Benoît, W., Briggs, G. A. D., Schönenberger, C., Catsicas, S., Forró, L., 2002. Nanomechanics of Microtubules. Phys. Rev. Lett. 89, 248101.

Klug, W. S., Bruinsma, R. F., Michel Jean-Philippe, Knobler C. M., Ivanovska I. L., Schmidt C. F., Wuite G. J. L., 2006. Failure of Viral Shells. Phys. Rev. Lett. 97, 228101.

Koga, T., Hoff, N., 1969. The axisymmetric buckling of initially imperfect complete spherical shell. Intern. J. Solids Structures 5, 679-697.

Koiter, W. T., 1969. The nonlinear buckling problem of a complete spherical shell under uniform external pressure. Proc. K. Ned. Akad. B-Ph. 72, 40-122.

Koiter, W. T., 1945. Over de stabiliteit van het elastisch evenwicht (The stability of elastic equilibrium) (in Dutch). Thesis, Technische Hooge School, Delft, The Netherlands, Paris, Amsterdam, (English translation: NASA Technical Translation F-10 1967, p. 883; available online:http://imechanica.org/node/1400).

Koiter, W. T., 1963. Elastic stability and post-buckling behavior. In: Langer, R. E. (Ed.), Proceedings of the Symposium on Nonlinear Problems. University of Wisconsin Press, pp. 257-275.

Kononova, O., Snijder, J., Kholodov, Y., Marx, K. A., Wuite, G. J. L., Roos, W. H., Barsegov, V., 2016. Fluctuating Nonlinear Spring Model of Mechanical Deformation of Biological Particles. PLoS Comput. Biol., 12, e1004729.

Kooiman, K., Bohmer, M. R., Emmer, M., Vos, H. J., Chlon, C., Shi, W. T., Hall, C. S., de Winter, S. H.P.M., Schroen, K., Versluis, M., de Jong, N., van Wamel, A., 2009. Oil-filled polymer microcapsules for ultrasound-mediated delivery of lipophilic drugs. J. Control Release, 133, 109–118.

Kraus, H., 1967. Thin Elastic Shells. Wiley, New York.

Krenzke, M. A., Kiernan, T. J., 1963. Elastic Stability of Near-Perfect Shallow Spherical Shells. AIAA J., 1, pp. 2855–2857.

Kučera, O., Havelka, D., Cifra, M., 2017. Vibrations of microtubules: Physics that has not met biology yet. Wave Motion. 72, 13-22.

Lamb, H., 1882. On the vibrations of a spherical shell. Proc. London Math. Soc. 14, 50-56.

Landau, L. D., Lifshitz, E. M., 1986. Theory of elasticity. Pergamon Press, Oxford.

Lee, A., Marthelot, J., Jimenez, F. L., Hutchinson, J. W., Reis, P. M., 2016. The geometric role of precisely engineered imperfections on the critical buckling load of spherical elastic shells. J. Appl.Mech. 83, 111005.

Lidmar, J., Mirny, L., Nelson, D. R., 2003. Virus shapes and buckling transitions in spherical shells. Phys. Rev. E 68, 051910.

Liew, K. M., Xiang, P., Zhang, L. W., 2015. Mechanical properties and characteristics of microtubules: A review. Compos. Struct. 123, 98-108.

Liu, Y., Miyoshi, H., Nakamura, M., 2006. Encapsulated ultrasound microbubbles: Therapeutic application in drug/gene delivery. J. Controlled Release 114, 89-99.

Mahajan, S., Sanejouand, Y. H., 2015. On the relationship between low-frequency normal modes and the large-scale conformational changes of proteins. Arch. Biochem. Biophys. 567, 59-65.

Marmottant, P., Bouakaz, A., de Jong, N., Quilliet, C., 2011. Buckling resistance of solid shell bubbles under ultrasound. J. Acoust. Soc. Am. 129, 1231-1239.

Marques, O., Sanejouand, Y. H., 1995. Hinge-bending motion in citrate synthase arising from normal mode calculations. Proteins 23, 557-560.

Mateu, M. G., 2012. Mechanical properties of viruses analyzed by atomic force microscopy: A virological perspective. Virus Res. 168, 1-22.

Mateu, M. G., 2013. The structural basis of virus function, in: Mateu, M. G. (Ed.), Structure and physics of viruses. Springer, Dordrecht, pp. 3-51.

May, E. R., Aggarwal, A., Klug, W. S., Brooks, III C. L., 2011. Viral capsid equilibrium dynamics reveals nonuniform elastic properties. Biophys. J. 100, L59-L61.

May, E. R., Brooks, III C. L., 2011. Determination of viral capsid elastic properties from equilibrium thermal fluctuations. Phys. Rev. Lett. 106, 188101.

May, E. R., Brooks, III C. L., 2012. On the Morphology of viral capsids: elastic properties and buckling transitions. J. Phys. Chem. B 116, 8604-8609.

May, E. R., 2014. Recent developments in molecular simulation approaches to study spherical virus capsids. Molec. Simul. 40, 878-888.

Mcgee, O. G., Spry, S. C., 1997. A three-dimensional analysis of the spheroidal and toroidal elastic vibrations of thick-walled spherical bodies of revolution. Int J Numer Meth Eng. 40, 1359-1382.

Mehrbod, M., Mofrad, M. R. K., 2011. On the Significance of Microtubule Flexural Behavior in Cytoskeletal Mechanics. PLoS ONE. 6, e25627.

Michel, J. P., Ivanovska, I. L., Gibbons, M. M., Klug, W. S., Knobler, C. M., Wuite, G. J. L., Schmidt, C. F., 2006. Nanoindentation studies of full and empty viral capsids and the effects of capsid protein mutations on elasticity and strength. Proc. Natl. Acad. Sci. U.S.A. 103, 6184-6189.

Murray, F. J., Wright, F. W., 1961. The buckling of thin spherical shells. AiAA J. 28, 223-236.

Nguyen, T. T., Bruinsma, R. F., Gelbart, W. M., 2005. Elasticity theory and shape transitions of viral shells. Phys. Rev. E 72, 051923.

Nguyen, T. T., Bruinsma, R. F., Gelbart, W. M., 2006. Continuum Theory of Retroviral Capsids. Phys. Rev. Lett. 96, 078102.

Nguyen-Thanh, N., Valizadeh, N., Nguyen, M. N., Nguyen-Xuan, H., Zhuang, X., Areias, P., Zi, G., Bazilevs, Y., De Lorenzis, L., Rabczuk, T., 2015. An extended isogeometric thin shell analysis based on Kirchhoff–Love theory. Comput.Methods Appl.Mech. 284, 265-291.

Niordson, F. I., 1984. Free Vibrations of thin elastic spherical shells. Int. J. Solids Struct., 20, 667–687.

Niordson, F. I., 1988. The spectrum of free vibrations of a thin elastic spherical shell. Int. J. Solids Struct., 24, 947–961.

Pampaloni, F., Lattanzi, G., Jonas, A., Surrey, T., Frey, E., Florin, E. L., 2006. Thermal fluctuations of grafted microtubules provide evidence of a length-dependent persistence length. Proc. Natl. Acad. Sci. U.S.A. 103, 10248.

Peeters, K., Taormina, A., 2008. Dynamics of icosahedral viruses: what does viral tiling theory teach us? Comput. Math. Methods Med. 9, 211-220.

Peeters, K., Taormina, A., 2009. Group theory of icosahedral virus capsid vibrations: a top-down approach. J. Theor. Biol. 256, 607-624.

Pentikainen, U., Pentikainen, O.T., Mulholland, A. J., 2008. Cooperative symmetric to asymmetric conformational transition of the apo-form of scavenger decapping enzyme revealed by simulations. Proteins 70, 498-508.

Qin, S., Caskey, C., Ferrara, K., 2009. Ultrasound contrast microbubbles in imaging and therapy: physical principles and engineering. Phys. Med. Biol. 54, R27-R57.

Reddy, J. N., Liu, C. F., 1985. A higher-order shear deformation theory of laminated elastic shells. Int. J. Eng. Sci. 23, 319-330.

Reddy, J. N., 2002. Energy Principles and Variational Methods in Applied Mechanics. Wiley, New York.

Reis, P. M., 2015. A perspective on the revival of structural (in) stability with novel opportunities for function: from buckliphobia to buckliphilia. J. Appl. Mech. 82, 111001.

Rochal, S. B., Konevtsova, O. V., Lorman, V. L., 2017. Static and dynamic hidden symmetries of icosahedral viral capsids. Nanoscale 9, 12449-12460.

Roos, W. H., Ivanovska, I. L., Evilevitch, A., Wuite, G. J. L., 2007. Viral capsids: Mechanical characteristics, genome packaging and delivery mechanisms. Cell. Mol. Life Sci. 64,1484-1497.

Ru, C. Q., 2009. Buckling of empty spherical viruses under external pressure. J. Appl. Phys. 105, 124701.

Sabir, A. B., 1964. Large deflection and buckling behavior of a spherical shell with inward point load and uniform external pressure. J. Mech. Eng. Sci. 6, 394-404.

Sanders, J. L., 1961. Nonlinear theories for thin shells. Quart. Appl. Math. 21, 21-36.

Sato, M., Konishi, Y., Park, S. J., 2015. Interlayer coupling effect on buckling modes of spherical bilayers. J. Mech. 31, 29-36.

Sboros, V., 2008. Response of contrast agents to ultrasound. Adv. Drug Delivery Rev. 60, 1117-1136.

Sboros, V., Glynos, E., Pye, S. D., Moran, C. M., Butler, M., Ross, J. A., McDicken, W. N., Koutsos, V., 2007. Nanomechanical probing of microbubbles using the atomic force microscope. Ultrasonics 46, 349-354.

Schwerin, E., 1922. Zur Stabilitat der dunnwandigen Hohlkugel unter glerchmaszigem Aussendruk. Z. Angew. Math. Mech. 2, 81-91.

Seaman, L., 1962. The Nature of Buckling in Thin Spherical Shells. Ph.D. thesis, Massachusetts Institute of Technology, Cambridge, MA.

Shen, H. S., 2010. Nonlinear vibration of microtubules in living cells. Curr. Appl. Phys. 11, 812-821.

Shi, Y. J., Guo, W. L., Ru, C. Q., 2008. Relevance of Timoshenko-beam model to microtubules of low shear modulus. Physica E 41, 213–219.

Siber, A., 2006. Buckling transition in icosahedral shells subjected to volume conservation constraint and pressure: Relations to virus maturation. Phys. Rev. E 73, 061915.

Siber, A., Podgornik, R., 2009. Stability of elastic icosadeltahedral shells under uniform external pressure: application to viruses under osmotic pressure. Phys. Rev. E 79, 011919.

Silbiger, A., 1962. Nonaxisymmetric Modes of Vibration of Thin Spherical Shells. J. Acoust. Soc. Am. 34, 862-863.

Sokolnikoff, I. S., 1956. Mathematical theory of elasticity. New York: McGraw-Hill, pp. 177-184.

Stephen, N. G., 1980. Timoshenko's shear coefficient from a beam subjected to gravity loading. J. Appl. Mech. 47, 121-127.

Talati, M., Jha, P. K., 2006. Acoustic phonon quantization and low-frequency Raman spectra of spherical viruses. Phys. Rev. E 73, 011901.

Tama, F., Brooks, III C. L., 2005. Diversity and identity of mechanical properties of icosahedral viral capsids studied with elastic network normal mode analysis. J. Mol. Biol. 345, 299-314.

Thompson, J. M. T., 1962. The elastic instability of a complete spherical shell. Aeronaut. Quart. 13, 189-202.

Toorani, M. H., Lakis, A. A., 2000. General equations of anisotropic plates and shells including transverse shear deformations, rotary inertia and initial curvature effects. 237(4), 561-615.

Tounsi, A., Heireche, H., Benhassaini, H., Missouri, M., 2010. Vibration and length-dependent flexural rigidity of protein microtubules using higher order shear deformation theory. J. Theor. Biol. 266, 250–255.

Tsen, K. T., Dykeman, E. C., Sankey, O. F., Tsen, S. W. D., Lin, N. T., Kiang, J. G., 2006. Raman scattering studies of the low-frequency vibrational modes of bacteriophage M13 in water-observation of an axial torsion mode. Nanotechnology 17, 5474-5479.

Tsen, K. T., Dykeman, E. C., Sankey, O. F., Tsen, S. W. D., Lin, N. T., Kiang, J. G., 2007. Probing the low-frequency vibrational modes of viruses with Raman scattering-bacteriophage M13 in water. J. Biomed. Opt. 12, 024009.

Tsien, H.-S., 1942. A Theory for the Buckling of Thin Shells. J. Aeronaut. Sci., 9, pp. 373–384.

Walker, A. C., 1968. An analytical study of the rotationally symmetric nonlinear buckling of a complete spherical shell under external pressure. Intern. J. Mech. Sci. 10, 695-710.

Wan, D., Bowick, M. J., Sknepnek, R., 2015. Effects of scars on icosahedral crystalline shell stability under external pressure. Phys. Rev. E 91, 033205.

Wang, B., Du, K., Hao, P., Zhou, C., Tian, K., Xu, S., Ma, Y., Zhang, X., 2016. Numerically and experimentally predicted knockdown factors for stiffened shells under axial compression. Thin-Walled Struct. 109, 13–24.

Wells, S. A., Van Der Kamp, M. W., Mcgeagh, J. D., Mulholland, A.J., 2015. Structure and function in homodimeric enzymes: simulations of cooperative and independent functional motions. PLoS One 10, e0133372.

van der Neut, A., 1932. Der Elastische Stabilitect van den Dunwandigen Bol. Thesis, Delft, Netherlands.

Verdaguer, N., Carriga, D., Fita, I., 2013. X-ray crystallography of viruses, in: Mateu, M. G. (Ed.), Structure and physics of viruses. Springer, Dordrecht, pp. 117-144.

von Karman, T., Tsien, H. S., 1939. The buckling of spherical shells by external pressure. J. Aeronaut. Sci. 7, 43-50.

Widom, M., Lidmar, J., Nelson, D.R., 2007. Soft modes near the buckling transition of icosahedral shells. Phys. Rev. E 76, 031911.

Wilkinson, J. P., 1965. Natural Frequencies of Closed Spherical Shells. J. Acoust. Soc. Am., 38, 367-368.

Wilkinson, J. P., 1966. Natural Frequencies of Closed Spherical Sandwich Shells. J. Acoust. Soc. Am. 40, 801-806.

Wilkinson, J. P., Kalnins, A., 1965. On Nonsymmetric Dynamic Problems of Elastic Spherical Shells. ASME J. Appl. Mech. 32, 525-532.

Xiang, P., Liew, K. M., 2013. A computational framework for transverse compression of microtubules based on a higher-order Cauchy–Born rule. Comput. Methods Appl. Mech. Engrg. 254, 14-30.

Yang, S. C., Lin, H. C., Liu, T. M., Lu, J. T., Hung, W. T., Huang, Y. R., Tsai, Y. C., Kao, C. L., Chen, S. Y., Sun, C. K., 2015. Efficient Structure Resonance Energy Transfer from Microwaves to Confined Acoustic Vibrations in Viruses. Sci. Rep. 5, 18030.

Yang, Z., Bahar, I., Widom, M., 2009. Vibrational Dynamics of Icosahedrally Symmetric Biomolecular Assemblies Compared with Predictions Based on Continuum Elasticity. Biophys. J. 96, 4438-4448.

Yin, Y., Chen, Y., Ni, D., Shi, H., Fan, Q., 2005. Shape equations and curvature bifurcations induced by inhomogeneous rigidities in cell membranes. J. Biomech. 38, 1433–1440.

Yu, C. L., Chen, Z. T., Chen, C., Chen, Y. T., 2017. Influence of initial imperfections on ultimate strength of spherical shells. Int. J. Nav. Archit. Ocean Eng. 9, 473–483.

Zandi, R., Reguera, D., 2005. Mechanical properties of viral capsids. Phys. Rev. E 72, 021917.

Zhang, J., Wang, C. Y., 2016. Free vibration analysis of microtubules based on the molecular mechanics and continuum beam theory. Biomech. Model Mechanobiol. 15, 1069–1078.

Zhang, L., Ru, C. Q., 2016. Imperfection sensitivity of pressured buckling of biopolymer spherical shells. Phys. Rev. E 93, 062403.

Zhang, L., Ru, C. Q., 2018. Post-buckling of a pressured biopolymer spherical shell with the mode interaction. Proc. R. Soc. A 474, 20170834.

Zink, M., Grubmuller, H., 2009. Mechanical properties of the icosahedral shell of southern bean mosaic virus: a molecular dynamics study. Biophys. J. 96, 1350–1363.

Zoelly, R., 1915. Ueber ein Knickungaproblem and der Kugelschale. Thesis, Zurich, Switzerland.

Appendix A: The Strain-displacement relations

This work is based on the the strain-displacement relations expressed in arbitrary orthogonal curvilinear coordinate system (Sokolnikoff, 1956). The normal and shear strain components are related to the components of the displacement vector by (Kraus, 1967; Sokolnikoff, 1956)

$$\begin{aligned}
\varepsilon_i &= \frac{\partial}{\partial \alpha_i}\left(\frac{U_i}{\sqrt{g_i}}\right)+\frac{1}{2g_i}\sum_{k=1}^{3}\frac{\partial g_i}{\partial \alpha_k}\frac{U_k}{\sqrt{g_k}}, \quad i=1,2,3,\\
\gamma_{ij} &= \frac{1}{\sqrt{g_i g_j}}\left[g_i\frac{\partial}{\partial \alpha_j}\left(\frac{U_i}{\sqrt{g_i}}\right)+g_j\frac{\partial}{\partial \alpha_i}\left(\frac{U_j}{\sqrt{g_j}}\right)\right], \quad i=1,2,3, \quad i\neq j,
\end{aligned} \tag{A.1}$$

where α_i, U_i and g_i are, respectively, the curvilinear coordinates of the surface, components of the displacement vector and geometrical scale factor quantities, and are defined below for application to spherical shells

$$\begin{aligned}
&\alpha_1=\varphi, \quad \alpha_2=\theta, \quad \alpha_3=z, \quad U_1=U, \quad U_2=V, \quad U_3=W,\\
&g_1=A_1^2\left(1+z/R\right)^2, \quad g_2=A_2^2\left(1+z/R\right)^2, \quad g_3=1,
\end{aligned} \tag{A.2}$$

where U, V, W are the displacement vector compentens, A_i are Lame's parameters (defined by $A_1=R$, $A_2=R\sin\varphi$ for spherical shells) (Toorani and Lakis, 2000). Substituting Eq. (A.2) into Eq. (A.1), we obtain the following strain-displacement equations in the spherical shell space

$$\begin{aligned}
\varepsilon_\varphi &= \frac{1}{R\left(1+z/R\right)}\left(\frac{\partial U}{\partial \varphi}+W\right), \qquad \varepsilon_\theta = \frac{1}{R\sin\varphi\left(1+z/R\right)}\left(\frac{\partial V}{\partial \theta}+\frac{U}{R}\cos\varphi+W\sin\varphi\right),\\
\gamma_{\varphi\theta} &= \sin\varphi\frac{\partial}{\partial \varphi}\left(\frac{V}{R\sin\varphi\left(1+z/R\right)}\right)+\frac{1}{\sin\varphi}\frac{\partial}{\partial \theta}\left(\frac{U}{R\left(1+z/R\right)}\right),\\
\gamma_{\varphi z} &= \frac{1}{R\left(1+z/R\right)}\frac{\partial W}{\partial \varphi}+R\left(1+z/R\right)\frac{\partial}{\partial z}\left(\frac{U}{R\left(1+z/R\right)}\right),\\
\gamma_{\theta z} &= \frac{1}{R\sin\varphi\left(1+z/R\right)}\frac{\partial W}{\partial \theta}+R\sin\varphi\left(1+z/R\right)\frac{\partial}{\partial z}\left(\frac{V}{R\sin\varphi\left(1+z/R\right)}\right),
\end{aligned} \tag{A.3}$$

where ε_φ, ε_θ and $\gamma_{\varphi\theta}$, $\gamma_{\varphi z}$, $\gamma_{\theta z}$ are, respectively, the normal and shearing strain components. We can assume that the displacement components are presented by the following relationships

$$\begin{aligned} U(\varphi,\theta,z) &= u(\varphi,\theta)+z\alpha(\varphi,\theta), \\ V(\varphi,\theta,z) &= v(\varphi,\theta)+z\beta(\varphi,\theta), \\ W(\varphi,\theta,z) &= w(\varphi,\theta). \end{aligned} \tag{A.4}$$

The α and β represent the rotation of tangents to the reference surface oriented along the parametric lines φ and θ respectively. Substituting Eq. (A.4) into Eq. (A.3)

$$\begin{aligned} &\varepsilon_\varphi = e_\varphi + z\kappa_\varphi, \quad \varepsilon_\theta = e_\theta + z\kappa_\theta, \quad \gamma_{\varphi\theta} = e_{\varphi\theta} + z\kappa_{\varphi\theta}, \\ &\gamma_{\varphi z} = e_{\varphi z} - z\frac{\alpha}{R} \approx e_{\varphi z}, \quad \gamma_{\theta z} = e_{\varphi z} - z\frac{\alpha}{R} \approx e_{\varphi z}, \end{aligned} \tag{A.5}$$

where the midface engineering strains are given by

$$\begin{aligned} e_\varphi &= \frac{1}{R}\frac{\partial u}{\partial\varphi}+\frac{w}{R}, \quad e_\theta = \frac{u}{R}\cot\varphi+\frac{1}{R\sin\varphi}\frac{\partial v}{\partial\theta}+\frac{w}{R}, \quad e_{\varphi\theta} = \frac{1}{R\sin\varphi}\frac{\partial u}{\partial\theta}+\frac{1}{R}\frac{\partial v}{\partial\varphi}-\frac{v}{R}\cot\varphi, \\ e_{\theta z} &= \frac{1}{R\sin\varphi}\frac{\partial w}{\partial\theta}-\frac{v}{R}+\beta, \quad e_{\varphi z} = \frac{1}{R}\frac{\partial w}{\partial\varphi}-\frac{u}{R}+\alpha, \end{aligned} \tag{A.6}$$

and the change in curvatures are given by

$$k_\varphi = \frac{1}{R}\frac{\partial\alpha}{\partial\varphi}, \quad k_\theta = \frac{\alpha}{R}\cot\varphi+\frac{1}{R\sin\varphi}\frac{\partial\beta}{\partial\theta}, \quad k_{\varphi\theta} = \frac{1}{R\sin\varphi}\frac{\partial\alpha}{\partial\theta}+\frac{1}{R}\frac{\partial\beta}{\partial\varphi}-\frac{\beta}{R}\cot\varphi \tag{A.7}$$

Appendix B: Axisymmetric post-buckling analysis of a pressured perfect biopolymer spherical shell

B1. Instability of post-buckling behavior of a pressured perfect biopolymer spherical shell

In order to determine the instability of post-buckling behavior, we should examine the sign of Eq. (2.32). First, the term $P_{11}\left[(u_1,w_1,\alpha_1),(u_2,w_2,\alpha_2);\frac{N_0}{Eh}\right]$ in Eq. (2.32) will vanish for any value of the load N_0 according to the orthogonality condition (2.28), which can also be confirmed by introducing the buckling modes (2.14) and (2.20) and the auxiliary displacements (2.29) into Eq. (C.3) and calculating with *Mathematica*. Also, it follows from Eqs. (C.1) (C.2) (C.4) (C.5) and (C.6) that the expressions of these equations are given by

$$
\begin{aligned}
&P_2\left[(u_1,w_1,\alpha_1),\frac{N_0}{Eh}\right]=A_2\left(\frac{N_0}{Eh}\right)=A_{20}+B_{20}\frac{N_0}{Eh},\quad P_3\left[u_1,w_1,\alpha_1\right]=A_3,\\
&P_4\left[u_1,w_1,\alpha_1\right]=A_{40},\quad P_{21}\left[(u_1,w_1,\alpha_1),(u_2,w_2,\alpha_2)\right]=-A_{42}-\sum_{k=0}^{n}{}^{*}A_k''C_{2k},\\
&P_2\left[(u_2,w_2,\alpha_2);\frac{N_0}{Eh}\right]=A_{41}+B_{41}C_0{}^2+\sum_{k=1}^{n}{}^{*}C_{2k}{}^2\left(A_k'+B_k'\frac{N_0}{Eh}\right),
\end{aligned}
\tag{B.1}
$$

where $A_{20},B_{20},A_3,A_{40},A_{41},B_{41},A_k',B_k',A_{42}$ and A_k'' can be obtained easily through *Mathematica* and the star attached to the summation sign indicates that the terms $k=n/2$ is omitted if n happens to be an even number.

Next, we introduce the critical buckling load given by (2.13) into the first equation of (B.1), and it turns out to be zero because (u_1,w_1,α_1) is the linearized buckling mode and the value of the load

corresponding to the linearized buckling mode is the critical buckling load given by (2.13). Therefore, to investigate the stability around the critical buckling state, we need to examine the higher order terms in (2.32), and the stability condition requests (Koiter, 1945, 1963, 1969)

$$\xi_0^{\,3} P_3\left[u_1, w_1, \alpha_1\right] + \xi_0^{\,4}\left(P_4\left[u_1, w_1, \alpha_1\right] + P_{21}\left[(u_1, w_1, \alpha_1), (u_2, w_2, \alpha_2)\right] + P_2\left[(u_2, w_2, \alpha_2); \frac{N_0}{Eh}\right]\right) > 0 \quad \text{(B.2)}$$

Thus, a necessary condition for stability is $P_3\left[u_1, w_1, \alpha_1\right] = A_3 = 0$ since otherwise an arbitrary choice of the sign of ξ_0 can make the third-order term negative. Then, for the case of buckling modes of an even degree *n*, $P_3\left[u_1, w_1, \alpha_1\right]$ do not vanish and (B.2) can be negative, we therefore arrive at the conclusion that the equilibrium at the critical buckling load is unstable for any even degree *n*. On the other hand, if the degree *n* of the buckling modes is odd, $P_3\left[u_1, w_1, \alpha_1\right] = A_3 = 0$. In this case, it will be necessary to investigate the fourth-order terms in (2.32), and the stability condition becomes (Koiter, 1945, 1963, 1969)

$$P_4\left[u_1, w_1, \alpha_1\right] + P_{21}\left[(u_1, w_1, \alpha_1), (u_2, w_2, \alpha_2)\right] + P_2\left[(u_2, w_2, \alpha_2); \frac{N_0}{Eh}\right] \geq 0 \quad \text{(B.3)}$$

We now investigate the minimum of the energy increment for any fixed value of the amplitude factor ξ_0. Minimizing the sum of $P_{21}\left[(u_1, w_1, \alpha_1), (u_2, w_2, \alpha_2)\right] + P_2\left[(u_2, w_2, \alpha_2); \frac{N_0}{Eh}\right]$ with respect to C_{2k} for any fixed value of the amplitude factor ξ_0, we obtain

$$\frac{\partial P_{21}\left[(u_1, w_1, \alpha_1), (u_2, w_2, \alpha_2)\right]}{\partial C_{2k}} + \frac{\partial P_2\left[(u_2, w_2, \alpha_2); \frac{N_0}{Eh}\right]}{\partial C_{2k}} = 0 \quad \text{(B.4)}$$

and C_{2k} is obtained by introducing the fourth and fifth expressions of (B.1) into (B.4)

$$C_{2k}=\begin{cases}\dfrac{A_0''}{2B_{41}} & k=0\\[2ex] \dfrac{A_k''}{2\left(A_k'+B_k'\dfrac{N_0}{Eh}\right)} & k=1,2,...n,\ but\ \ k\neq\dfrac{n}{2}\ \ if\ \ n\ is\ even\end{cases} \tag{B.5}$$

Then introducing the resulting expressions C_{2k} (B.5) into the fourth and fifth expressions of (B.1) and adding all the coefficients of fourth-order terms gives

$$\begin{aligned}A_4\left(\frac{N_0}{Eh}\right)&=P_4\left[u_1,w_1,\alpha_1\right]+\underset{\xi=const.}{Min}\left\{P_{21}\left[(u_1,w_1,\alpha_1),(u_2,w_2,\alpha_2)\right]+P_2\left[(u_2,w_2,\alpha_2);\frac{N_0}{Eh}\right]\right\}\\&=A_{40}+A_{41}-A_{42}-\frac{\left(A_0''\right)^2}{4B_{41}}-\sum_{k=1}^{n}{}^{*}\frac{\left(A_k''\right)^2}{4\left(A_k'+B_k'\dfrac{N_0}{Eh}\right)}\end{aligned} \tag{B.6}$$

where the star attached to the summation sign still indicates that the terms $k=n/2$ is omitted, if n happens to be an even number.

Therefore, according to Koiter's general nonlinear theory of elastic stability (Koiter, 1945, 1963), the further necessary condition for stability, more restrictive than (B.3), is that (B.6) must be non-negative for arbitrary values of ξ_0. Now introducing the critical buckling load (2.13) into (B.6), we find that (B.6) is negative for a buckling mode of an odd degree *n*, which shows that post-buckling behavior of the pre-buckling equilibrium state at the critical buckling load is also unstable when the integer n is an odd number. Therefore, post-buckling behavior of a pressured perfect biopolymer spherical shell defined by the present refined model is unstable, and the linearized critical value $\left(\dfrac{N_0}{Eh}\right)_{cr}$ given by (2.13) is actually the maximum loading a prefect biopolymer spherical shell can sustain because it cannot sustain any pressure higher than the critical value given by (2.13).

B2. Calculation of potential energy functional (2.32)

Based on the Koiter's general nonlinear theory of elastic stability (Koiter, 1945, 1963), to the lowest-order approximation, the potential energy functional (2.32) becomes

$$P[\hat{u}] = 2\pi Eh^3 \left\{ \xi_0^{\,2} A_2 \left(\frac{N_0}{Eh} \right) + \xi_0^{\,3} A_3 \right\} \tag{B.7}$$

for buckling modes of an even degree n (at which $P_3[u_1, w_1, \alpha_1] = A_3 \neq 0$), or becomes

$$P[\hat{u}] = 2\pi Eh^3 \left\{ \xi_0^{\,2} A_2 \left(\frac{N_0}{Eh} \right) + \xi_0^{\,4} A_4 \left(\frac{N_0}{Eh} \right) \right\} \tag{B.8}$$

for buckling modes of an odd degree n (at which $P_3[u_1, w_1, \alpha_1] = A_3 = 0$).

However, according to Koiter's investigation of post-buckling behavior of a complete spherical shell for the classical buckling model (Koiter, 1969), neglecting the fourth-order term in Eq. (B.7) is questionable and the third-order term is negligibly small over most of the post-buckling range, which indicates that Eq. (B.8) will be used to described the post-buckling behavior for both an even and an odd degree n. Therefore, we further investigate if it still holds for biopolymer spherical shells defined by the present refined model.

Figure B.1 shows that the relative magnitude of the coefficient of fourth-order term and the coefficient of third-order term ($\tau = A_4 \left(\frac{N_0}{Eh} \right) \Big/ A_3$) over the post-buckling range ($\phi = \left(\frac{N_0}{Eh} \right) \Big/ \left(\frac{N_0}{Eh} \right)_{cr}$) for buckling modes of an even degree n. The value of ϕ is smaller than or equal to one since $\left(\frac{N_0}{Eh} \right)_{cr}$ is the maximum loading a prefect spherical shell can sustain. Figure A.1a shows the results for the classical case, which is given by the present refined model with $h_0 = h$ and $G^*/G = \infty$. It is seen from Fig. B.1a

that, consistent with Koiter's conclusion (Koiter, 1969), the coefficient of fourth-order term at the critical load ($\phi = 1$) is nearly an order n larger than the coefficient of third-order term, which indicates that the fourth-order term $\xi_0^{\,4} A_4 \left(\frac{N_0}{Eh} \right)$ becomes already non-negligible for values of the amplitude factor ξ_0 of order of magnitude n^{-1}. In other words, neglecting the fourth-order term is already questionable when the dimples amount to a fraction n^{-1} of the average shell thickness h. Also, as shown in Fig. B.1a, during the post-buckling range which means that ϕ decrease from 1, although the relative magnitude decreases rapidly, it still keeps a value greater than 1 especially in the neighborhood of the bifurcation point. In addition, since the value of ξ_0 will keep increasing with the decrease of ϕ, consistent with Koiter's (Koiter, 1969), the third-order term is negligibly small over most of the post-buckling range and the fourth-order term is essential for a proper understanding of the post-buckling behavior. In terms of the other two key parameters G^*/G and h_0/h, as shown in Fig. B.1b and B.1c, the variation of G^*/G and h_0/h within a physically realistic range strengthens the tendency that the third-order term can be omitted for an even degree *n*.

Therefore, the potential energy functional (2.32) is finally simplified to Eq. (B.8) for both an odd and an even degree *n*, which explains that, appealing to our physical intuition, the choice of an even or an odd integer *n* controlled by the small changes of $R/h, G^*/G, h_0/h$ through (2.15) will not have any significant consequences for the post-buckling behavior of a biopolymer spherical shell defined by the present refined model. And the post-buckling equilibrium state in the neighborhood of the bifurcation point is specified by the stationary value of Eq. (B.8) as a function of the amplitude factor ξ_0.

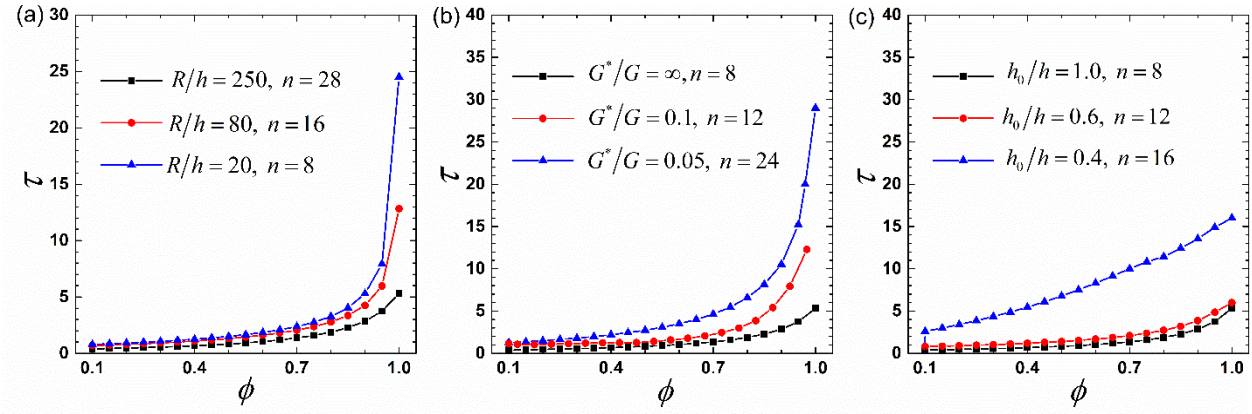

Fig. B.1 The relative magnitude of the coefficients of fourth and third order terms over the post-buckling range with fixed (a) $G^*/G=\infty$, $h_0/h=1.0$ (b) $R/h=20$, $h_0/h=1.0$ (c) $R/h=20$, $G^*/G=\infty$

Appendix C: Detailed expression of terms in Eq. (2.32)

$$P_2\left[(u_1,w_1,\alpha_1),\frac{N_0}{Eh}\right]=$$
$$\int_0^{\pi}\left\{\frac{1}{2(1-\mu^2)}\left[\left(\frac{\partial u_1}{h\partial\varphi}+\frac{w_1}{h}\right)^2+\left(\frac{u_1}{h}\cot\varphi+\frac{w_1}{h}\right)^2+2\mu\left(\frac{\partial u_1}{h\partial\varphi}+\frac{w_1}{h}\right)\left(\frac{u_1}{h}\cot\varphi+\frac{w_1}{h}\right)\right]\right.$$
$$+\frac{1}{2}\frac{N_0}{Eh}\left(\frac{\partial w_1}{h\partial\varphi}\right)^2+\frac{1}{24(1-\mu^2)}\left(\frac{h}{h_0}\right)^3\left[\left(\frac{\partial\alpha_1}{\partial\varphi}\right)^2+(\alpha_1\cot\varphi)^2+2\mu\left(\frac{\partial\alpha_1}{\partial\varphi}\right)(\alpha_1\cot\varphi)\right] \quad (C.1)$$
$$\left.+\frac{1}{4(1+\mu)}k_s\frac{G^*}{G}\left(\frac{\partial w_1}{h\partial\varphi}+\frac{R}{h}\alpha_1\right)^2\right\}\sin\varphi d\varphi$$

$$P_3\left[u_1,w_1,\alpha_1\right]=\int_0^{\pi}\left\{\frac{1}{2(1-\mu^2)}\frac{h}{R}\left[\left(\frac{\partial u_1}{h\partial\varphi}+\frac{w_1}{h}\right)+\mu\left(\frac{u_1}{h}\cot\varphi+\frac{w_1}{h}\right)\right]\left(\frac{\partial w_1}{h\partial\varphi}\right)^2\right\}\sin\varphi d\varphi \quad (C.2)$$

$$P_{11}\left[(u_1,w_1,\alpha_1),(u_2,w_2,\alpha_2);\frac{N_0}{Eh}\right]=$$
$$\int_0^{\pi}\left\{\frac{1}{(1-\mu^2)}\left[\left(\frac{\partial u_1}{h\partial\varphi}+\frac{w_1}{h}\right)\left(\frac{\partial u_2}{h\partial\varphi}+\frac{w_2}{h}\right)+\left(\frac{u_1}{h}\cot\varphi+\frac{w_1}{h}\right)\left(\frac{u_2}{h}\cot\varphi+\frac{w_2}{h}\right)\right.\right.$$
$$\left.+\mu\left(\frac{\partial u_1}{h\partial\varphi}+\frac{w_1}{h}\right)\left(\frac{u_2}{h}\cot\varphi+\frac{w_2}{h}\right)+\mu\left(\frac{\partial u_2}{h\partial\varphi}+\frac{w_2}{h}\right)\left(\frac{u_1}{h}\cot\varphi+\frac{w_1}{h}\right)\right]$$
$$+\frac{N_0}{Eh}\left(\frac{\partial w_1}{h\partial\varphi}\right)\left(\frac{\partial w_2}{h\partial\varphi}\right)+\frac{1}{12(1-\mu^2)}\left(\frac{h}{h_0}\right)^3\left[\left(\frac{\partial\alpha_1}{\partial\varphi}\right)\left(\frac{\partial\alpha_2}{\partial\varphi}\right)+(\alpha_1\cot\varphi)(\alpha_2\cot\varphi)\right. \quad (C.3)$$
$$\left.+\mu\left(\frac{\partial\alpha_1}{\partial\varphi}\right)(\alpha_2\cot\varphi)+\mu\left(\frac{\partial\alpha_2}{\partial\varphi}\right)(\alpha_1\cot\varphi)\right]$$
$$\left.+\frac{1}{2(1+\mu)}k_s\frac{G^*}{G}\left(\frac{\partial w_1}{h\partial\varphi}+\frac{R}{h}\alpha_1\right)\left(\frac{\partial w_2}{h\partial\varphi}+\frac{R}{h}\alpha_2\right)\right\}\sin\varphi d\varphi$$

$$P_4\left[u_1,w_1,\alpha_1\right]=\int_0^{\pi}\left[\frac{1}{8(1-\mu^2)}\left(\frac{h}{R}\right)^2\left(\frac{\partial w_1}{h\partial\varphi}\right)^4\right]\sin\varphi d\varphi \quad (C.4)$$

$$P_{21}\left[(u_1,w_1,\alpha_1),(u_2,w_2,\alpha_2)\right]=$$

$$\int_0^{\pi}\frac{1}{2(1-\mu^2)}\left(\frac{h}{R}\right)\left\{2\left(\frac{\partial u_1}{h\partial\varphi}+\frac{w_1}{h}\right)\left(\frac{\partial w_1}{h\partial\varphi}\frac{\partial w_2}{h\partial\varphi}\right)+\left(\frac{u_2}{h}\cot\varphi+\frac{w_2}{h}\right)\left(\frac{\partial w_1}{h\partial\varphi}\right)^2\right. \tag{C.5}$$

$$\left.+\mu\left[2\left(\frac{u_1}{h}\cot\varphi+\frac{w_1}{h}\right)\left(\frac{\partial w_1}{h\partial\varphi}\frac{\partial w_2}{h\partial\varphi}\right)+\left(\frac{u_2}{h}\cot\varphi+\frac{w_2}{h}\right)\left(\frac{\partial w_1}{h\partial\varphi}\right)^2\right]\right\}\sin\varphi d\varphi$$

$$P_2\left[(u_2,w_2,\alpha_2),\frac{N_0}{Eh}\right]=$$

$$\int_0^{\pi}\left\{\frac{1}{2(1-\mu^2)}\left[\left(\frac{\partial u_2}{h\partial\varphi}+\frac{w_2}{h}\right)^2+\left(\frac{u_2}{h}\cot\varphi+\frac{w_2}{h}\right)^2+2\mu\left(\frac{\partial u_2}{h\partial\varphi}+\frac{w_2}{h}\right)\left(\frac{u_2}{h}\cot\varphi+\frac{w_2}{h}\right)\right]\right.$$

$$+\frac{1}{2}\frac{N_0}{Eh}\left(\frac{\partial w_2}{h\partial\varphi}\right)^2+\frac{1}{24(1-\mu^2)}\left(\frac{h}{h_0}\right)^3\left[\left(\frac{\partial\alpha_2}{\partial\varphi}\right)^2+\left(\alpha_2\cot\varphi\right)^2+2\mu\left(\frac{\partial\alpha_2}{\partial\varphi}\right)\left(\alpha_2\cot\varphi\right)\right] \tag{C.6}$$

$$\left.+\frac{1}{4(1+\mu)}k_s\frac{G^*}{G}\left(\frac{\partial w_2}{h\partial\varphi}+\frac{R}{h}\alpha_2\right)^2\right\}\sin\varphi d\varphi$$

Appendix D: Determination of $(u_2^*, v_2^*, w_2^*, \alpha_2^*, \beta_2^*)$

In order to solve Eq. (3.22), similar to the determination of ($u_2^*, v_2^*, w_2^*, \alpha_2^*, \beta_2^*$), let us define u_2^*, v_2^* and $Q_{\varphi 2}^*, Q_{\theta 2}^*$ in terms of two new functions $f_2^*(\varphi,\theta)$ and $g_2^*(\varphi,\theta)$ as

$$\begin{aligned} u_2^* &= \frac{\partial f_2^*}{\partial \varphi},\ v_2^* = \frac{\partial f_2^*}{\partial \theta}\csc\varphi, \\ Q_{\varphi 2}^* &= \frac{\partial g_2^*}{\partial \varphi},\ Q_{\theta 2}^* = \frac{\partial g_2^*}{\partial \theta}\csc\varphi, \end{aligned} \tag{D.1}$$

Inserting Eq. (D.1) and ($u_1^*, v_1^*, w_1^*, \alpha_1^*, \beta_1^*$) (Eqs. (3.19) and (3.21)) into Eq. (3.22) leads to three equations for (f_2^*, w_2^*, g_2^*)

$$\begin{aligned} \left[R^2\nabla^2 + (1-\mu)\right] f_2^* + (1+\mu) w_2^* + F &= 0 \\ R\nabla^2 g_2^* - \frac{Eh}{1-\mu}\left(\nabla^2 f_2^* + \frac{2w_2^*}{R^2}\right) + N_0\nabla^2 w_2^* + L &= 0 \\ \left(R\nabla^2 + \frac{1-\mu}{R} - \frac{R}{D}k_s G^* h\right) g_2^* - \left(k_s G^* h\nabla^2 + k_s G^* h\frac{1-\mu}{R^2}\right) w_2^* &= 0 \end{aligned} \tag{D.2}$$

where the expression of F is determined by introducing w_1^* (Eq. (3.19)) into the fourth, fifth and sixth terms of first and second equation of (3.22) and the expression of L is determined by introducing ($u_1^*, v_1^*, w_1^*, \alpha_1^*, \beta_1^*$) (Eqs. (3.19) and (3.21)) into the sixth, seventh and eighth terms of the third equation of (3.22). The specific expressions of F and L are given by

$$
\begin{aligned}
(F;L) = h\Bigg\{ & \sum_{k=0}^{n} (\xi_0)^2 \, (F0_{2k}^{0}; L0_{2k}^{0}) P_{2k}(\cos\varphi) \\
& + \sum_{m=1}^{n} \xi_0 \left(\xi_m \cos m\theta + \kappa_m \sin m\theta\right) \sum_{k=\lceil m/2 \rceil}^{n} (F1_{2k}^{m}; L1_{2k}^{m}) \bar{P}_{2k}^{m}(\cos\varphi) \\
& + \sum_{i,j=1 \text{ and } j\geq i}^{n} \left(\xi_i\xi_j - \kappa_i\kappa_j\right) \cos\left[(i+j)\theta\right] \sum_{k=\lceil (i+j)/2 \rceil}^{n} (F2i_{2k}^{i+j}; L2i_{2k}^{i+j}) \bar{P}_{2k}^{i+j}(\cos\varphi) \\
& + \sum_{i,j=1 \text{ and } j\geq i}^{n} \left(\xi_i\xi_j + \kappa_i\kappa_j\right) \cos\left[(j-i)\theta\right] \sum_{k=\lceil (j-i)/2 \rceil}^{n} (F3i_{2k}^{j-i}; L3i_{2k}^{j-i}) \bar{P}_{2k}^{j-i}(\cos\varphi) \\
& + \sum_{i,j=1 \text{ and } j\geq i}^{n} \left(\xi_i\kappa_j + \xi_j\kappa_i\right) \sin\left[(i+j)\theta\right] \sum_{k=\lceil (i+j)/2 \rceil}^{n} (F4i_{2k}^{i+j}; L4i_{2k}^{i+j}) \bar{P}_{2k}^{i+j}(\cos\varphi) \\
& + \sum_{i,j=1 \text{ and } j>i}^{n} \left(\xi_i\kappa_j - \xi_j\kappa_i\right) \sin\left[(j-i)\theta\right] \sum_{k=\lceil (j-i)/2 \rceil}^{n} (F5i_{2k}^{j-i}; L5i_{2k}^{j-i}) \bar{P}_{2k}^{j-i}(\cos\varphi) \Bigg\},
\end{aligned}
\tag{D.3}
$$

where P_{2k} are Legendre functions of degree $2k$ and $\bar{P}_{2k}^{l}(\cos\varphi)$ are the associated normalized Legendre-polynomial of degree $2k$ and order l. The value of $(F0_{2k}^{0}; L0_{2k}^{0})$, $(F1_{2k}^{m}; L1_{2k}^{m})$, $(F2i_{2k}^{i+j}; L2i_{2k}^{i+j})$, $(F3i_{2k}^{j-i}; L3i_{2k}^{j-i})$, $(F4i_{2k}^{i+j}; L4i_{2k}^{i+j})$ and $(F5i_{2k}^{j-i}; L5i_{2k}^{j-i})$ can be obtained easily through *Mathematica*.

Then, it follows from Eq. (D.2) that the formulas of w_2^*, f_2^*, g_2^* are similar to F and L, which are given by

$$
\begin{aligned}
\left(w_2^*; f_2^*; g_2^*\right) = h\Bigg\{ & \sum_{k=0}^{n} \left(\xi_0\right)^2 \left(w0_{2k}^0; f0_{2k}^0; g0_{2k}^0\right) P_{2k}\left(\cos\varphi\right) \\
& + \sum_{m=1}^{n} \xi_0 \left(\xi_m \cos m\theta + \kappa_m \sin m\theta\right) \sum_{k=\lceil m/2 \rceil}^{n} \left(w1_{2k}^m; f1_{2k}^m; g1_{2k}^m\right) \bar{P}_{2k}^m\left(\cos\varphi\right) \\
& + \sum_{i,j=1 \text{ and } j\geq i}^{n} \left(\xi_i\xi_j - \kappa_i\kappa_j\right) \cos\left[\left(i+j\right)\theta\right] \sum_{k=\lceil (i+j)/2 \rceil}^{n} \left(w2i_{2k}^{i+j}; f2i_{2k}^{i+j}; g2i_{2k}^{i+j}\right) \bar{P}_{2k}^{i+j}\left(\cos\varphi\right) \\
& + \sum_{i,j=1 \text{ and } j\geq i}^{n} \left(\xi_i\xi_j + \kappa_i\kappa_j\right) \cos\left[\left(j-i\right)\theta\right] \sum_{k=\lceil (j-i)/2 \rceil}^{n} \left(w3i_{2k}^{j-i}; f3i_{2k}^{j-i}; g3i_{2k}^{j-i}\right) \bar{P}_{2k}^{j-i}\left(\cos\varphi\right) \\
& + \sum_{i,j=1 \text{ and } j\geq i}^{n} \left(\xi_i\kappa_j + \xi_j\kappa_i\right) \sin\left[\left(i+j\right)\theta\right] \sum_{k=\lceil (i+j)/2 \rceil}^{n} \left(w4i_{2k}^{i+j}; f4i_{2k}^{i+j}; g4i_{2k}^{i+j}\right) \bar{P}_{2k}^{i+j}\left(\cos\varphi\right) \\
& + \sum_{i,j=1 \text{ and } j>i}^{n} \left(\xi_i\kappa_j - \xi_j\kappa_i\right) \sin\left[\left(j-i\right)\theta\right] \sum_{k=\lceil (j-i)/2 \rceil}^{n} \left(w5i_{2k}^{j-i}; f5i_{2k}^{j-i}; g5i_{2k}^{j-i}\right) \bar{P}_{2k}^{j-i}\left(\cos\varphi\right) \Bigg\}
\end{aligned}
\tag{D.4}
$$

where $\left(w0_{2k}^0; f0_{2k}^0; g0_{2k}^0\right)$, $\left(w1_{2k}^m; f1_{2k}^m; g1_{2k}^m\right)$, $\left(w2i_{2k}^{i+j}; f2i_{2k}^{i+j}; g2i_{2k}^{i+j}\right)$, $\left(w3i_{2k}^{j-i}; f3i_{2k}^{j-i}; g3i_{2k}^{j-i}\right)$, $\left(w4i_{2k}^{i+j}; f4i_{2k}^{i+j}; g4i_{2k}^{i+j}\right)$ and $\left(w5i_{2k}^{j-i}; f5i_{2k}^{j-i}; g5i_{2k}^{j-i}\right)$ are some undetermined coefficients. Accordingly, with the use of Eqs. (3.13) and (3.20), the first Laplacian of w_2^*, f_2^*, g_2^* gives

$$
\begin{aligned}
\left(\nabla^2 w_2^*; \nabla^2 f_2^*; \nabla^2 g_2^*\right) = h\Bigg\{ & \sum_{k=0}^{n} \left(\xi_0\right)^2 \left(w0_{2k}^0; f0_{2k}^0; g0_{2k}^0\right) \frac{-2k(2k+1)}{R^2} P_{2k}\left(\cos\varphi\right) \\
& + \sum_{m=1}^{n} \xi_0 \left(\xi_m \cos m\theta + \kappa_m \sin m\theta\right) \sum_{k=\lceil m/2 \rceil}^{n} \left(w1_{2k}^m; f1_{2k}^m; g1_{2k}^m\right) \frac{-2k(2k+1)}{R^2} \bar{P}_{2k}^m\left(\cos\varphi\right) \\
& + \sum_{i,j=1 \text{ and } j\geq i}^{n} \left(\xi_i\xi_j - \kappa_i\kappa_j\right) \cos\left[\left(i+j\right)\theta\right] \sum_{k=\lceil (i+j)/2 \rceil}^{n} \left(w2i_{2k}^{i+j}; f2i_{2k}^{i+j}; g2i_{2k}^{i+j}\right) \frac{-2k(2k+1)}{R^2} \bar{P}_{2k}^{i+j}\left(\cos\varphi\right) \\
& + \sum_{i,j=1 \text{ and } j\geq i}^{n} \left(\xi_i\xi_j + \kappa_i\kappa_j\right) \cos\left[\left(j-i\right)\theta\right] \sum_{k=\lceil (j-i)/2 \rceil}^{n} \left(w3i_{2k}^{j-i}; f3i_{2k}^{j-i}; g3i_{2k}^{j-i}\right) \frac{-2k(2k+1)}{R^2} \bar{P}_{2k}^{j-i}\left(\cos\varphi\right) \\
& + \sum_{i,j=1 \text{ and } j\geq i}^{n} \left(\xi_i\kappa_j + \xi_j\kappa_i\right) \sin\left[\left(i+j\right)\theta\right] \sum_{k=\lceil (i+j)/2 \rceil}^{n} \left(w4i_{2k}^{i+j}; f4i_{2k}^{i+j}; g4i_{2k}^{i+j}\right) \frac{-2k(2k+1)}{R^2} \bar{P}_{2k}^{i+j}\left(\cos\varphi\right) \\
& + \sum_{i,j=1 \text{ and } j>i}^{n} \left(\xi_i\kappa_j - \xi_j\kappa_i\right) \sin\left[\left(j-i\right)\theta\right] \sum_{k=\lceil (j-i)/2 \rceil}^{n} \left(w5i_{2k}^{j-i}; f5i_{2k}^{j-i}; g5i_{2k}^{j-i}\right) \frac{-2k(2k+1)}{R^2} \bar{P}_{2k}^{j-i}\left(\cos\varphi\right) \Bigg\}
\end{aligned}
\tag{D.5}
$$

Then substituting Eq. (D.3), (D.4) and (D.5) into Eq. (D.2), these undetermined coefficients can be calculated and then combining with Eqs. (D.1) and (3.2), the non-axisymmetric second-order deviations $u_2^*, v_2^*, w_2^*, \alpha_2^*, \beta_2^*$ can be finally determined in terms of $\frac{N_0}{Eh}$.

Then consider the orthogonality condition, expressed by the equation (Koiter, 1969)

$$\int_0^{\pi}\int_0^{2\pi}\left(\frac{\partial w_1^*}{\partial \varphi}\right)\left(\frac{\partial w_2^*}{\partial \varphi}\right)R^2 \sin\varphi d\varphi d\theta = 0 \tag{D.6}$$

The orthogonality condition requests that the expansion of w_2^* in a series of Legrende function shall not contain any term of degree n (Koiter, 1969). In the case of an odd critical degree n of the buckling mode, it follows immediately from the expression of w_2^*, f_2^*, g_2^* in (D.4) that the orthogonality condition (D.6) is satisfied. On the other hand, for an even value of n, this orthogonality condition requires $(w0_{2k}^0; f0_{2k}^0; g0_{2k}^0) = (w1_{2k}^m; f1_{2k}^m; g1_{2k}^m) = (w2i_{2k}^{i+j}; f2i_{2k}^{i+j}; g2i_{2k}^{i+j}) = (w3i_{2k}^{j-i}; f3i_{2k}^{j-i}; g3i_{2k}^{j-i})$

$= (w4i_{2k}^{i+j}; f4i_{2k}^{i+j}; g4i_{2k}^{i+j}) = (w5i_{2k}^{j-i}; f5i_{2k}^{j-i}; g5i_{2k}^{j-i})$ for $k = n/2$.

Appendix E: Detailed expression of terms in Eq. (3.24)

$$
\begin{aligned}
&P_2\left[(u_1^*, v_1^*, w_1^*, \alpha_1^*, \beta_1^*); \frac{N_0}{Eh}\right] = \\
&\int_0^{2\pi}\int_0^{\pi}\left\{\frac{1}{2(1-\mu^2)}\left[\left(\frac{\partial u_1^*}{h\partial\varphi}+\frac{w_1^*}{h}\right)^2+\left(\frac{u_1^*}{h}\cot\varphi+\frac{1}{h\sin\varphi}\frac{\partial v_1^*}{\partial\theta}+\frac{w_1^*}{h}\right)^2\right.\right. \\
&\qquad\left.\left.+2\mu\left(\frac{\partial u_1^*}{h\partial\varphi}+\frac{w_1^*}{h}\right)\left(\frac{u_1^*}{h}\cot\varphi+\frac{1}{h\sin\varphi}\frac{\partial v_1^*}{\partial\theta}+\frac{w_1^*}{h}\right)\right]\right. \\
&\quad+\frac{1}{4(1+\mu)}\left(\frac{1}{h\sin\varphi}\frac{\partial u_1^*}{\partial\theta}+\frac{\partial v_1^*}{h\partial\varphi}-\frac{v_1^*}{h}\cot\varphi\right)^2 \\
&\quad+\frac{1}{24(1-\mu^2)}\left(\frac{h_0}{h}\right)^3\left[\left(\frac{\partial\alpha_1^*}{\partial\varphi}\right)^2+\left(\alpha_1^*\cot\varphi+\frac{1}{\sin\varphi}\frac{\partial\beta_1^*}{\partial\theta}\right)^2+2\mu\left(\frac{\partial\alpha_1^*}{\partial\varphi}\right)\left(\alpha_1^*\cot\varphi+\frac{1}{\sin\varphi}\frac{\partial\beta_1^*}{\partial\theta}\right)\right] \\
&\quad+\frac{1}{48(1+\mu)}\left(\frac{h_0}{h}\right)^3\left[\left(\frac{1}{\sin\varphi}\frac{\partial\alpha_1^*}{\partial\theta}+\frac{\partial\beta_1^*}{\partial\varphi}-\beta_1^*\cot\varphi\right)^2\right] \\
&\quad\left.+\frac{k_s}{4(1+\mu)}\frac{G^*}{G}\left[\left(\frac{R}{h}\alpha_1^*+\frac{\partial w_1^*}{h\partial\varphi}\right)^2+\left(\frac{R}{h}\beta_1^*+\frac{1}{h\sin\varphi}\frac{\partial w_1^*}{\partial\theta}\right)^2\right]\right\}\sin\varphi d\varphi d\theta \\
&+\int_0^{2\pi}\int_0^{\pi}\left\{\frac{1}{2}\frac{N_0}{Eh}\left[\left(\frac{\partial w_1^*}{h\partial\varphi}\right)^2+\left(\frac{1}{h\sin\varphi}\frac{\partial w_1^*}{\partial\theta}\right)^2\right]\right\}\sin\varphi d\varphi d\theta
\end{aligned}
\tag{E.1}
$$

$$
\begin{aligned}
&P_3\left[u_1^*, v_1^*, w_1^*, \alpha_1^*, \beta_1^*\right] = \\
&\int_0^{2\pi}\int_0^{\pi}\left\{\frac{1}{2(1-\mu^2)}\frac{h}{R}\left[\left(\left(\frac{\partial u_1^*}{h\partial\varphi}+\frac{w_1^*}{h}\right)+\mu\left(\frac{u_1^*}{h}\cot\varphi+\frac{1}{h\sin\varphi}\frac{\partial v_1^*}{\partial\theta}+\frac{w_1^*}{h}\right)\right)\left(\frac{\partial w_1^*}{h\partial\varphi}\right)^2\right.\right. \\
&\qquad\left.\left.+\left(\mu\left(\frac{\partial u_1^*}{h\partial\varphi}+\frac{w_1^*}{h}\right)+\left(\frac{u_1^*}{h}\cot\varphi+\frac{1}{h\sin\varphi}\frac{\partial v_1^*}{\partial\theta}+\frac{w_1^*}{h}\right)\right)\left(\frac{1}{h\sin\varphi}\frac{\partial w_1^*}{\partial\varphi}\right)^2\right]\right. \\
&\quad\left.+\frac{1}{2(1+\mu)}\frac{h}{R}\left[\left(\frac{1}{h\sin\varphi}\frac{\partial u_1^*}{\partial\theta}+\frac{\partial v_1^*}{h\partial\varphi}-\frac{v_1^*}{h}\cot\varphi\right)\left(\frac{\partial w_1^*}{h\partial\varphi}\right)\left(\frac{1}{h\sin\varphi}\frac{\partial w_1^*}{\partial\varphi}\right)\right]\right\}\sin\varphi d\varphi d\theta
\end{aligned}
\tag{E.2}
$$

$$P_{11}\left[(u_1^*,v_1^*,w_1^*,\alpha_1^*,\beta_1^*),(u_2^*,v_2^*,w_2^*,\alpha_2^*,\beta_2^*);\frac{N_0}{Eh}\right]=$$

$$\int_0^{2\pi}\int_0^{\pi}\left\{\frac{1}{(1-\mu^2)}\left[\left(\frac{\partial u_1^*}{h\partial\varphi}+\frac{w_1^*}{h}\right)\left(\frac{\partial u_2^*}{h\partial\varphi}+\frac{w_2^*}{h}\right)+\left(\frac{u_1^*}{h}\cot\varphi+\frac{1}{h\sin\varphi}\frac{\partial v_1^*}{\partial\theta}+\frac{w_1^*}{h}\right)\left(\frac{u_2^*}{h}\cot\varphi+\frac{1}{h\sin\varphi}\frac{\partial v_2^*}{\partial\theta}+\frac{w_2^*}{h}\right)\right.\right.$$
$$\left.\left.+\mu\left(\left(\frac{\partial u_1^*}{h\partial\varphi}+\frac{w_1^*}{h}\right)\left(\frac{u_2^*}{h}\cot\varphi+\frac{1}{h\sin\varphi}\frac{\partial v_2^*}{\partial\theta}+\frac{w_2^*}{h}\right)+\left(\frac{\partial u_2^*}{h\partial\varphi}+\frac{w_2^*}{h}\right)\left(\frac{u_1^*}{h}\cot\varphi+\frac{1}{h\sin\varphi}\frac{\partial v_1^*}{\partial\theta}+\frac{w_1^*}{h}\right)\right)\right]$$
$$+\frac{1}{2(1+\mu)}\left[\left(\frac{1}{h\sin\varphi}\frac{\partial u_1^*}{\partial\theta}+\frac{\partial v_1^*}{h\partial\varphi}-\frac{v_1^*}{h}\cot\varphi\right)\left(\frac{1}{h\sin\varphi}\frac{\partial u_2^*}{\partial\theta}+\frac{\partial v_2^*}{h\partial\varphi}-\frac{v_2^*}{h}\cot\varphi\right)\right]$$
$$+\frac{1}{12(1-\mu^2)}\left(\frac{h_0}{h}\right)^3\left[\left(\frac{\partial\alpha_1^*}{\partial\varphi}\right)\left(\frac{\partial\alpha_2^*}{\partial\varphi}\right)+\left(\alpha_1^*\cot\varphi+\frac{1}{\sin\varphi}\frac{\partial\beta_1^*}{\partial\theta}\right)\left(\alpha_2^*\cot\varphi+\frac{1}{\sin\varphi}\frac{\partial\beta_2^*}{\partial\theta}\right)\right.$$
$$\left.+\mu\left(\left(\frac{\partial\alpha_1^*}{\partial\varphi}\right)\left(\alpha_2^*\cot\varphi+\frac{1}{\sin\varphi}\frac{\partial\beta_2^*}{\partial\theta}\right)+\left(\frac{\partial\alpha_2^*}{\partial\varphi}\right)\left(\alpha_1^*\cot\varphi+\frac{1}{\sin\varphi}\frac{\partial\beta_1^*}{\partial\theta}\right)\right)\right]$$
$$+\frac{1}{24(1+\mu)}\left(\frac{h_0}{h}\right)^3\left[\left(\frac{1}{\sin\varphi}\frac{\partial\alpha_1^*}{\partial\theta}+\frac{\partial\beta_1^*}{\partial\varphi}-\beta_1^*\cot\varphi\right)\left(\frac{1}{\sin\varphi}\frac{\partial\alpha_2^*}{\partial\theta}+\frac{\partial\beta_2^*}{\partial\varphi}-\beta_2^*\cot\varphi\right)\right]$$
$$\left.+\frac{k_s}{2(1+\mu)}\frac{G^*}{G}\left[\left(\frac{R}{h}\alpha_1^*+\frac{\partial w_1^*}{h\partial\varphi}\right)\left(\frac{R}{h}\alpha_2^*+\frac{\partial w_2^*}{h\partial\varphi}\right)+\left(\frac{R}{h}\beta_1^*+\frac{1}{h\sin\varphi}\frac{\partial w_1^*}{\partial\theta}\right)\left(\frac{R}{h}\beta_2^*+\frac{1}{h\sin\varphi}\frac{\partial w_2^*}{\partial\theta}\right)\right]\right\}\sin\varphi d\varphi d\theta$$
$$+\int_0^{2\pi}\int_0^{\pi}\left\{\frac{N_0}{Eh}\left[\left(\frac{\partial w_1^*}{h\partial\varphi}\right)\left(\frac{\partial w_2^*}{h\partial\varphi}\right)+\left(\frac{1}{h\sin\varphi}\frac{\partial w_1^*}{\partial\theta}\right)\left(\frac{1}{h\sin\varphi}\frac{\partial w_2^*}{\partial\theta}\right)\right]\right\}\sin\varphi d\varphi d\theta$$

(E.3)

$$P_{21}\left[(u_1^*,v_1^*,w_1^*,\alpha_1^*,\beta_1^*),(u_2^*,v_2^*,w_2^*,\alpha_2^*,\beta_2^*)\right]=$$

$$\int_0^{2\pi}\int_0^{\pi}\left\{\frac{1}{(1-\mu^2)}\left(\frac{h}{R}\right)\left[\left(\frac{\partial u_1^*}{h\partial\varphi}+\frac{w_1^*}{h}\right)\left(\frac{\partial w_1^*}{h\partial\varphi}\right)\left(\frac{\partial w_2^*}{h\partial\varphi}\right)+\left(\frac{u_1^*}{h}\cot\varphi+\frac{1}{h\sin\varphi}\frac{\partial v_1^*}{\partial\theta}+\frac{w_1^*}{h}\right)\left(\frac{1}{\sin\varphi}\frac{\partial w_1^*}{h\partial\theta}\right)\left(\frac{1}{\sin\varphi}\frac{\partial w_2^*}{h\partial\theta}\right)\right.\right.$$
$$\left.\left.+\mu\left(\left(\frac{\partial u_1^*}{h\partial\varphi}+\frac{w_1^*}{h}\right)\left(\frac{1}{\sin\varphi}\frac{\partial w_1^*}{h\partial\theta}\right)\left(\frac{1}{\sin\varphi}\frac{\partial w_2^*}{h\partial\theta}\right)+\left(\frac{u_1^*}{h}\cot\varphi+\frac{1}{h\sin\varphi}\frac{\partial v_1^*}{\partial\theta}+\frac{w_1^*}{h}\right)\left(\frac{\partial w_1^*}{h\partial\varphi}\right)\left(\frac{\partial w_2^*}{h\partial\varphi}\right)\right)\right]$$
$$+\frac{1}{2(1+\mu)}\left(\frac{h}{R}\right)\left[\left(\frac{1}{h\sin\varphi}\frac{\partial u_1^*}{\partial\theta}+\frac{\partial v_1^*}{h\partial\varphi}-\frac{v_1^*}{h}\cot\varphi\right)\left(\left(\frac{\partial w_1^*}{h\partial\varphi}\right)\left(\frac{1}{\sin\varphi}\frac{\partial w_2^*}{h\partial\theta}\right)+\left(\frac{\partial w_2^*}{h\partial\varphi}\right)\left(\frac{1}{\sin\varphi}\frac{\partial w_1^*}{h\partial\theta}\right)\right)\right]$$
$$+\frac{1}{2(1-\mu^2)}\left(\frac{h}{R}\right)\left[\left(\frac{\partial u_2^*}{h\partial\varphi}+\frac{w_2^*}{h}\right)\left(\frac{\partial w_1^*}{h\partial\varphi}\right)^2+\left(\frac{u_2^*}{h}\cot\varphi+\frac{1}{h\sin\varphi}\frac{\partial v_2^*}{\partial\theta}+\frac{w_2^*}{h}\right)\left(\frac{1}{\sin\varphi}\frac{\partial w_1^*}{h\partial\theta}\right)^2\right.$$
$$\left.+\mu\left(\left(\frac{\partial u_2^*}{h\partial\varphi}+\frac{w_2^*}{h}\right)\left(\frac{1}{\sin\varphi}\frac{\partial w_1^*}{h\partial\theta}\right)^2+\left(\frac{u_2^*}{h}\cot\varphi+\frac{1}{h\sin\varphi}\frac{\partial v_2^*}{\partial\theta}+\frac{w_2^*}{h}\right)\left(\frac{\partial w_1^*}{h\partial\varphi}\right)^2\right)\right]$$
$$\left.+\frac{1}{2(1+\mu)}\left(\frac{h}{R}\right)\left[\left(\frac{1}{h\sin\varphi}\frac{\partial u_2^*}{\partial\theta}+\frac{\partial v_2^*}{h\partial\varphi}-\frac{v_2^*}{h}\cot\varphi\right)\left(\frac{\partial w_1^*}{h\partial\varphi}\right)\left(\frac{1}{\sin\varphi}\frac{\partial w_1^*}{h\partial\theta}\right)\right]\right\}\sin\varphi d\varphi d\theta$$

(E.4)

$$P_2\left[(u_2^*, v_2^*, w_2^*, \alpha_2^*, \beta_2^*); \frac{N_0}{Eh}\right] =$$

$$\int_0^{2\pi}\int_0^{\pi}\left\{\frac{1}{2(1-\mu^2)}\left[\left(\frac{\partial u_2^*}{h\partial\varphi}+\frac{w_2^*}{h}\right)^2+\left(\frac{u_2^*}{h}\cot\varphi+\frac{1}{h\sin\varphi}\frac{\partial v_2^*}{\partial\theta}+\frac{w_2^*}{h}\right)^2\right.\right.$$
$$\left.+2\mu\left(\frac{\partial u_2^*}{h\partial\varphi}+\frac{w_2^*}{h}\right)\left(\frac{u_2^*}{h}\cot\varphi+\frac{1}{h\sin\varphi}\frac{\partial v_2^*}{\partial\theta}+\frac{w_2^*}{h}\right)\right]$$
$$+\frac{1}{4(1+\mu)}\left(\frac{1}{h\sin\varphi}\frac{\partial u_2^*}{\partial\theta}+\frac{\partial v_2^*}{h\partial\varphi}-\frac{v_2^*}{h}\cot\varphi\right)^2$$
$$+\frac{1}{24(1-\mu^2)}\left(\frac{h_0}{h}\right)^3\left[\left(\frac{\partial\alpha_2^*}{\partial\varphi}\right)^2+\left(\alpha_2^*\cot\varphi+\frac{1}{\sin\varphi}\frac{\partial\beta_2^*}{\partial\theta}\right)^2+2\mu\left(\frac{\partial\alpha_2^*}{\partial\varphi}\right)\left(\alpha_2^*\cot\varphi+\frac{1}{\sin\varphi}\frac{\partial\beta_2^*}{\partial\theta}\right)\right]$$
$$+\frac{1}{48(1+\mu)}\left(\frac{h_0}{h}\right)^3\left[\left(\frac{1}{\sin\varphi}\frac{\partial\alpha_2^*}{\partial\theta}+\frac{\partial\beta_2^*}{\partial\varphi}-\beta_2^*\cot\varphi\right)^2\right]$$
$$\left.+\frac{k_s}{4(1+\mu)}\frac{G^*}{G}\left[\left(\frac{R}{h}\alpha_2^*+\frac{\partial w_2^*}{h\partial\varphi}\right)^2+\left(\frac{R}{h}\beta_2^*+\frac{1}{h\sin\varphi}\frac{\partial w_2^*}{\partial\theta}\right)^2\right]\right\}\sin\varphi d\varphi d\theta$$
$$+\int_0^{2\pi}\int_0^{\pi}\left\{\frac{1}{2}\frac{N_0}{Eh}\left[\left(\frac{\partial w_2^*}{h\partial\varphi}\right)^2+\left(\frac{1}{h\sin\varphi}\frac{\partial w_2^*}{\partial\theta}\right)^2\right]\right\}\sin\varphi d\varphi d\theta \qquad \text{(E.5)}$$

$$P_4\left[u_1^*, v_1^*, w_1^*, \alpha_1^*, \beta_1^*\right] =$$

$$\int_0^{2\pi}\int_0^{\pi}\left\{\frac{1}{8(1-\mu^2)}\left(\frac{h}{R}\right)^2\left[\left(\frac{\partial w_1^*}{h\partial\varphi}\right)^4+\left(\frac{1}{h\sin\varphi}\frac{\partial w_1^*}{\partial\theta}\right)^4+2\mu\left(\frac{\partial w_1^*}{h\partial\varphi}\right)^2\left(\frac{1}{h\sin\varphi}\frac{\partial w_1^*}{\partial\theta}\right)^2\right]\right.$$
$$\left.+\frac{1}{4(1+\mu)}\left(\frac{h}{R}\right)^2\left[\left(\frac{\partial w_1^*}{h\partial\varphi}\right)^2\left(\frac{1}{h\sin\varphi}\frac{\partial w_1^*}{\partial\theta}\right)^2\right]\right\}\sin\varphi d\varphi d\theta \qquad \text{(E.6)}$$

Appendix F: Derivation of Equations (4.23)-(4.25)

Substitution of (4.1), (4.2) and (4.22) into Eqs. (4.4) results in

$$
\begin{aligned}
&\frac{\partial}{\partial\varphi}\left[\left(\nabla^2+A_1\right)f+\frac{R}{Eh}A_2 g+A_3 w\right]+\frac{\partial^2\left(-\psi\sin\varphi\right)}{\partial\varphi^2}+\frac{1-\mu}{2}\frac{\partial^2\left(-\psi\sin\varphi\right)}{\partial\theta^2}\csc^2\varphi\\
&+\frac{\partial\left(-\psi\sin\varphi\right)}{\partial\varphi}\cot\varphi-\left(\mu+\cot^2\varphi\right)\left(-\psi\sin\varphi\right)-\frac{R\left(1-\mu^2\right)}{Eh}\left(\Lambda\sin\varphi\right)\\
&+\Omega^2\left(1-\mu^2\right)\left[k_1\left(-\psi\sin\varphi\right)+k_2\left(\frac{R}{k_s G^* h}\left(-\Lambda\sin\varphi\right)-\psi\sin\varphi\right)\right]=0,\\
&\frac{\partial}{\partial\theta}\left[\left(\nabla^2+A_1\right)f+\frac{R}{Eh}A_2 g+A_3 w+\left(\frac{1+\mu}{2}\frac{\partial\left(-\psi\sin\varphi\right)}{\partial\varphi}+\frac{3-\mu}{2}\left(-\psi\sin\varphi\right)\cot\varphi\right)\right]=0,\\
&B_1\nabla^2 f+\frac{R}{Eh}\left(B_2\nabla^2+B_3\right)g-\left(\nabla^2-B_4\right)w+\frac{R\left(1+\mu\right)}{2}\\
&\left[\left(\frac{1}{k_s G^* h}\frac{\partial\left(-\Lambda\sin\varphi\right)}{\partial\varphi}+\frac{1}{R}\frac{\partial\left(-\psi\sin\varphi\right)}{\partial\varphi}\right)+\frac{3-\mu}{1+\mu}\left(\frac{1}{k_s G^* h}\left(-\Lambda\sin\varphi\right)+\frac{1}{R}\left(-\psi\sin\varphi\right)\right)\cot\varphi\right]=0,\\
&\frac{\partial}{\partial\varphi}\left(\frac{Eh}{R}C_1\nabla^2 f+\nabla^2 g+\frac{Eh}{R}C_2 w\right)+k_s G^* h\left\{\left(\frac{1}{k_s G^* h}\frac{\partial^2\left(-\Lambda\sin\varphi\right)}{\partial\varphi^2}+\frac{1}{R}\frac{\partial^2\left(-\psi\sin\varphi\right)}{\partial\varphi^2}\right)\right.\\
&+\cot\varphi\left(\frac{1}{k_s G^* h}\frac{\partial\left(-\Lambda\sin\varphi\right)}{\partial\varphi}+\frac{1}{R}\frac{\partial\left(-\psi\sin\varphi\right)}{\partial\varphi}\right)-\left(\mu+\cot^2\varphi\right)\left(\frac{1}{k_s G^* h}\left(-\Lambda\sin\varphi\right)+\frac{1}{R}\left(-\psi\sin\varphi\right)\right)\\
&+\frac{1-\mu}{2}\csc^2\varphi\left(\frac{1}{k_s G^* h}\frac{\partial^2\left(-\Lambda\sin\varphi\right)}{\partial\theta^2}+\frac{1}{R}\frac{\partial^2\left(-\psi\sin\varphi\right)}{\partial\theta^2}\right)-\frac{R^2}{D}\left(-\Lambda\sin\varphi\right)\\
&\left.+\Omega^2\left(1-\mu^2\right)\left(\frac{h}{h_0}\right)\left[\frac{2}{R}\left(-\psi\sin\varphi\right)+k_r\left(\frac{1}{k_s G^* h}\left(-\Lambda\sin\varphi\right)-\frac{\psi}{R}\sin\varphi\right)\right]\right\}=0,\\
&\frac{\partial}{\partial\theta}\left[\frac{Eh}{R}C_1\nabla^2 f+\nabla^2 g+\frac{Eh}{R}C_2 w+\left(\frac{\partial\left(-\psi\sin\varphi\right)}{\partial\varphi}+\left(-\psi\sin\varphi\right)\cot\varphi\right.\right.\\
&\left.\left.-\frac{Eh}{R\left(1-\mu\right)}\left(\frac{\partial\left(-\Lambda\sin\varphi\right)}{\partial\varphi}+\left(-\Lambda\sin\varphi\right)\cot\varphi\right)\right]=0.
\end{aligned}
\tag{F.1}
$$

Integration of the second equation of (F.1) with respect to θ, followed by differentiation with respect to φ and subtraction from the first equation of (F.1) gives

$$\left(1-\mu\right)R^2\nabla^2\psi+2A_1\psi+2A_2\Lambda=0. \tag{F.2}$$

Similarly, integration of the fifth equation of (F.1) with respect to θ, followed by differentiation with respect to φ and subtraction from the fourth equation of (F.1) gives

$$(1-\mu)B_2R^2\nabla^2\Lambda-2\left(A_2-B_3\right)\Lambda-2\left(A_1-B_1\right)\psi=0. \tag{F.3}$$

Thus, an uncoupled equation in ψ can be obtained through Eqs. (F.2) and (F.3):

$$V_1\nabla^4\psi+V_2\nabla^2\psi+V_3\psi=0. \tag{F.4}$$

In order to obtain a single uncoupled equation in w, the auxiliary functions f and g are eliminated from the third equation of (F.1) with the aid of the second and fifth equations of (F.1). With this manipulation, furthermore, the terms containing ψ and Λ can be eliminated after the use of (F.2) and (F.3), and the uncoupled equation in w is obtained as

$$\nabla^6w+W_1\nabla^4w+W_2\nabla^2w+W_3w=0. \tag{F.5}$$

The expression for the determination of the auxiliary function Λ can be derived from Eq. (F.2) in the form

$$\Lambda=-\frac{Eh}{R}\frac{1}{A_2}\left(\frac{1-\mu}{2}\nabla^2\psi+A_1\psi\right) \tag{F.6}$$

and f and g can be derived from the second, third and fifth equations of (F.1) in the form

$$\begin{aligned}
&F_1f=F_2R^4\nabla^4w+F_3R^2\nabla^2w+F_4w+F_5\frac{\partial\psi}{\partial\varphi}\sin\varphi+F_6\frac{\partial\Lambda}{\partial\varphi}\sin\varphi,\\
&RG_1g=Eh\left(G_2R^4\nabla^4w+G_3R^2\nabla^2w+G_4w+G_5\frac{\partial\psi}{\partial\varphi}\sin\varphi+G_6\frac{\partial\Lambda}{\partial\varphi}\sin\varphi\right),
\end{aligned} \tag{F.7}$$

where

$$F_1 = A_2B_1^2 - 2A_1B_1B_3 + A_2^2B_1C_1 - A_2^2B_1B_2C_1^2 - A_2B_1B_3C_1 - A_1A_2B_3C_1 + A_1A_2B_2B_3C_1^2 + A_1B_3^2C_1 - A_1A_2B_1 + A_1A_2B_1B_2C_1 + A_1B_1B_3 + A_1^2B_3 - A_1^2B_2B_3C_1, \quad \text{(F.8)}$$

$$F_2 = -A_2 + A_2B_2C_1 + B_3, \quad \text{(F.9)}$$

$$F_3 = -A_2B_2C_2 + A_2B_2^2C_1C_2 + B_2B_3C_2 + A_2B_4 - A_2B_2B_4C_1 - B_3B_4 - A_2A_3 - A_2A_3B_2^2C_1^2 + 2A_2A_3B_2C_1 + A_3B_3 - A_3B_2B_3C_1 + A_2B_1 + A_2^2C_1 - A_2^2B_2C_1^2 - A_2B_3C_1 - A_1A_2 + A_1A_2B_2C_1, \quad \text{(F.10)}$$

$$F_4 = A_2^2C_2 + B_3^2C_2 - 2A_2^2B_2C_1C_2 - 2A_2B_3C_2 + A_2B_2B_3C_1C_2 + A_2B_1B_2C_2 + A_3B_1B_3 - A_2B_1B_4 + A_2^2B_2C_1C_2 - A_1A_2B_2C_2 + A_1A_2B_2^2C_1C_2 + A_2A_3B_3C_1 - A_1A_3B_3 - A_2A_3B_2B_3C_1^2 + A_1A_3B_2B_3C_1 - A_3B_3^2C_1 - A_2^2B_4C_1 + A_1A_2B_4 + A_2^2B_2B_4C_1^2 - A_1A_2B_2B_4C_1 + A_2B_3B_4C_1, \quad \text{(F.11)}$$

$$F_5 = \frac{1-\mu}{2}\left(-A_1A_2B_2C_1 + A_1B_2B_3C_1 + A_1A_2 - A_1B_3 - A_2B_1 + B_1B_3 - A_2^2C_1 - B_3^2C_1 + A_2^2B_2C_1^2 + 2A_2B_3C_1 - A_2B_2B_3C_1^2\right), \quad \text{(F.12)}$$

$$F_6 = \frac{1-\mu}{2}\left(-A_2^2B_2C_1 + A_2B_2B_3C_1 - A_2B_1B_2 + A_1A_2B_2 - A_1A_2B_2^2C_1 + A_2^2B_2^2C_1^2\right), \quad \text{(F.13)}$$

$$G_1 = A_2B_1^2 - 2A_1B_1B_3 + A_2^2B_1C_1 - A_2^2B_1B_2C_1^2 - A_2B_1B_3C_1 - A_1A_2B_3C_1 + A_1A_2B_2B_3C_1^2 + A_1B_3^2C_1 - A_1A_2B_1 + A_1A_2B_1B_2C_1 + A_1B_1B_3 + A_1^2B_3 - A_1^2B_2B_3C_1, \quad \text{(F.14)}$$

$$G_2 = A_1 - A_1B_2C_1 - B_1, \quad \text{(F.15)}$$

$$G_3 = -A_1A_2C_1 + A_1A_2B_2C_1^2 + A_1^2 - A_1^2B_2C_1 - A_1B_1 + A_1B_2C_2 - A_1B_4 - A_1B_2^2C_1C_2 + A_1B_2B_4C_1 - B_1B_2C_2 + B_1B_4 + A_1A_3 - 2A_1A_3B_2C_1 + A_1A_3B_2^2C_1^2 - A_3B_1 + A_3B_1B_2C_1 + A_1B_3C_1, \quad \text{(F.16)}$$

$$G_4 = -A_3B_1^2 + A_1A_2B_4C_1 - A_1A_2B_2B_4C_1^2 + A_3B_1B_3C_1 + A_1^2B_2C_2 - A_1^2B_4 - A_1^2B_2^2C_1C_2 + A_1^2B_2B_4C_1 - A_1B_1B_2C_2 + A_1B_1B_4 - A_1A_2C_2 + A_1A_2B_2C_1C_2 + A_1B_3C_2 + A_2B_1C_2 - A_2B_1B_2C_1C_2 - B_1B_3C_2 - A_2A_3B_1C_1 + A_1A_3B_1 + A_2A_3B_1B_2C_1^2 - A_1A_3B_1B_2C_1 - A_1B_3B_4C_1, \quad \text{(F.17)}$$

$$G_5 = \frac{1-\mu}{2}\left(-A_1^2 - B_1^2 + 2A_1B_1 + A_1^2B_2C_1 - A_1B_1B_2C_1 + A_1A_2C_1 - A_1A_2B_2C_1^2 - A_1B_3C_1 + A_2B_1B_2C_1^2 + B_1B_3C_1 - A_2B_1C_1\right), \quad \text{(F.18)}$$

$$G_6 = \frac{1-\mu}{2}\left(A_1A_2B_2C_1 - A_1^2B_2 + A_1^2B_2^2C_1 + A_1B_1B_2 - A_1A_2B_2^2C_1^2 - A_1B_2B_3C_1\right). \quad \text{(F.19)}$$